The Dissertation Committee for Anne Marie Mikelonis Certifies that this is the approved version of the following dissertation:

Adhesion of Silver Nanoparticle Amendments to Ceramic Water Filters

Committee:

Desmond F. Lawler, Supervisor

Lynn E. Katz

Mary Jo Kirisits

Desiderio Kovar

Katherine A. Willets

Adhesion of Silver Nanoparticle Amendments to Ceramic Water Filters

by

Anne Marie Mikelonis, B.S.C.E., M.E.C.E.

Dissertation

Presented to the Faculty of the Graduate School of

The University of Texas at Austin

in Partial Fulfillment

of the Requirements

for the Degree of

Doctor of Philosophy

The University of Texas at Austin

August 2015

Dedication

To my parents, for your enthusiasm, support, and unconditional love.

Acknowledgements

My favorite Maya Angelou quote is: “I’ve learned that people will forget what you said, people will forget what you did, but people will never forget how you made them feel.” During this experience, I have had the great fortune of being surrounded by a talented community that makes me feel unforgettably supported. When I first toyed with the idea of pursuing a Ph.D., several friends advised me to select a program based on who would be my advisor. It was the one piece of advice I carefully followed, and I am very grateful I did. Des, thank you for your mentorship, support to pursue my interests, and unwavering confidence. Your dedication to your students and craft amazes me. Lynn, Kallie, Desi, and Mary Jo, thank you for your enthusiasm for my ideas and access to your labs. I am very fortunate you agreed to be on my committee. Eric and Susan, your continued support since my time at MIT has been incredible, thank you!

To the members of EWRE past and present, thank you for so many great memories inside and out of ECJ. I am particularly grateful for the comradery and assistance of the Lawler “nano group” of Ijung, Tongren, Sungmin, and Stetson. Ijung, I will never forget the first day we saw our (snowflake) nanoparticles on the TEM. Tongren, your helpfulness in the lab has left a huge impression on me; thank you for washing so many of my dishes. Sungmin, thank you for your substantial contributions to Chapters 4 and 5 and the many hours spent discussing technical details. I feel very lucky that we were placed in the same office and that someone else finds DLVO related journal articles from the 1940s-1970s so fascinating. Stetson, I am thrilled to see how you take ceramic water filters to another level. Over the years, many undergraduate and graduate students have helped me with small pieces of this research. Thank you for your many hours! In particular, Raul and Samantha your energy and enthusiasm for learning was

contagious and enriched my Ph.D. experience tremendously. Thank you for choosing to work with me. I would also like to thank Charlie Perego and Hugo Celio for numerous instances of technical assistance and my many officemates in 7.206, you made coming to work each day fun. Also, thank you to the GETA community, spearheaded by Pam Dahl, who made me feel more connected to UT as a whole. I am also very grateful for the financial support of NSF, AWWA, and AAUW over the course of this work and Mary Kay Jackson and the Pure Home Water staff for facilitating my work in Ghana.

Words cannot properly express my gratitude for the joy and friendship so many have shared with me while in Austin. Aurore, my fondest memories are colored by times during our three years as roommates. Thank you seems inadequate for the countless hours you listened and helped me troubleshoot life and lab issues. I am grateful for your friendship more than you can ever imagine. Bryant, Celina, Clayton, Ellison, Farith, Fernando, Francesca, Ginnie, Georges, JP, Justin, Katie, Matt, Mo, Ryan, Sarah (x2), Cindy, and Niamh thank you for so many great discussions and reoccurring adventures. To all the ladies who welcomed me on their tennis teams and Kelly, Lisa, Mark, Nando, Stephanie, and Wil who spent many hours just hitting/talking life, I hope you realize that time kept me sane. To the dinner club: Aurore, Catherine, Cédric, Clément, Eléna, Fernando and Natalia, you are more than friends, you are family. Finally, I would like to acknowledge a few in my support system not in Austin. In particular, Blake, Crystal, Emily, and Ravi thank you for never losing tabs of me, even when I'm hard to keep track of. Most importantly, Mom, Dad, Greta, and Tony your support made this possible, thank you for always being my home regardless of the miles.

Adhesion of Silver Nanoparticle Amendments to Ceramic Water Filters

Anne Marie Mikelonis, Ph.D.

The University of Texas at Austin, 2015

Supervisor: Desmond F. Lawler

Silver nanoparticles (Ag NPs) are frequently added as a disinfectant to ceramic filters used for household drinking water treatment. To provide suspension phase particle stability, Ag NPs can be synthesized using a number of different molecules to cap the metal core. The goal of this doctoral work was to advance the fundamental understanding of how stabilizing agents influence the attachment and detachment of Ag NPs from ceramic water filters. To achieve this goal, deposition experiments onto Al_2O_3 membranes and clay-based ceramic filters were performed using Ag NPs stabilized by three different agents: citrate, polyvinylpyrrolidone (PVP), and branched polyethylenimine (BPEI). Laboratory and field- scale filtration experiments were also conducted to evaluate the removal of Ag NPs from ceramics under different water conditions – the presence of hardness and natural organic matter (NOM). Citrate-stabilized Ag NPs were found to have the highest attachment densities, regardless of filter material. Differing attachment densities for the three types of Ag NPs were extensively explained using a combination of classic Derjaguin, Landau, Verwey and Overbeek (DLVO) theory, steric forces, and particle-particle interaction energy calculations. A

multilevel statistical model was built to describe the removal of Ag NPs from ceramic water filters under different water conditions. The type of Ag NP was found to affect the initial release of Ag from the filters, while the interaction of the type of Ag NP and water were found to affect the rate of removal. Hardness and NOM prolonged the release of Ag from ceramic water filters.

Table of Contents

List of Tables

List of Figures

Chapter 1: Introduction

PROBLEM STATEMENT

Disinfection is an essential part of drinking water treatment. Conventional treatment involves two separate processes: removal of particles and inactivation of pathogens. However, the sustainability of disinfection via this route is threatened by rising costs of chemicals, health concerns, and even societal resistance. In the United States, disinfection systems produce carcinogenic disinfection byproducts (DBPs) that stem from chemical reactions between natural organic matter (NOM) and chlorine (Edzwald, 2011). Further, mandated chlorine residuals have inspired an entire industry of household water treatment products that remove chlorine from tap water because many find the taste of chlorine disagreeable. Thus, current disinfection practices are ripe for change. Inspiration may be drawn from a technology pioneered by local nongovernmental organizations in developing countries. For decades, safe drinking water advocates have combined disinfection and particle removal into a single step by incorporating a colloidal silver coating into ceramic water filters used for household water treatment. Silver-coated ceramic water filters have found widespread acceptance, notwithstanding a lack of fundamental research that examines their lifetime effectiveness.

OBJECTIVES

This research explores an innovative approach to current disinfection options through studying the attachment and release of silver nanoparticles (Ag NPs), a known disinfectant (Eckhardt et al., 2013) to ceramic water filters. Paramount to creating a safe

and reliable single step disinfection process is a mechanistic understanding of the forces that attract Ag NPs to ceramic surfaces. Ag NPs are generated by a wide range of techniques, each of which use a variety of different "stabilizing" agents to control the size of the NPs. Different stabilizers produce different configurations on the particle surface, which in turn affect particle-surface interaction energies. The primary objectives of this research are to:

1) *Characterize the attachment density of Ag NPs on porous ceramic filters.*

2) *Identify the dominant interaction energies involved in Ag NP-ceramic deposition.*

3) *Describe how water chemistry affects the detachment and dissolution of Ag from ceramics.*

The overall goal of this research is to produce a much deeper understanding of the differences in attachment and detachment of Ag NPs, when stabilized by different ligands, to and from porous ceramic water filters.

DISSERTATION STRUCTURE

This dissertation is organized into chapters containing the following information:

Chapter 2: Background

Contains an overview of ceramic water filtration, Ag NP toxicology, and properties of the three stabilizing agents used in this work.

Chapter 3: Materials and Methods

Includes detailed procedures and characterization of materials used in the experimental portion of research. Some of this information is repeated, as relevant, in subsequent chapters so that each chapter can stand alone.

Chapter 4: DLVO Approximation Methods for Predicting the Attachment of Silver Nanoparticles to Ceramic Membranes

Reviews methods for estimating van der Waals and electrical double layer energies of interaction, and addresses Objective 1 by comparing with existing models. Includes results of Ag NP deposition experiments on Al_2O_3 membranes and discusses adherence to modeling results.

Chapter 5: Extended DLVO: The Influence of Nontraditional Interactions in Ag NP-Ceramic Water Filter Systems

Addresses Objective 2 through an evaluation of the role of Lewis acid-base interactions, steric interactions, and competing particle-particle forces. Contains experimental characterization of the thickness of the stabilizing layer and Ag NP deposition experiments to clay based ceramics.

Chapter 6: Multilevel Modeling of Retention and Disinfection Efficacy of Silver Nanoparticles on Ceramic Water Filters

Documents field testing performed at the ceramic water filter factory, Pure Home Water in Tamale, Ghana, and develops a statistical model to evaluate Objective 3, the impact of different water characteristics and stabilizing molecules on the retention. Additionally, this chapter examines the disinfection efficacy of Ag NPs.

Chapter 7: The Effects of Water Chemistry on the Desorption and Dissolution of Ag from Ceramic Water Filters

Addresses Objective 3 through laboratory-based testing of the removal of Ag NPs from ceramic water filters using four different water types.

Chapter 8: Conclusions and Recommendations

Outlines major findings pertaining to the three main objectives of this work. Also provides suggestions for next steps in advancing this research.

Chapter 2: Background

Ceramic water filtration falls into two broad categories: membranes and household water filters, as shown in Figure 2-1. The ceramic membranes produced in developed countries (Figure 2-1a) are made to exact specifications and manufactured under high quality controls. Japanese companies have pioneered the development of ceramic membranes for treatment of municipal water supplies. On the other hand, household ceramic water filters (Figure 2-1b) made in developing countries vary substantially in overall design, production method, clay, quality control, burnout material, and chemical amendments. As expected, the membrane filters in developed countries are of very high quality. Surprisingly, the household pot filters have also demonstrated high levels of effectiveness as household water treatment devices (Rayner et al., 2013; Bielefeldt, 2009; Brown 2007). Their relatively simple design and operation offer a good, low-cost, point-of-use water treatment system in developing countries.

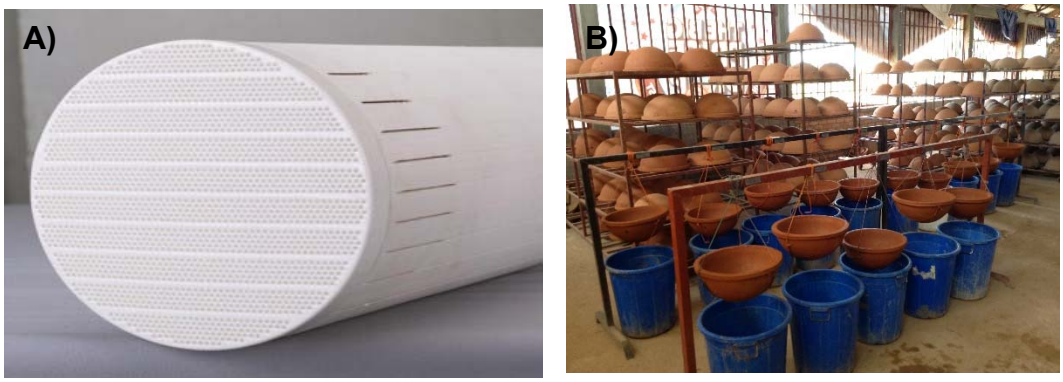

Figure 2-1: A) Ceramic Membrane Element, B) Household Water Filters, PHW, Tamale, Ghana, Image A) was used with permission of Metawater

CERAMIC MEMBRANES

The use of porous ceramics in modern drinking water treatment plants is relatively recent. Ceramic membrane filters have been made most commonly from alumina (produced by NGK Insulators LTD, and distributed by Metawater, Kruger, PWN Technologies, and Veolia). Other materials include titanium dioxide (Purifics, Inopor), and zirconia oxides (Inopor). These materials impart high levels of thermal and chemical stability which prevent distortions during operation. Ceramic membranes are primarily produced in a round multi-channel construction and operated in a cross-flow filtration mode. Typically, nominal pore sizes are 0.1 μm, and operating fluxes are in the range of 170-340 L/m^2-h. They are more frequently used in sectors such as the food and beverage and pharmaceutical industries rather than for municipal water treatment. The exception is Japan where, as of 2010, ceramic membranes had been installed at 100 treatment plants for a total capacity of 486,400 m^3/day (Metawater, 2015). The first US installation of ceramic membranes for municipal water treatment was in the Parker Water and Sanitation District in Colorado (Kruger, 2011). There, 560 membranes were installed to provide 10 MGD of treatment capacity. Ceramic membranes' resistance to high temperatures, pressures, and corrosive solutions has made them an attractive option for water purification where polymeric based membranes are not suitable (Lv et al., 2009; Padilla et al., 1997). For example, some recent promising research (Galjaard et al., 2013; Ha et al., 2013) would couple ozonation with ceramic membranes. This combination was previously unexplored, due to a fear of the extreme damage the powerful oxidant might impart on polymeric membranes. In both recent studies, the hydroxyl radical formation

resulting from decomposition of the ozone within the ceramic membrane significantly reduced membrane fouling.

Ceramic membranes were selected for this research for several reasons. The filters are made from oxides that have been used effectively as sorbents for years, so attachment of NPs is promising. Secondly, the higher durability of ceramics in comparison to polymeric membranes translates to a much longer lifespan and potential sustainability. Finally, the membranes are quite new to the U.S. market, so this is an advantageous time to study the introduction of new features. Excluding water filters used for camping, there are no reports of commercial products integrating Ag NP amendments to ceramic membranes.

HOUSEHOLD CERAMIC WATER FILTERS

Household ceramic water filters are produced in a variety of designs including disks, pots, and hollow cylindrical "candle" shaped elements. The filters are simple to use and have proven effective for both particle and microbial removal (Rayner et al., 2013; Lantagne, 2010; Bielefeldt, 2009; Brown, 2007). Local earthenware clays are employed in the production of ceramic water filters. Earthenware clays contain iron oxides and other mineral impurities that allow them to reach maturity at temperatures less than 1100 °C. Lower firing temperatures leaves the ceramic more porous compared to refractory clays such as stoneware and porcelain. While the earthenware clays vary in composition from factory to factory, the ratio of elements is fairly similar. Table 2-1 summarizes elemental data collected from pot filters from four different manufacturers. The data

were obtained and using energy dispersive X-ray spectroscopy (EDS) on a FEI Quanta 650 Scanning Electron Microscope (SEM). (Note, it is difficult to measure elements with low atomic numbers with any accuracy using this system. The values for carbon and oxygen should not be interpreted as absolute).

Table 2-1: Elemental Weight % of Four Pot Filters

Element	Ghana	Guatemala	Nicaragua	Unknown Origin
C	12.91	0.9	0.43	5.37
O	51.75	55.3	54.41	59.8
Mg	1.21	1.64	0.84	0.37
Al	8.78	11.25	10.1	7.68
Si	17.56	22.95	27.48	19.66
K	2.19	3.29	1.4	1.15
Fe	4.97	4.26	4.87	5.06
Ag	0.64	0.41	0.47	0.91

To increase porosity, a finely sieved, combustible material, such as rice husks, sawdust, or corn husks, is also mixed into the clay prior to forming the shape of the water filter. At many factories, Ag NPs are applied to the filters for disinfection instead of using chlorine. The majority of operations paint a solution of colloidal silver onto the filters post firing. However, a few factories dip the filters in a silver solution. Some factories even mix the silver in with the clay prior to firing (Ceramics Working Group, 2011).

The initial, widespread dissemination of household ceramic water filters was launched by a US-based nonprofit, Potters for Peace, in 1998 after Hurricane Mitch devastated Central America. The organization continues to provide technical assistance in establishing new filter factories across the world through helping local artisans and

entrepreneurs with startup. Additionally, the organization maintains many open source documents and research reports on their website (Potters for Peace, 2015). Larger scale, private manufacturers that sell ceramic water filters and advance the technology, are Resource Development International Cambodia (RDIC) and Ecofiltro in Guatemala.

The work presented in Chapter 6 was facilitated through a collaboration with the filter factory, Pure Home Water (PHW) (Figure 2-2). PHW is a nonprofit organization, located in the Northern Region of Ghana, committed to providing safe household drinking water to the surrounding communities. The organization was started by Susan Murcott, a Lecturer at the Massachusetts Institute of Technology. It has distributed ceramic pot filters since 2005. After exceeding the capacities of its supplier, PHW constructed a factory in 2013, and has demonstrated continued commitment to advancing the science behind the technology. The factory is managed and staffed entirely by locals. The "AfriClay" filter design, a 10 L hemispheric- shaped pot filter, was used in all experiments described in Chapter 6.

Figure 2-2: Pure Home Water, Tamale, Ghana A) Factory worker smoothing filter rims, B) Filters drying prior to firing, C) Downtown market store, D) Filters ready for unloading from kiln, E) Filters soaking prior to flow rate testing, F) PHW employee surveying filter user for correct usage.

SILVER NANOPARTICLE DISINFECTION

The strong toxicity of ionic silver to a wide range of microorganisms is well known. Due to differences in structural integrity of mammalian cells, some limited human health effects have been documented in relation to use of silver. Known cases deal only with a form of skin discoloration called *argyria* or *argyrosis* (ATSDR 2009; Varner, 2010). The EPA maximum contaminant level (MCL), as well as the WHO secondary standard, for silver in drinking water is 0.1 mg/L. Fortunately, the effective

lethal concentration for many bacteria of concern (Carlson et al., 2008; El Badaway et al., 2010) is below this level. Relevant research indicates that metabolic inhibition of human cells occurs at a substantially higher level of 25 mg/L (AshaRani et al., 2009). That being said, an awareness of the potentially unintended adverse effects that the Ag NPs could have on microbial communities exists. As such, the goal of this dissertation is to fundamentally understand attachment and release so that disinfection properties can be responsibly used to our advantage.

Toxicology

Research has shown that the ionic form of silver (Ag^+) can enter cells and disrupt enzyme synthesis by binding to the sulfur in thiol groups (Kim et al., 2008). Moreover, additional uncoupling of oxidative phosphorylation causes cell death (Holt et al., 2005). Over the last decade, the precise mechanism of the toxicity of silver nanoparticles has been subject to much debate. Some believe toxicity stems from the release of Ag^+, while others postulate that the particle size and other features cause primary toxicity. Recent work from Xiu et al. (2012) and Chambers et al. (2014) shows that Ag^+ is the dominant toxicant. This finding concurs with previous research (Carlson et al., 2008; Yen et al., 2009) that demonstrated that the size of nanoparticles has a bearing on the necessary, effective lethal dosage. Smaller sizes reduce the required mass dosage. This size effect is logical because approximately 40% of atoms are located at the surface of 10 nm particles, whereas < 20% are located on the surface for particles > 30 nm (Auffan et al., 2009). Further, Ma et al. (2012) found that, in suspension, the solubility of particles coated with

different organic stabilizers is dominated by the size of the particles, not the cap. Although most of the toxicology research has been performed in suspension, it is still applicable to this research (in which the nanoparticles will be attached to the filter surfaces). Prior toxicology findings mean that adjustable features, such as particle size, shape, and coating, can be manipulated to limit the release of Ag^+ to a value below the EPA MCL, and yet still be sufficient to cause microbial inactivation.

STABILIZING AGENTS

Stabilizing agents (also referred to as capping agents) are commonly employed during synthesis of metallic nanoparticles to prevent aggregation and provide surface passivation. Stabilization is provided through one of three primary mechanisms: electrostatic, steric, or electrosteric interactions. Electrostatic stabilization occurs due to charged functional groups, adsorption/isomorphic substitution of ions, or accumulation/depletion of electrons at the surface of the nanoparticle (Cao, 2004). The surface charge density from one of these sources produces electrostatic forces between the particles. If the electrostatic repulsion (from the double layer of counterions around the metal core) is larger than van der Waals attraction between particles, then aggregation will be prevented. On the other hand, steric stabilization is provided by polymers that are either anchored or adsorbed to the nanoparticle surface. When sterically stabilized particles approach one another, interpenetration and/or compression of the polymer layers occurs. This leads to an increase in the Gibbs free energy of the particles and results in repulsion (Cao, 2004). Electrosterically stabilized particles prevent aggregation using a

mixture of both electrostatic and steric mechanisms through charged functional groups on the branches of polymers. In addition to affecting stability and reactivity, stabilizers can also affect solubility, particle shape and size, and catalytic activity (Tolymat et al. 2010; Shen et al. 2014).

Several studies have demonstrated differences in adhesion to surfaces and toxicity due to the nanoparticle's stabilizing agent. Adhesive forces between the particles and the ceramic surface are crucial to keeping the particles attached to the surface of the clay filters used in this work. Measured using Atomic Force Microscopy (AFM), silver nanoparticles stabilized with proteins had an average adhesion force of 125 +/- 32 nN vs. 29 +/- 11 nN for unstabilized, bare silver to a clay ceramic (Yakub and Soboyejo, 2012). Research using carefully purified suspensions to remove Ag^{+} suggests that surface contact between the bacterium and the Ag NP is critical for toxicity (El Badawy et al., 2011). The impact of particle shape and size is minimal if the electrostatic barrier between bacteria and Ag NP cannot be overcome. Similar work, but with different microorganisms (*Escherichia coli* and *Daphnia magna*), has come to similar conclusions (Silva et al., 2014). Silva et al.'s work investigated three different types of Ag NPs (branched polyethylenimine (BPEI), citrate, and polyvinylpyrrolidone (PVP)) for the influence of particle size and surface potential on toxicity. For both microorganisms, they found that BPEI Ag NPs (with opposite sign surface potential than the microorganisms) were the most toxic followed by citrate, and then PVP (with same sign particle and microorganism). *E. coli* required higher dosages than *D. magna* to induce mortality.

These findings highlight that, for the work in this dissertation, there is a competition among optimal conditions and goals for the three surfaces (particle, bacteria, and filter). For example, an electrostatic barrier could prevent biofilm growth on the surface of the filter and thus avoid fouling. On the other hand, deploying opposite sign potentials could be a technique for achieving more potentate toxicity.

Researchers have found that stabilizers also interact with natural water constituents. In some of the early work, ligands that coordinate more strongly with silver (i.e., chloride) promoted much faster rates of Ag NP dissolution (Linnert et al., 1990). Similarly, elemental silver is sensitive to the presence of oxidants (Li et al., 2010). Further, it has been demonstrated that releases from citrate-stabilized particles result from oxidation caused by interactions with dissolved oxygen and H^+ (Liu and Hurt, 2010). Interactions among silver nanoparticles, raw water, and the stabilizing agent will be particularly influential in the lifespan and efficiency of the Ag NPs when they are used in water filters.

Despite their influence, stabilizer structures and attachment mechanisms are normally neglected in the literature. Stabilizer properties are challenging to measure with routine analytical methods. A laboratory with the requisite expertise and access to several advanced complementary analysis methods is required. Thickness and coverage of organic coatings on flat surfaces are typically studied using scanning tunneling microscopy and AFM. For NPs, the small size and large curvature present measurement challenges in terms of mounting and elimination of contaminants. For AFM analysis, the

tip size, material, shape, and change in spring constant (if the tip is modified) can all affect the measurement. The coatings on NPs can be difficult to see using transmission or scanning electron microscopy (TEM and SEM) due to interference from the background of the grids, drying artifacts, resolution limitations, and beam damage to the samples. Some researchers have successfully used thermal gravimetric analysis (TGA) (Yu et al., 2009) or X-ray photoelectron spectroscopy (XPS) (Battocchio et al., 2014) to look at thickness and conformation, but these techniques require very detailed knowledge of the particle shape. To get good data from XPS, often specialized versions, such as synchrotron or high pressure XPS, are necessary. Even after, mounting of the particles, buildup of charge on the aggregates, surface roughness, effects of size and curvature on signal strength, and lack of necessary degree of spatial resolution in 3D limit the use of this technique. To complicate matters further, for all of these techniques, aqueous samples often require expensive specialized holders and consumables not typically used. Considering these challenges, it is clear why NP surfaces are not routinely characterized to the extent desired for modeling. A huge measurement hurdle exists for accomplishing efficient innovation of NP coatings in academic and industrial settings.

In an extensive review of the literature, Tolymat et al. (2010) identify the most common agents used by researchers to stabilize Ag NPs. At 27% use by occurrence, citrate is the most frequently used stabilizer, followed by PVP at 18% and amines at 8%. The different Ag NPs tested during the course of this work include particles stabilized with citrate, PVP, and BPEI. These particular stabilizing agents were selected not only

for their widespread use, but also for their differences in functional groups/stabilization mechanisms. Citrate is electrostatically stabilized; PVP is sterically stabilized; and BPEI electrosterically stabilized. Further, the surface potential at natural water conditions (pH 7-9) for all of these stabilized particles varies. PVP and citrate are negative (and differ in the magnitude of surface potential by up to 4.5 times), whereas BPEI has a positive charge. The following section summarizes the current state of knowledge of the citrate, PVP, and BPEI stabilizers used in this work.

Citrate

Citrate (Figure 2-3) has many practical uses in our daily lives. It is used as a food additive, anticoagulant in blood transfusions, and in boiler descaling. It is also commonly used as a buffer. The pK_a's for citric acid are 3.13, 4.76, and 6.4. The pK_a values of citrate on Ag NPs are likely higher than in solution. Force microscopy studies investigating carboxylic acid terminated self-assembled monolayers on gold coated Si substrates show it is more difficult to ionize acids on metal surfaces than in free solution (i.e., pK_a 5.2 vs. 4.8) (Hu and Bard, 1997; van der Vegte and Hadziioannou, 1997). This can be attributed to strong intermolecular hydrogen bonding that occurs laterally when on the metal.

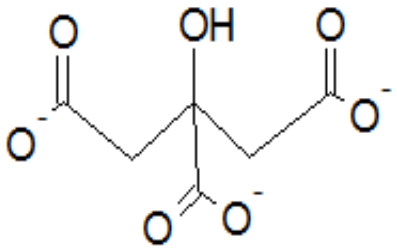

Figure 2-3: Molecular Structure of Citrate

The conformation of the citrate on the surface of Ag NPs is not well documented. Park (2013) performed one of the few detailed spectroscopic studies of citrate molecules

adsorbed on gold and Ag NPs. The work combined attenuated total reflectance infrared (ATR-IR) spectroscopy, transmission FTIR spectroscopy, and X-ray photoelectron spectroscopy (XPS) with geometry-based modeling utilizing Scanning Tunneling Microscopy (STM) and TEM images from the literature. Park concluded that the adsorbed citrate coordinates to the surface of the NPs by bidentate binding. The citrate's central and one of its' terminal carboxylate groups participate in the attachment to the metal core. As a result, there is a dangling carboxyl group available for binding to other surfaces or itself. Park hypothesized that the negatively charged dangling carboxylate does not bind to the metal surface due to charge balance requirements on the surface or the presence of counter ions. Wulandari (2015) reached the same conclusion about a dangling carboxyl group. Using FTIR data reinforced with molecular orbital (MO) calculations an enhanced excitation of the 1382 cm^{-1} band was interpreted as a perpendicular carboxyl on the Ag NP surface. Citrate also has a hydroxyl group available for binding. However, the hydroxyl group acts as a supporting donor group for the central carboxylate rather than participating in bonding to the metal (Park, 2013).

The presence of the dangling carboxyl group facilitates the formation of polymeric citrate chains assembled on the surface of the nanoparticle through hydrogen bonds between the terminal carboxylic acid groups. The chains interact with each other through van der Waals attraction between CH_2, thus forming bilayers of citrate on the silver nanoparticle surface. Surface coverage of citrate is relatively low at 1.86×10^{-10} mol/cm^2 (Park).

Polyvinylpyrrolidone (PVP)

PVP $(C_6H_9NO)_n$ (Figure 2-4) was developed by Professor Walter Reppe in the 1930s in Germany at the chemical conglomerate I.G. Farben. It is a polymer of N-vinyl-2-pyrrolidone and goes by a number of names including polyvinylpyrrolidone, povidone, and polyvidone. The backbone forms a hydrophobic region; whereas the rings form hydrophilic regions that interact with water (Zhang, 1996). Originally, it was used as a blood-plasma substitute and extender during World War II. Because it has been found to safely pass through humans, it has been used in the pharmaceutical, food and beverage, and cosmetic industries. For example, it is used as a binder in pharmaceutical tablets. The WHO acceptable daily intake is 0-50 mg/kg/day. It is also used in dyes and inks, detergents, paints and coatings (Robinson, 1990).

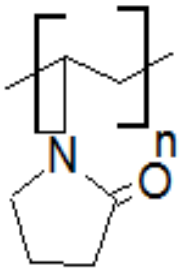

Figure 2-4: Molecular Structure of PVP

PVP typically has a molecular weight of 2,500 to 1,200,000 Daltons. Different grades of PVP are expressed in terms of Fikentscher's viscosity coefficient, also referred to as the K-value. K values are determined based on kinematic viscosity measurements (Swei and Talbot, 2003). The higher the K-value, the higher viscosity and molecular weight of the PVP molecule. K-12, 15, 17, and 30 are deemed suitable for injection in humans and animals and K-25 and 30 are acceptable for use in pharmaceutical, food, and cosmetics applications. The PVP used in this research is K-30 and corresponds to a molecular weight of 40,000 Daltons. PVP is known to exhibit inert behavior towards salts and acids (no buffering capacity) (Robinson, 1990). Free PVP decomposes at

330 ˚C (Shen 2014). Light scattering has shown the end to end distance of the coiled polymer ranges from 2.3 nm to 93 nm (Robinson, 1990).

Again, there are few studies that investigate the conformation and attachment of PVP on Ag NP surfaces. The studies that do exist are difficult to compare because the Ag NPs are made using different reducing agents and procedures for addition of the PVP (e.g., introduction of PVP during or after the reduction and different PVP K-values and amount added to solution). Several of the studies look at nanowires instead of particles (Mdluli, 2011; Goa, 2004).

Researchers agree to three logical attachment points for the PVP to the silver core: the oxygen in the carboxylic group, the nitrogen in the ring, or attachment via both the nitrogen and the oxygen. XPS was used to study PVP on Ag NPs (diameters 13-28.7 nm) synthesized using photoreduction of silver nitrate and conclude that the polymer was attached to Ag NP surface via the oxygen in the carboxylic group (Huang et al., 1996). In this work, they saw a positive shift in the oxygen 1s binding energy and a negative shift in binding energy in the silver $3d_{5/2}$ and concluded the attachment mechanism was to the oxygen. Others have postulated that the attachment mode could depend on the size of the NPs (Wang et al., 2005). For particles with diameters less than 50 nm, they proposed that the nitrogen in PVP coordinates with silver, whereas for larger particles (500-1000 nm), both the nitrogen and oxygen coordinate separately. The oxygen was still the dominant mechanism. This conclusion was drawn from IR spectra where the resonance peak of C=O saw no change for PVP

stabilized silver nanoparticles less than 50 nm, but the C-N peaks at 1019 cm^{-1} and 1074 cm^{-1} were red shifted to 1035 and 1076 while the N-OH complex was greatly weakened. For the larger particles, the C-N peak was strengthened (meaning reduction in Ag-N interaction) and the C-O peak was red shifted. This work did not contain any theoretical calculations to support the interpretation of the spectra, and provided no detailed methods of sample preparation. Zhang et al. (1996) interpreted spectra to similar effect and Shen (2014) has found size dependent chemisorption modes of pyrolidone rings for different sizes of Pt and Rh NPs.

Surface Enhanced Raman Spectroscopy (SERS) combined with theoretical density function theory (DFT) calculations have also been used with a silver nitrate - citrate reduction - PVP stabilized, Ag NP synthesis method (Mdluli, 2009). To simplify the system, the authors used pyrolidinone and N-methyl-2-pyroolidinone (monomers of PVP) rather than the entire chain. They concluded that the primary attachment was via the carboxylate group. Their calculations indicated that oxygen attachment is kinetically favorable compared to the nitrogen, but that the nitrogen can, and occasionally does, form a weak interaction via charge transfer between the nitrogen and the silver core. Further, their work demonstrates that attachment via both the nitrogen and the oxygen is very unlikely to occur because the ring would need to bend. The authors think that the orientation of the PVP is perpendicular to the metal surface because of an observed peak at 226 cm^{-1}, indicating carboxylate stretching. In summary, the literature agrees that the primary attachment mechanism is through the lone pair electrons on the oxygen, but

much work still needs to be done to understand the details of the conditions under which nitrogen interactions also occur and how the PVP lays on the surface.

Branched Polyethylenimine (BPEI)

Branched Polyethylenimine (Figure 2-5) contains repeating methylene units and primary, secondary, and tertiary amino groups. It is synthesized using a ring opening polymerization of aziridine. Because of BPEI's attraction to a large variety of cells (due to its high charge density), it is one of the most frequently used cationic polymers used for delivering nucleic acid therapeutics. It has pH tunable, hydrophobic cavities formed from the methylene backbone/amino arm combination that are very efficient for loading hydrophobic cancer drugs during research (Cho et. al, 2014). Despite this feature, BPEI is rarely used in clinical trials because of its non-specific interactions with serums (Tripathi et. al, 2013). Outside of the gene delivery research community, BPEI is also added to a wide range of products from detergents and printing inks to water treatment flocculants and adhesives (ChemicalBook, 2015). BPEI has a melting point of 59-60 ˚C, boiling point of 250 ˚C, density of 1.03 g/mL at 25 ˚C, and a refractive index of 1.53 (ChemicalBook, 2015).

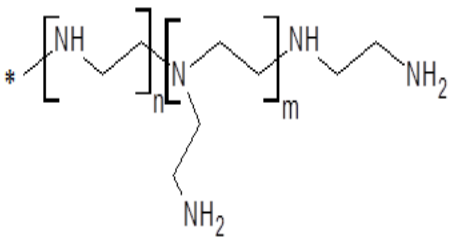

Figure 2-5: Molecular Structure of BPEI

The protonation state of BPEI is very complicated because, as protons are added, conformation changes occur along the polymer's backbone due to electrostatic repulsions

between the amino groups. The literature suggests that 10-30% of the amines are protonated at pH values near neutral, but this can vary depending on chain length, salt concentration, or even the presence of a nearby negatively charged object. For example, higher salt concentrations screen electrostatic repulsions and allow for a greater degree of protonation. Since not all amino groups are protonated, the molecule has the capability to act as a "proton sponge," thus providing some buffering capacity **(**Ziebarth and Wang, 2010).

Cytotoxicity is a concern for many mammalian cell lines, particularly at BPEI molecular weights larger than 25 kDa (Moghimi et al., 2005). Research has shown BPEI induces greater cytotoxicity than linear PEI, most likely because the branches in BPEI provide substantially more interaction with cellular components than the polymer's linear version (Tobita and Yasuda, 2008). Toxicity is typically observed around 20 mg/L BPEI (Hunter, 2006). In the research reported herein, low molecular weight BPEI was used (1.8 kDa), and the Ag NPs were triple washed to remove BPEI from solution. While it is unlikely that the BPEI concentrations reach harmful levels in my research, it is still necessary to recognize that more work should be done to study the human risk associated with ingesting BPEI-coated Ag NPs before any widespread technology introduction. Further, since few researchers use BPEI as a stabilizing agent, robust spectroscopic studies do not exist in the literature. As a result, the orientation of the BPEI molecule on the surface of Ag NPs is unknown.

CONCLUSIONS

While many have laid a solid foundation of Ag NP research, there are many gaps in the literature. Different types of Ag NPs have been studied extensively in suspension, but the influence of stabilizers on attachment to porous ceramics is unexplored. Ag NPs have been used on clay-based ceramic water filters used in developing countries, but have never been integrated into the Al_2O_3 membranes used for municipal water treatment in developed countries. Further, the existing work with Ag NPs on clay-based ceramic water filters only investigates detachment and does not explore the influence of different stabilizing molecules on the initial attachment process or subsequent release. The current literature does not identify the predominant energies of interaction controlling Ag NP-ceramic water filter systems. The work in this dissertation will address these areas.

Chapter 3: Materials and Methods

Several specific filter substrates and Ag NPs were used during the experiments conducted in connection with this work. This chapter documents each material's synthesis procedure, characterization, and the protocols followed for each type of experiment in which they were used. As relevant and helpful to the narrative, excerpts from this chapter are repeated in subsequent chapters because the later chapters are, or are expected, to be published papers.

SUBSTRATES

Al_2O_3 Membranes

Experiments used porous aluminum oxide (Al_2O_3) ceramic disks (with 0.1 μm diameter pores, and also known as Whatman Anodiscs or simply Anodiscs), and clay disks produced in-house as part of this work. The Whatman Anodiscs represent membranes used for municipal water treatment in developed countries. The clay disks represent the pot filters used in developing countries. The Whatman Anodiscs have highly uniform porosity (Figure 3-1a). The channels are 0.2 μm in diameter for the majority of their length, but taper to a 0.1 μm effective diameter on one side of the surface (Figure 3-1b).

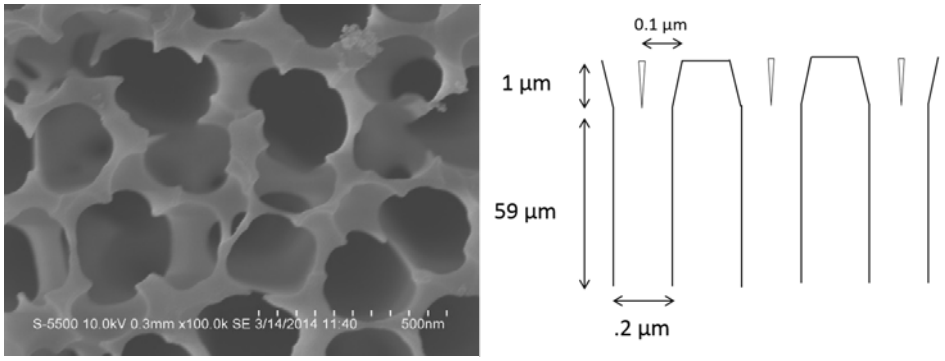

Figure 3-1: A) Planar View and B) Side View of Anodisc. Planar view obtained on a Hitachi S5500 Scanning Electron Microscope (SEM).

Their extremely uniform pores are created via an anodic oxidation of aluminum metal foil, in a process similar to that described by Furneaux et al. (1989). Most commercial, ceramic membranes used in water treatment are made via sintering. When dry, the commercial ceramic membranes' crystalline structure is believed to be α-alumina. However, despite prodigious efforts, samples were not obtained to confirm that belief. The ordering of pores in Anodiscs results in increased permeability due to low pore resistance (Ha et al., 2013). An EDS spectrum obtained by the author was used to confirm that the Anodiscs are pure Aluminum and Oxygen (Figure 3-2). The carbon peak to the far left is due to a polymeric support ring that surrounds the 25 mm diameter-sized filter. Thirteen mm diameter filters were used

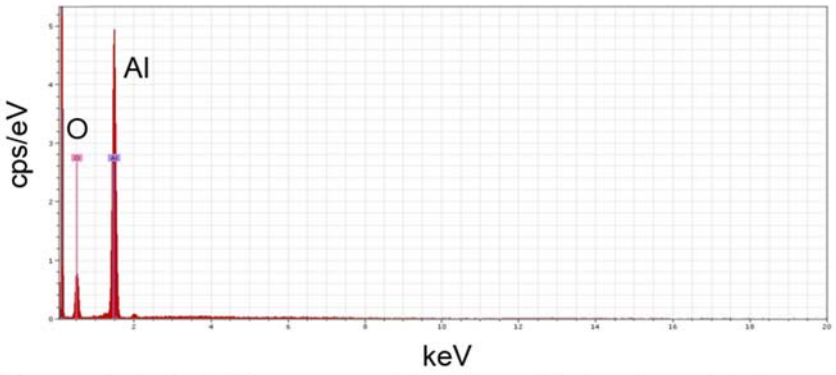

Figure 3-2: EDX Spectrum of Anodisc. Obtained on a FEI Quanta 650 SEM.

throughout the rest of this work, and they did not have the polymeric support ring. XRD results clearly demonstrate that the Anodiscs are amorphous in structure (Figure 3-3). The spectrum was measured using a Scintag X1 diffractometer with Cu k-alpha radiation, and a solid state detector. Samples were placed on a zero background quartz plate.

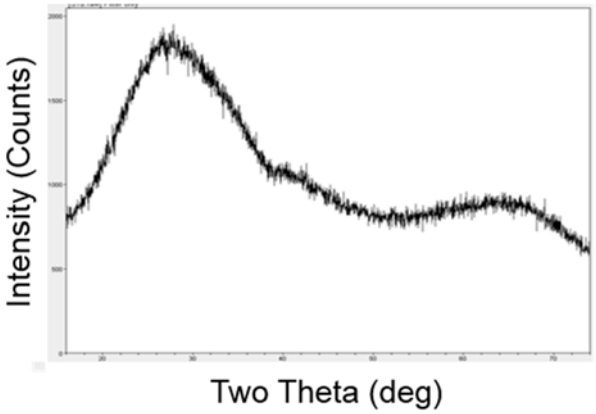

Figure 3-3: XRD Spectrum of Anodisc

Clay Filters

Pot filters made from indigenous, local clays are highly heterogeneous. The same is true for any clay filters produced in-house. Resco red art clay was selected for use to compare with previously published work (Oyanedel-Craver and Smith, 2008), and because it has similar mineral composition to the clay filters produced by the different factories that were described in Chapter 2. The Resco clay is illite/kaolinite in nature with approximately 20% Si, 10% Al, 2% K, and 3% Fe by mass (as measured via EDX). Untreated, white pine sawdust was obtained from Fine Lumber and Plywood, Inc., Austin, TX and used as the combustible to create pores. The sawdust was finely chopped in a standard kitchen blender, then sieved through a 0.42 mm mesh opening. For a 13 mm filter, a 375 mg mixture of clay and sawdust were uniaxially, dry-pressed, using carbide and steel tooling (2 class z no-go plug gauges, 1 press-fit drill bushing from McMaster-

Carr, and a PVC pipe in order to release the filter disk from the mold), as illustrated in Figure 3-4. A Carver hydraulic laminating press was employed to apply a load of 10,000 psi during the dry-press process. This mimics forces used in the field factories for producing pot filters (The Ceramics Manufacturing Working Group, 2011). The clay disks were then fired in a Lindbergh tube furnace with a ramp rate of 2˚C/min. Upon reaching 1100 ˚C, the disks were held at that temperature for one hour prior to slowly cooling.

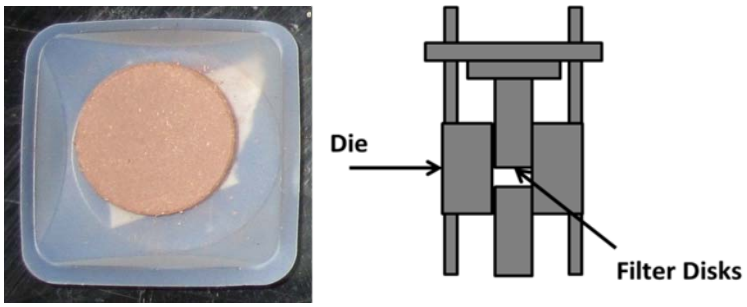

Figure 3-4: Dry Pressed Filter Disk and Apparatus

On average, the produced filters had an open porosity of 45%, as measured via a Quantachrome Ultrapyc, 1200e gas pycnometer. The pycnometer uses the displacement of helium gas to measure the volume of the sample. The open porosity is calculated by subtraction from the geometric volume.

Various mixtures of clay and sawdust by weight were tested before arriving at the final filter recipe. Ultimately, a ratio of 10% sawdust to clay (by weight) was chosen because it had a porosity roughly comparable to the filters produced in the field. That being said, the amount of sawdust used was 5-10% lower than many filters produced in the field (The Ceramics Manufacturing Working Group, 2011). Nonetheless, the data

from this research show that a mixture of Resco Red Art Clay and 10-15% Austin sawdust produces a range of porosity comparable to field filters (Oyanedel Craver and Smith, 2008).

To produce effective clay filters, the firing temperature is very important. As depicted in Figure 3-5 (n=3 per bar), an increase in firing temperature results in more sintering and effectively lowers the open porosity of the filter. A setpoint of 1100 °C is on the higher end of firing temperatures used in the field, but was selected to provide greater strength to the filter. Any temperature lower than 900 °C will produce a clay filter that crumbles.

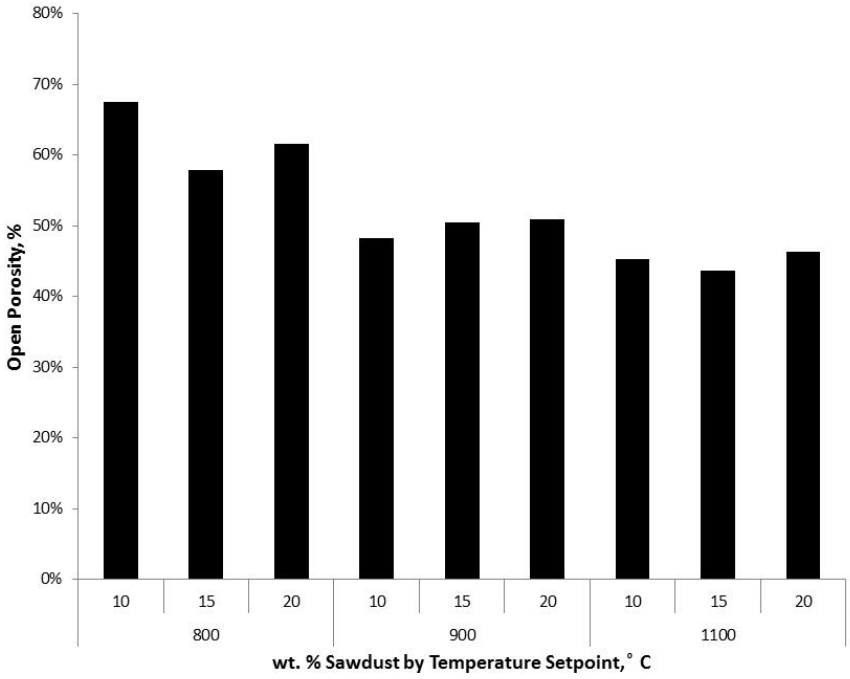

Figure 3-5: Open Porosity by % Sawdust and Firing Temperature

No standard technique is available for measuring the pore size distribution of clay disks, so it was necessary to explore multiple techniques. Gas adsorption/desorption techniques using nitrogen, coupled with the Barrett-Joyner-Halenda (BJH) analysis for pore size, was tried, but proved unsuccessful due to the low surface area per filter. Another candidate was Capillary Flow Porometry. This technique measures the pore size distribution of through-pores only, an advantageous measurement for water filtration. The technique's implementation involves increasing the applied pressure to the influent side of the filter and monitoring effluent pressure and flow. Pore size is then calculated using the Washburn equation. After numerous trials, sample adjustments, and discussions with Quantachrome's analytical services, it turned out that the clay disks were too brittle for the measurement procedure. Unfortunately, they could not be kept from breaking during the analysis. Eventually, only Mercury Intrusion Porosimetry proved to be an effective technique for measuring the pore size distribution within the filters. Although it provides information for both through and dead-end pores, it also provides some indication of the straining properties of clay filters. Test results indicate that when the filters contain a majority of pores less than 20 μm in size (Figure 3-6), the size distribution is similar to filters made with clays from Mexico and Guatemala (Oyanedel-Craver and Smith, 2008). The data from Quantachrome indicate that filter one has a high fraction of the pores with diameters less than 30 nm (0.03 μm), which is why these filters are excellent at removing particles from water.

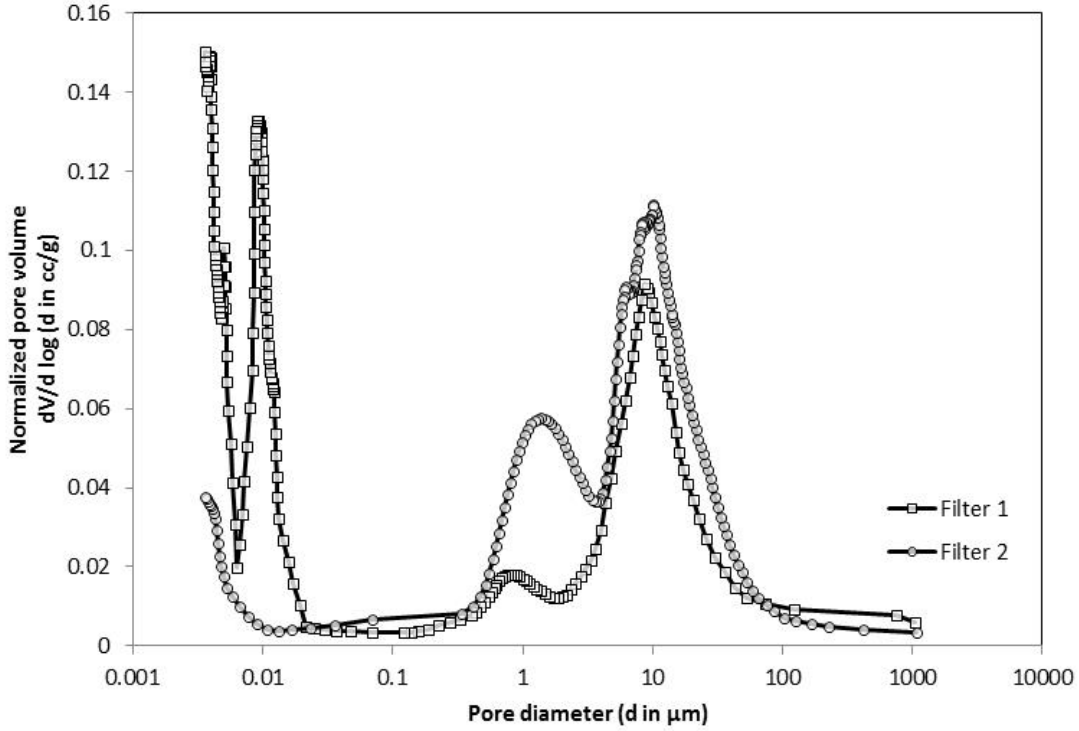

Figure 3-6: Pore Size Distributions of Two Clay Filters

Surface Potential

Crucial to the modeling work performed in Chapters 4 and 5, high quality surface potential measurements are required for both types of filters. Two different methods for making these measurements were investigated. A newer technique, employing a dip cell with a Malvern Zetasizer instrument and a tracer particle, was tested. A small piece of sample disk was fastened to the dip cell. Then, the sample was carefully positioned to just block the laser. Next, over the course of an hour, the sample was raised to five different positions above the starting data point. These six data points, along with the surface charge of the tracer particle, are used by the software to calculate a surface

potential of the solid at a particular pH value. Mineral oil was used as a tracer particle. However, since mineral oil has a negative surface charge, the newer technique only worked well for a solid sample that also had a negative surface charge (namely, the clay filter) because the two substances did not interact. The technique did not work for the Anodisc because of its higher point of zero charge. Besides using the Malvern method, the filters were sent to Anton Paar where a SurPass electrokinetic analysis was performed on both types of filters. This technique measures streaming potential (or current). For planar solids, two identical samples are mounted on either side of an adjustable gap cell. The streaming potential measurement is converted to zeta potential using the Fairbrother-Mastin equation (Anton Paar, 2012). The zeta potential at different pH values (Figure 3-7) indicates that the point of zero charge for the Anodisc is at a pH value of approximately 5.5.

Colloidal α-alumina particles have a significantly different point of zero charge, closer to a pH value of 9, than the value of 5.5 measured for the Anodisc. The disparity exists because submicron particles contain singly coordinated surface hydroxyl groups (due to many vacancies and other surface defects), whereas planar surfaces are primarily composed of surface hydroxyl groups with double coordination (because a larger fraction of the total area is expressed in low index planes). Hydroxyl groups that have double coordination have a pK_a around pH values of 4-6, which is consistent with the point of zero charge found for the Anodisc (Franks and Gan, 2007).

For the clay filters, the point of zero charge is at a pH value close to or less than 2. The curves were obtained at a constant ionic strength of 10 mM, maintained using KNO_3. The pH was adjusted by KOH and HNO_3.

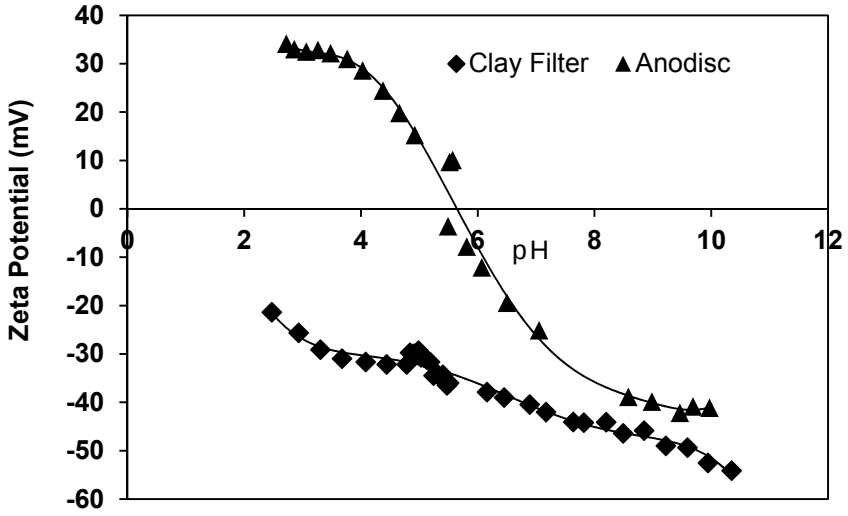

Figure 3-7: Zeta Potential Curves for Anodisc and Clay Filters at 10 mM Ionic Strength

Contact Angles

Contact angles between an Anodisc and 1-Bromonapthaline, glycerol, and water were measured using a Ramé-Hart contact angle goniometer. The DROPimage software package was used for the analysis. The clay filters absorbed the water droplets faster than could be measured, so no data on the contact angle are available. For the Anodisc, contact angle measurements were obtained, but they were not used in this work, because similar measurements for the Ag NPs were not obtained (both are necessary for Lewis acid base energy of interaction calculations). The data collected are documented in Table 3-1 for potential use in future projects.

Table 3-1: Anodisc Contact Angles with Polar and Nonpolar Solvents

Material	Contact Angle (°)
1-Bromonaphtaline on Anodisc	11
Glycerol on Anodisc	21
Water on Anodisc	25

SILVER NANOPARTICLES

Synthesis

Due to the large quantities of NPs needed over the course of the experiments, different Ag NPs were synthesized and cleaned in-house. The different Ag NPs used during the course of this research include particles stabilized by citrate, PVP, and BPEI. The following procedures were followed for making each batch:

PVP/ BPEI Ag NPs

- Prepare:
    - 6 mM $NaBH_4$ (23 mg in 100 mL ultrapure H_2O)
    - 3 mM $AgNO_3$ (51 mg in 100 mL ultrapure H_2O)
    - 40 K PVP to be 0.2% in final solution (450 mg in 25 mL ultrapure H_2O) OR
    - Stock Solution of 1,800 MW BPEI in ultrapure water.

      (Note, BPEI is very viscous and cannot be pipetted. Add a small measured mass of BPEI directly into the beaker where the water will be added.)

- Add entire $AgNO_3$ to stirred $NaBH_4$ (surrounded by ice) 1 mL at a time (1:1 volume)
- Add either PVP (0.2% by mass) or BPEI (0.5 g/L)

Citrate Ag NPs

- This is the Gorham et al. (2012) method.
- Prepare:
    - 58.8 mM $AgNO_3$ (250 mg in 25 mL ultrapure H_2O)*
    - 34 mM sodium citrate (250 mg in 25 mL ultrapure H_2O)*
    - 100 mM $NaBH_4$ (94.58 mg in 25 mL ultrapure H_2O)

    *Can be stored in the dark at 4 °C for several months for future use.
- Boil 400 mL of ultrapure H_2O mostly covered with a watch glass to collect steam
- Add 1.69 mL of the $AgNO_3$ solution and 2.92 mL of the sodium citrate solution and stir rapidly
- Add 2 mL $NaBH_4$ dropwise in 100 uL additions
- Stir 30 min at a slow boil
- Cool to room temperature on a hot plate

Cleaning/Concentrating Method

- Separate 40 mL of stock solution into 6 Oakridge centrifuge tubes
- Centrifuge at 17,000 g, 4 °C for 2 hours
- Remove 20 mL of supernatant
- Sonicate remaining solution in bath sonicator

- Add 10 mL of Millipore H_2O
- Centrifuge at 17,000 g, 4 ^{o}C for 2 hours
- Remove 10 mL of supernatant
- Sonicate remaining solution in bath sonicator
- Add 10 mL of Millipore H_2O
- Centrifuge at 17,000 g, 4 ^{o}C, for 2 hours
- Pour out remaining supernatant until point of pellet disruption
- Sonicate remaining solution in bath sonicator

Result: Concentrates particles approximately 4.5x synthesis silver concentration. Each batch measured using inductively coupled plasma optical emission spectrometry (ICP-OES) prior to experiments.

Silver Concentration Measurements

An Agilent ICP-OES was used to measure silver concentration. Samples were prepared in 15 mL polypropylene tubes by placing the Ag NP sample in direct contact with HNO_3 prior to adding dilution water. Enough HNO_3 was added to each sample so that, after final dilution, the sample contained 6% HNO_3. For higher concentration Ag NP suspensions, if the protocol of introducing the acid before the water was not followed, mass balances on silver were difficult to achieve due to partial digestion of the samples. A wavelength of 328 nm was used for silver detection. All standards were prepared using a 1000 μg/mL ICP NIST traceable standard purchased from Inorganic Ventures (Christiansburg, VA). The silver instrument detection limit corresponded to 1 μg/L.

Zeta Potential

The surface charge at natural water conditions (pH 7-9) for all of these particles vary, as shown in Figure 3-8. The zeta potential measurements were performed on a Malvern Zetasizer. The ionic strength was held constant at 10 mM. The pH was adjusted using concentrated HNO_3 and NaOH. The magnitude of the zeta potential varies substantially by stabilizing molecule. BPEI Ag NPs are highly positive, citrate Ag NPs highly negative, and PVP Ag NPs a much lower negative value. Citrate and BPEI Ag NPs show a pH-dependent zeta potential value due to the protonation and deprotonation of the carboxyl and amino groups, whereas PVP Ag NPs have a zeta potential of approximately -10 mV across the range of pH values.

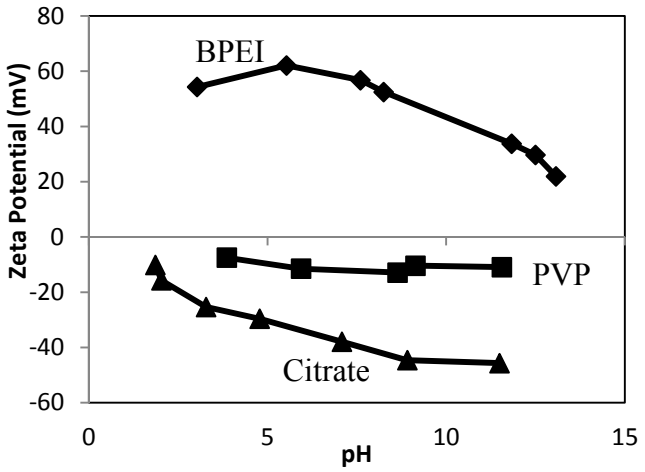

Figure 3-8: Effect of Capping Agent on Silver Nanoparticle Zeta Potential

Surface Tension

Surface tensions of three Ag NP-water suspensions (Citrate-Ag NPs, PVP-Ag NPs, and BPEI-Ag NPs) were measured with a Ramé-Hart contact angle goniometer using the pendant drop method. The surface tension measurements were not employed in the modeling portion of the work. These measurement data are documented in Table 3-2 for potential use in future projects.

Table 3-2: Ag NPs Suspensions' Surface Tensions

100 mg/L Aqueous Suspensions	**Surface Tension (mJ/m^2)**
Citrate-Ag NPs	68
PVP-Ag NPs	63
BPEI-Ag NPs	72

Particle Size

Representative particle size distributions obtained using multiple images taken on a FEI Tecnai TEM (Figure 3-9) (employing ImageJ (NIH) software) indicate that, on

average, the particles are 10-15 nm in diameter (Figure 3-10a). The particles aggregate at different rates under the experimental conditions used in this study (Figure 3-10b and c).

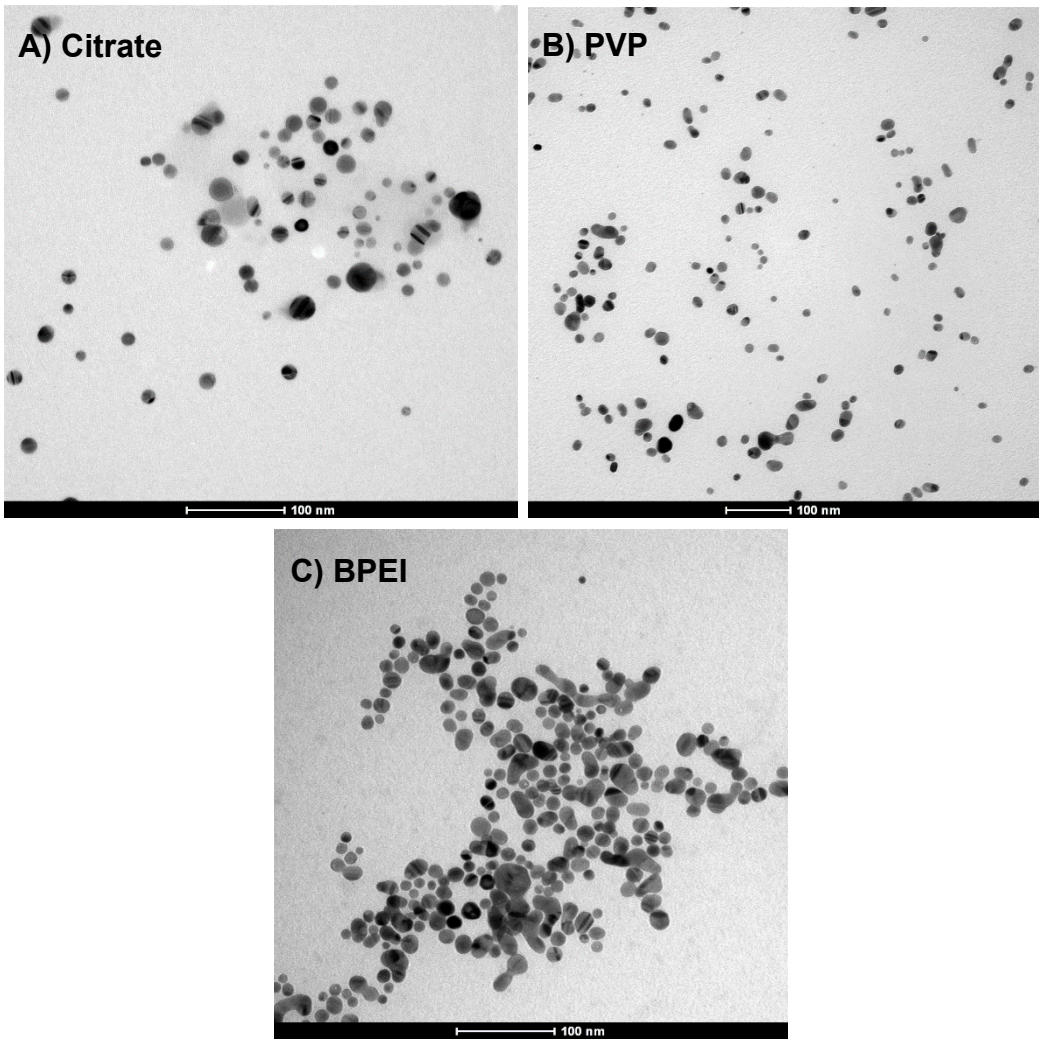

Figure 3-9: TEM Images of Differently Stabilized Ag NPs

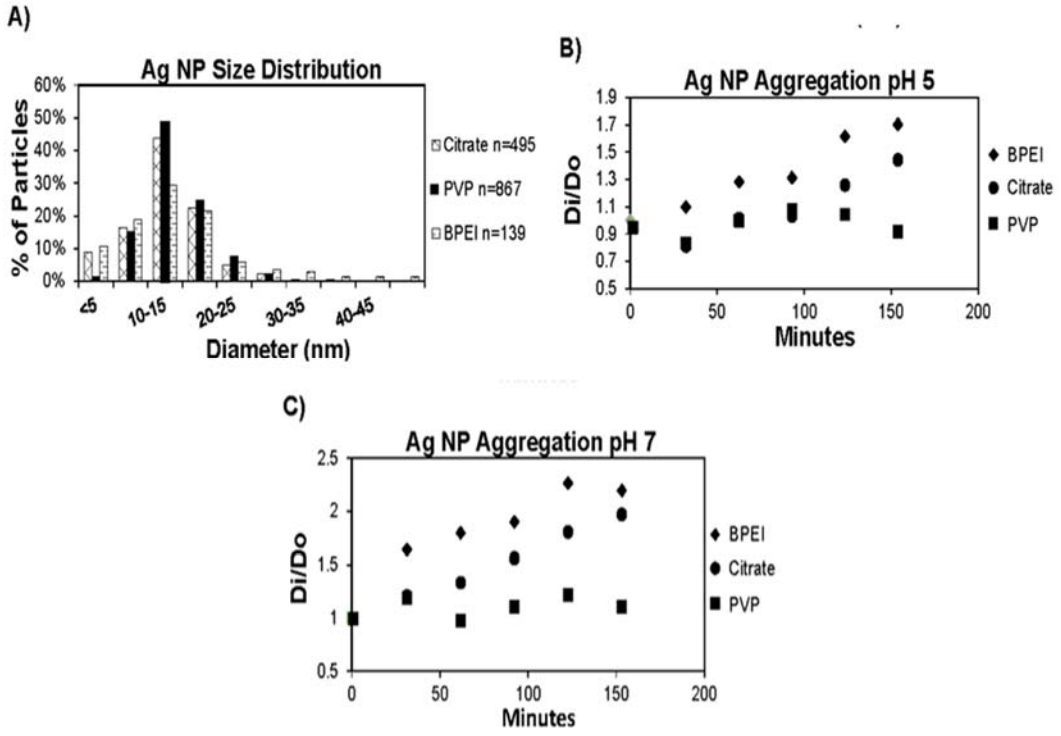

Figure 3-10: A) Ag NP Size Analysis From Multiple TEM Images. B) and C) Ag NP Aggregation Rates. Determined using a NanoSight particle size analyzer at a constant ionic strength of 10 mM, added as KNO_3.

ATTACHMENT EXPERIMENTS

Procedure for Soaking Filters in Ag NP Suspensions

1) Record mass of filter. (Use a pair of needle nose pliers instead of tweezers when handling the Anodiscs. This minimizes filter breakage).
2) Label amber glass jars (Use amber jars because silver is sensitive to light and glass because Teflon was found to adsorb the silver nanoparticles).
3) Inside the jars put one filter held upright in a glass holder made to specification by the UT Austin glass blower (Figure 3-11a).
4) Sonicate and vortex Ag NP stock solutions (known concentration).

5) In a separate beaker, dilute Ag NP stock to desired concentration. Prepare a total volume that will completely submerge the filters (20 mL for the amber jars used in this work)
6) Adjust beaker solution to desired pH using concentrated HNO_3 or KOH.
7) Add KNO_3 to beaker such that ionic strength, I = 10 mM
8) Pour beaker suspension into amber jars with holders (It is important to prepare the solution in a separate beaker to minimize filter breakage.)
9) Secure lid on amber jars (The lid consists of septa with a hole cut out for insertion of a pH probe).
10) Insert pH probes, making sure the filter is on the opposite side of the jar.
11) Insert two hypodermic needles into the headspace of each amber jar and put tubing connected to N_2 gas into one needle (turn on N_2 gas to lowest flow rate that the regulator allows).
12) Place jars on shaker table for 3 hours (Figure 3-11b).
13) Monitor and maintain constant pH by using 1:1000 dilutions of concentrated KOH or HNO_3 throughout the course of the experiment.
14) After the experiment, clean all glassware with soap and water, followed by soaking in a microbath solution (2% aqueous solution of Micro-90®
overnight, and a 10% acid bath for a minimum of 30 minutes.
15) Measure amount of Ag NPs deposited on filter using ICP-OES by digesting filter in 1 mL of concentrated HNO_3, followed by adding 10 mL of water. (Further

dilution will be necessary under favorable attachment conditions). Also measure solution phase Ag using a digestion of 6% concentrated HNO_3

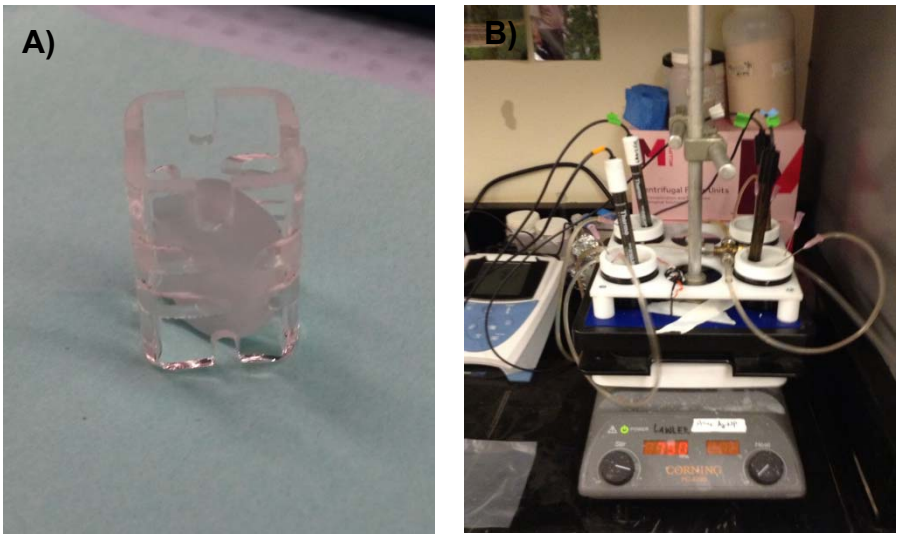

Figure 3-11: A) Anodisc in Glass Filter Holder B) Attachment Setup

ALUMINUM SOLUBILITY EXPERIMENTS

Individual Anodisc membranes were submerged, upright, in water with a background ionic strength of 10 mM, added as KNO_3. The containers were gently mixed for 1, 3, 6, or 12 hours and maintained at different pH values between 4 and 12 using concentrated HNO_3 or KOH. After the desired duration, total aluminum concentration was measured using ICP-OES at a wavelength of 396.15 nm. The samples were digested using 2% concentrated HNO_3. The instrument detection limit for aluminum was measured to be 2.2 µg/L. Results of the solubility experiment, reported by the duration that the Anodisc was submerged are displayed in Figure 3-12.

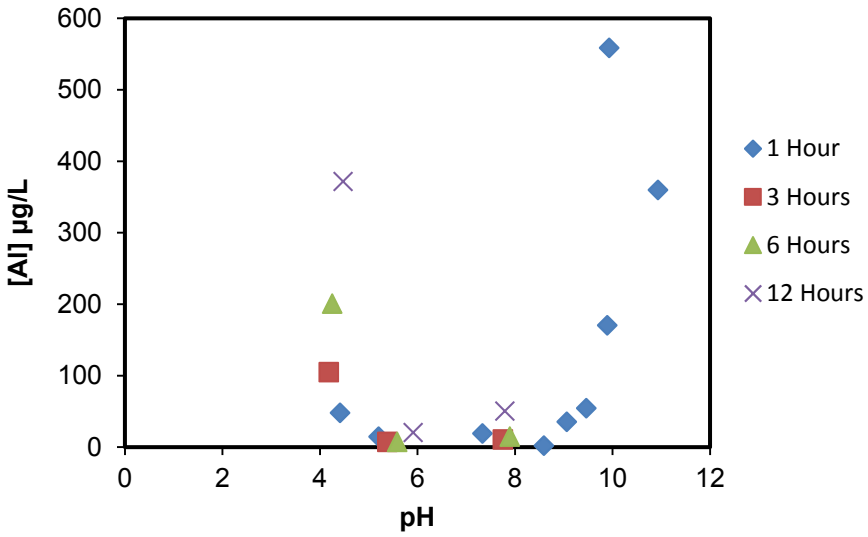

Figure 3-12: Anodisc Aluminum Solubility Results

Chapter 4: DLVO Approximation Methods for Predicting the Attachment of Silver Nanoparticles to Ceramic Membranes

INTRODUCTION

A recent trend in the field of membrane research is the attachment of nanoparticles (NPs) to the membrane's surface to harness the NPs' reactive and catalytic properties (Ng et al., 2013; Wegmann et al., 2008; Chen et al., 2013). NPs such as silver (Ag), iron, titanium, and magnesium oxides are often studied because they impart useful features such as degradation of challenging contaminants (*e.g.*, arsenic, trichloroethylene, nitrobenzene, and lead) or reduction in total organic carbon, a precursor for disinfection byproducts formed after chlorination in drinking water treatment (Byun et al., 2011; Golas et al., 2010; Goldstein and Greenlee, 2012). In particular, Ag NPs, the focus of this study, have garnered substantial attention in terms of disinfection and biofouling reduction on ceramic water filters (Bielefeldt et al., 2009; Kallman et al., 2011; Oyanedel-Craver and Smith, 2008). Although it is well known that particle deposition onto surfaces is a complex process that involves many factors such as particle size, surface charge heterogeneity, surface roughness, and steric and hydrophobic interactions, electrostatic interactions are still expected to play a significant role in the process (Benjamin and Lawler, 2013; Adamczyk and Warszynski, 1996).

Sungmin Youn, a PhD student in the Environmental Engineering program at UT Austin, significantly contributed to this chapter through collaborative modeling and review. Sungmin improved and converted excel spreadsheets into Matlab code found in Appendices A and B.

The objective of this work is to evaluate if approximations of Derjaguin-Landau-Verway-Overbeek (DLVO) theory can accurately predict Ag NP deposition preference onto ceramic membranes for particles stabilized by different organic ligands. A combination of experimental and modeling approaches were used to test two hypotheses: 1) pH conditions can be selected which promote attachment and 2) systems with lower predicted DLVO energy barriers will experience greater Ag deposition.

Background

NPs are generated by a wide range of techniques, many of which use stabilizing molecules during synthesis to prevent aggregation and provide surface passivation. Stabilization of the metal core is provided through one of three primary mechanisms: electrostatic, steric, or electrosteric interactions between the metal and stabilizer (Cao, 2004). In an extensive review of the literature, the most common agents used by researchers to stabilize Ag NPs were citrate at 27% use by occurrence, followed by polyvinylpyrrolidone (PVP) at 18%, and amines at 8%. These coatings produce diverse conformations and charge distributions on the particle surface, which in turn affect particle-particle and particle-flat surface interactions (Tolaymat et al., 2010). Currently, stabilizers are selected using arduous trial-and-error methods with the majority of synthesis goals focused on size and shape control, rather than post processing attachment to surfaces. Although a few studies have demonstrated differences in toxicity due to NP's stabilizing agent, the influence of stabilizer structure is normally neglected in the literature because stabilizer properties are challenging to measure with routine analytical

methods (El Badawy et al., 2011; Silva et al., 2014). The small size and large curvature of NPs present measurement challenges and require several advanced complementary analysis methods such as Atomic Force Microscopy (AFM), X-Ray Photoelectron Spectroscopy (XPS), Transmission Electron Microscopy (TEM), and Thermal Gravimetric Analysis (TGA) to glean useful information about the thickness and density distribution of the stabilizer. Consequently, the incorporation of steric forces into deposition models is limited due to practical constraints, whereas the more straightforward measurements of surface potential and size required for DLVO calculations are more accessible. As a result, identification of situations where DLVO theory is useful in controlling NP deposition holds great potential for routine application in a wide range of disciplines.

DLVO Exact Solution

DLVO theory predicts colloidal stability by summing the potential energy associated with the interaction of the electrical double layers of two surfaces and the van der Waals interactions (Israelachvili, 1992). The calculation of the van der Waals energies for a particle (p) and flat surface (f) is straightforward:

$$\boldsymbol{V_{A,pf} = \frac{Aa_p}{6s}\left(1 + \frac{14s}{\lambda}\right)^{-1}} \qquad (4\text{-}1)$$

Where s represents separation distance, A the Hamaker constant, λ the characteristic wavelength of interaction, and a_p the particle radius (Benjamin and Lawler, 2013). A value of 100 nm is typically appropriate for λ (Anandarajah and Chen, 1995).

On the other hand, exact computation of the energy associated with the double layers is much more complicated and requires numerical methods. Further, to solve for the energy associated with the overlapping double layers, it is necessary to specify if the charged surfaces are at constant surface potential or at constant surface charge upon approach. The use of one assumption over the other reflects different views of the relevant physical phenomena at close separation distances. For example, counterions can adsorb as the two surfaces grow nearer or escape because of the geometry of the surfaces (constant potential assumption more applicable), particles such as clays and latex can have a fixed charge (constant charge assumption more applicable), or interactions of double layers may be so brief under Brownian motion that equilibrium is maintained (constant charge assumption more applicable) (Gregory, 1973). At large separation distances, regardless of which assumption is made, the calculated interaction energies for the exact solution are in close agreement. However, the two assumptions lead to drastic differences in energies of interaction at short separation distances, differences which are magnified when the potentials are of different magnitudes for each surface. Intuitively perplexing, unequal surface potentials with the same sign will give attraction at small separation distances under the constant potential assumption, and repulsion will occur for opposite sign surface potentials with the constant charge assumption (Gregory, 1975). In general, the constant surface charge assumption can be considered an upper limit to the possible energy of interaction, whereas the constant surface potential corresponds to the lower limit (Israelachvili, 1992).

DLVO Double Layer Approximations

For routine use, such as selecting the optimal NP attachment conditions, it is more convenient to use an approximate expression than numerical methods that are required for the exact solution. Approximation methods still face the issue of disagreement at short separation distances between the constant potential and constant charge assumption. The linear superposition approximation (LSA), an approximation method that can use either the constant charge or constant potential assumptions, always lies somewhere in the middle (Figure 4-1). Care must be taken to use the scenarios within the bounds of acceptable error for each particular application because the approximations, particularly linearized versions, add more limitations to the magnitude and sign of the charges/surface potentials. Additionally, the double layer interaction energy is geometry specific and, for the scenario at hand, must be adapted to a particle and a flat plate configuration. An extensive body of work in the field of Environmental Engineering examines particle removal in aqueous solutions using granular media filtration. At the microscopic level, the size difference between the particles and the grains of the filter media are so different

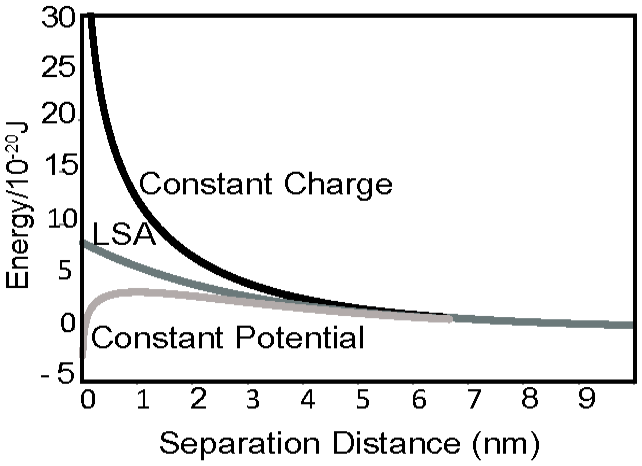

Figure 4-1: Electrical Double Layer Energy of Interaction for a Particle (33.8 mV) and Flat Plate (14.5 mV), the BPEI Ag NP Experimental Condition. The graph demonstrates the solution dependence on the boundary condition assumption employed during the calculation.

that the particle “sees” the filter media as a flat plate, just as the NPs interact with the surface of a membrane in this study. The equations for the most frequently used approximation methods are summarized in Table 4-1 and discussed subsequently. Additionally, a very detailed discussion of particle-particle electrical double layer approximations can be found in Elimelech et al. (2013).

Table 4-1: Electrical Double Layer Approximation Methods

Assumption	Method	Geometry	Double Layer Interaction Energy (V)	References
Constant Charge	Compression Method	Flat Plate-Flat Plate	$V_{R,ff} = \frac{2nk_BT}{\kappa}\left[(y_1+y_2)\ln\left(\frac{B+\left(\frac{y_1+y_2}{2}\right)\coth\left(\frac{\kappa s}{2}\right)}{1+\left(\frac{y_1+y_2}{2}\right)}\right) - \ln\left(\left(\frac{y_1+y_2}{2}\right)^2 + \cosh\kappa s + B\sinh\kappa s\right) + \kappa s\right]$ (4-2a) $B = \sqrt{\left[1+\left(\frac{y_1+y_2}{2}\right)^2 \operatorname{csch}^2(\kappa d/2)\right]}$ (4-2b)	(Gregory, 1975)
	Linearized Poisson Boltzmann	Particle-Particle	$V_{R,pp} = \frac{a_{p1}a_{p2}}{a_{p1}+a_{p2}}\frac{2\pi nk_BT}{\kappa^2}(y_1^2+y_2^2)\times \left[\frac{2y_1y_2}{y_1^2+y_2^2}\ln\left(\frac{1+e^{-\kappa s}}{1-e^{-\kappa s}}\right) - \ln[1-e^{-2\kappa s}]\right]$ (4-3)	(Usui, 1973)
	Linearized Poisson Boltzmann	Particle-Flat Plate	$V_{R,pf} = \pi\varepsilon_o\varepsilon_r a_p \left\{ \begin{array}{c} 2\Psi_{d_f}\Psi_{d_p}\ln\left[\frac{1+e^{(-\kappa s)}}{1-e^{(-\kappa s)}}\right] - \\ \left(\Psi_{d_f}^2+\Psi_{d_p}^2\right)\ln\left[1-e^{(-2\kappa s)}\right] \end{array} \right\}$ (4-4)	*
Constant Potential	Linearized Poisson Boltzmann	Particle-Flat Plate	$V_{R,pf} = \pi\varepsilon_o\varepsilon_r a_p \left\{ \begin{array}{c} 2\Psi_{d_f}\Psi_{d_p}\ln\left[\frac{1+e^{(-\kappa s)}}{1-e^{(-\kappa s)}}\right] + \\ \left(\Psi_{d_f}^2+\Psi_{d_p}^2\right)\ln\left[1-e^{(-2\kappa s)}\right] \end{array} \right\}$ (4-5)	(Hogg et al., 1966)
	Linear Superposition Approximation (LSA)	Particle-Flat Plate	$V_{R,pf} = a_{p1}\frac{128\pi nk_B}{\kappa^2}\gamma_1\gamma_2 e^{-\kappa s}$ (4-6a) $\gamma = tanh(y/4)$ (4-6b)	**

* Geometry converted from Usui (1973) and notation transformed to be in terms of potential
** Geometry converted from Gregory (1975)
Where ε represents permittivity, a_p the particle radius, s separation distance, Ψ surface potential, κ the Debye length, n the number concentration, $\kappa^2 = 2e^2nz^2/\varepsilon k_BT$, and $y = ze\,\Psi/k_BT$ (e is the elementary charge and z is the valency of the ions in solution). The value y corresponds to the reduced, dimensionless form of the surface potential Ψ.

For the constant charge assumption, two approximation methods have been developed. The "compression method" (Equation 4-2a) uses the notion that, as the two surfaces approach each other, the charge density in the region between the surfaces increases. Using the Poisson equation, which relates charge to potential, estimates of the

potential as it changes at different separation distances, can be made without direct measurement. The compression method has been shown to agree very well with exact solutions for plates of both equal and unequal double layers (Gregory, 1973; Gregory, 1975). Unfortunately, the expression developed using the compression method cannot be easily integrated (which is necessary to change geometry). If numerical methods are to be avoided, it is only helpful in solving for double layer interaction energies of two flat plates. A linearized version of the Poisson Boltzmann equation has also been developed for the constant charge assumption and will be employed in this paper (Equation 4-4) (Usui, 1973). It overestimates the repulsion at close approach, because the linearization is based on a simplification of the Taylor series where only the two first terms are considered. This assumption leads to error if the surface potential is greater than |25 mV| (Verwey and Overbeek, 1948). At short separation distances, the linearization at constant charge breaks down. For two oppositely charged surfaces, the energy of interaction will become repulsive. However, the constant charge linearization captures attraction between oppositely charged surfaces at these short separation distances where other approximations fail because of the mathematical simplifications.

For the constant potential assumption, a linearized version of the Poisson Boltzmann equation and the Derjaguin approximation is also used to solve for the energy of interaction (Equation 4-5). For water treatment applications most researchers use the work derived by Hogg et al. (1966). These calculations require relatively straight forward measurements of particle size and the surface potential for the particle and the flat plate

collector. As previously mentioned for the linearization at constant charge, the assumptions made during the derivation require that the surface potentials be less than |25 mV|, and similar in value, to give good agreement with the exact solution for short separation distances (which is where the energy barrier occurs). While this method has proven applicable in many environmental engineering situations, where natural organic matter is ubiquitous and coats both surfaces rendering them similar, the relationship is limited for the more pristine manufacturing conditions where NPs, due to stabilizing agents, have very different surfaces than the membrane. NPs by design often have large surface potentials in order to prevent aggregation and also have a different surface charge than the membrane.

LSA (Equation 4-6a) can use either the assumption of constant potential or constant charge, but is most frequently used with constant potential to correct for the underestimation of the energy barrier at short separation distances. LSA, at the constant potential assumption, has been found applicable for situations of particle deposition (Adamczyk and Warszynski, 1996). It assumes each surface is isolated, but that a region exists between the two surfaces where potential is small and obeys the linearized Poisson-Boltzmann equation. This allows contributions from each surface to be added together to obtain an overall potential energy (Elimelech et al., 2013). The advantage of the LSA model is that it is valid for any arbitrary surface potentials, electrolyte composition, and particle size and does not underestimate the energy barrier like the linearized Poisson Boltzmann estimation method for constant potential does (Adamczyk

and Warszynski, 1996). It adheres to derivation assumptions for small surface potentials and separation distances of κs>1 (Gregory, 1975).

A few items are important to note about the approximations. First, by convention, negative energies represent attraction and positive energies repulsion. Secondly, after converting to a particle and flat plate, it is possible to put Equation 4-3 in terms of surface potential (the experimentally measured variable). One will observe that the only difference in (Eqn. 4-4) and (Eqn. 4-5) is that, at constant surface potential, the $\left(\boldsymbol{\Psi_{d_f}^2 + \Psi_{d_p}^2}\right)\boldsymbol{\ln\left[1 - e^{(-2Ks)}\right]}$ term is added, whereas it is subtracted at constant charge. This explains why the constant surface potential underestimates its exact solution for unequal and high surface potentials, but the constant charge leads to overestimates of its exact solution of repulsion at close approach for surfaces that are of unequal and/or high surface potentials (it is in good agreement with exact solutions for attractive scenarios).

In summary, the most widely used and accessible approximations are based on the linearized Poisson Boltzmann equation. At constant charge, the energy barrier is overestimated, whereas at constant potential, the energy barrier is underestimated at short separation distances. The underestimation at constant potential can be corrected in part by using the LSA method. In reality, it is challenging to know which extreme case, constant charge or constant potential, or some intermediate scenario is likely to occur so all scenarios should be considered.

EXPERIMENTAL

Materials.

Trace metal grade HNO_3, standardized KOH, NIST traceable Ag ICP standard, and ACS grade reagents were used for the experiments reported. Citrate, PVP, and branched polyethylenimine (BPEI) Ag NPs were synthesized in our laboratory and used for this study. These stabilizing agents were selected to represent the three common modes of stabilization, which are electrostatic (citrate), steric (PVP), and electrosteric (BPEI). Synthesis methods, cleaning procedures, images, and zeta potential values for the particles at different pH values are described in Chapter 3. Representative particle size distributions obtained using multiple images taken on a FEI Tecnai TEM and ImageJ software indicate that, on average, the particles are 10-15 nm in diameter (Figure 4-2a). The particles aggregate at different rates under the experimental conditions used in this study (Figure 4-2b and c).

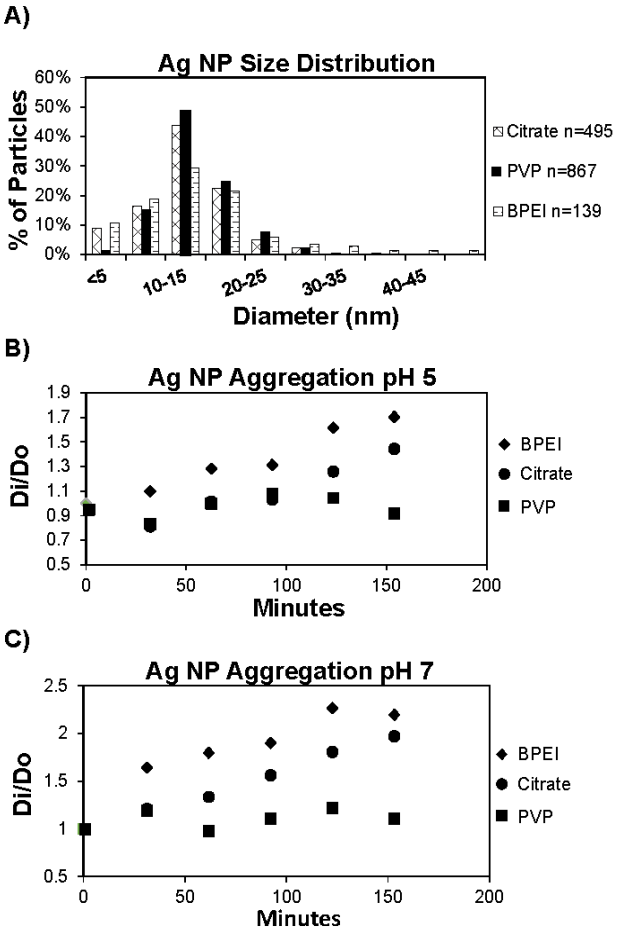

Figure 4-2: A) Ag NP Size Analysis From Multiple Images Analyzed using ImageJ, B) and C) Ag NP Aggregation Rates determined using a NanoSight particle size analyzer at a constant ionic strength of 10 mM, added as KNO_3. B) is at pH 5 and C) at pH 7.

The aggregation rates are used later in the paper to estimate particle sizes at experimentally relevant time points.

Porous aluminum oxide (Al_2O_3) ceramic disks with an effective pore size 0.1 μm (diameter) and disk diameter 13 mm (Whatman Anodiscs) were used to represent ceramic membranes used at drinking water treatment plants. The Al_2O_3, "Anodisc," substrates have highly uniform porosity created via an anodic oxidation of aluminum metal foil, in a process similar to that described by Furneaux et al. (1989). The point of zero charge for the Anodisc is at a pH of approximately 5.5 (Figure 4-3).

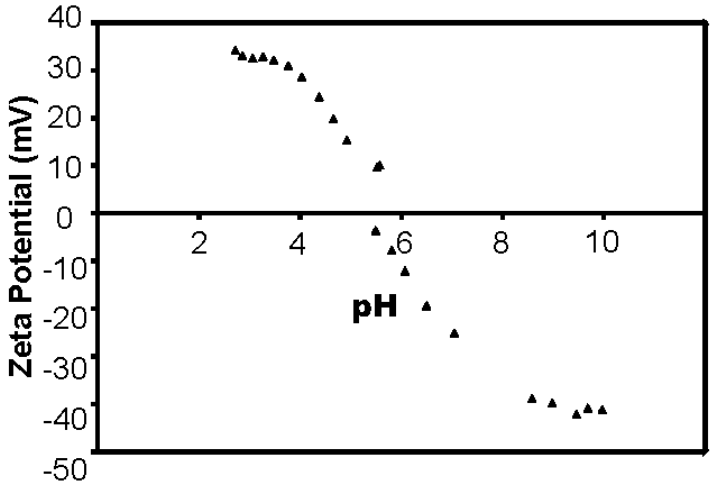

Figure 4-3: Zeta Potential of Whatman Anodisc at 10 mM Ionic Strength (as KNO_3). Measured using an Anton Paar surPASS Electrokinetic Analyzer.

Methods

To study the attachment of NPs to membranes, experiments were conducted at a constant ionic strength of 10 mM KNO_3. The membranes were submerged in Ag NP suspensions for three hours and pH was held constant using concentrated HNO_3 and KOH. A nitrogen blanket was used to minimize the introduction of atmospheric CO_2. Amber glass containers were used to avoid degradation of the Ag by light and the

containers were placed on a shaker table throughout the experiment so that the suspensions remained mixed and to prevent Ag NPs from settling. The membranes were kept upright by a glass holder so that both sides were in contact with the Ag NP suspension at all times. Total suspension phase Ag concentration was measured using a Varian ICP-OES. To determine the amount of Ag deposited on the Anodisc, the filters were digested in concentrated HNO_3 to desorb and dissolve the Ag.

Hypothesis one (that pH conditions can be selected according to DLVO theory which promote attachment) was tested by performing deposition experiments at both pH 5 and pH 7. These pH values were selected for several reasons. First, the pH values are below and above the point of zero charge for the Anodisc, but the sign of the charge for all three types of Ag NPs stayed the same. This allowed for testing scenarios where the particles and filters are of opposite sign (pH 5 for citrate and PVP Ag NPs, pH 7 for BPEI Ag NPs) and the same sign (pH 7 for citrate and PVP Ag NPs, pH 5 for BPEI Ag NPs). Secondly, the magnitude of the surface potential of the Anodisc stayed within the ±25 mV constraint of using the linearized version of the

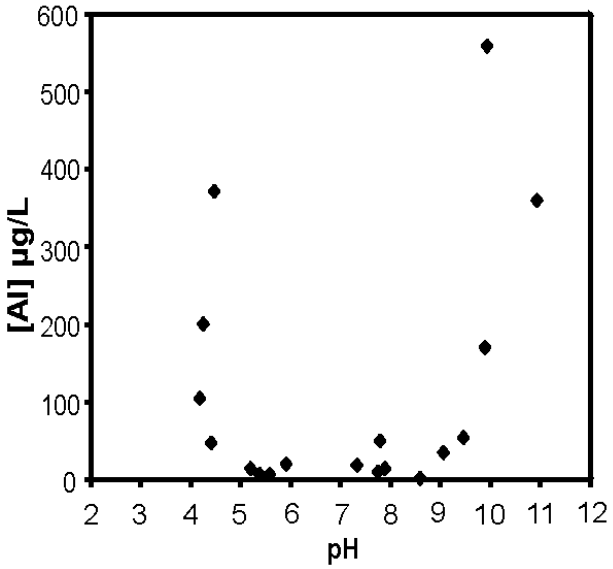

Figure 4-4: Anodisc's Aluminum Solubility. Measured using a Varian ICP-OES. Aluminum concentrations are very low for pH values of 5 to 9, the range of the experiments performed.

double layer energy approximations. Finally, these pH values did not promote dissolution of aluminum, so competitive adsorption is not a concern (Figure 4-4).

To test hypothesis two (systems with lower predicted DLVO energy barriers will experience greater Ag deposition), modeling was performed using Matlab on a number of scenarios that represent the experimental conditions (Table 4-2). Equations (4-4), (4-5), and (4-6a) (at constant potential) were used for comparison to experimental data. Experimentally obtained zeta potential measurements were converted to estimated surface potential values using the Gouy-Chapman model for characterizing the diffuse layer:

$$\psi = \frac{4kT}{ze} tanh^{-1}\left(tanh\left(\frac{ze\xi}{4kT}\right) x \frac{1}{Kd}\right) \quad (4\text{-}7)$$

Where ξ symbolizes zeta potential. A value of 5 angstroms was used for the distance, d, between the surface of the charged particle and the slipping plane (van Oss, 1990). In the van der Waals attractive energy calculations, a value of 5.2×10^{-20} J was used for the Hamakar constant; this value was calculated using values for Ag, water, and Al_2O_3 provided in Israelachvili (1992). Starting particle sizes were estimated from the particle size distributions in Figure 4-2a. Ending particle sizes were estimated using linear regression on the aggregation data presented in Figure 4-2b and c. Particle sizes for the 90th percentile (R90) size radii were obtained using Nanosight after two and a half hours of aggregation. The DLVO model was also tested at constant 5 nm and 10 nm radius values for all of the particles because, as the particle radius changes, the DLVO energy barrier varies. Matlab code for calculation of DLVO energy curves under different

boundary condition assumptions can be found in Appendix A.

Table 4-2. Attachment Experimental Conditions

Ag NP	pH	Ag NP Surface Potential (mV)	Anodisc Surface Potential (mV)	Average Particle Radius (nm) Starting	Ending	R90
Citrate	5	-23.4	14.5	6.5	9.2	44
	7	-29.1	-24.4		13.8	54
PVP	5	-9.8	14.5	7	10.8	101
	7	-9.3	-24.4		8.4	108
BPEI	5	33.8	14.5	7.8	14.5	123
	7	28.4	-24.4		20.9	173

RESULTS

The magnitude of repulsive energy between the particles and membranes and, therefore, the height of the energy barrier depend on the approximation method (Figure 4-5). The constant charge assumption produces the largest repulsive energies, followed by (constant potential) LSA, and constant potential. Although the energy barrier increases with increasing particle size, the order of repulsion/attraction among the different particle types and pH conditions does not change by approximation method when run at radii of 5 nm, 10 nm, and experimentally estimated starting and ending values (not shown).

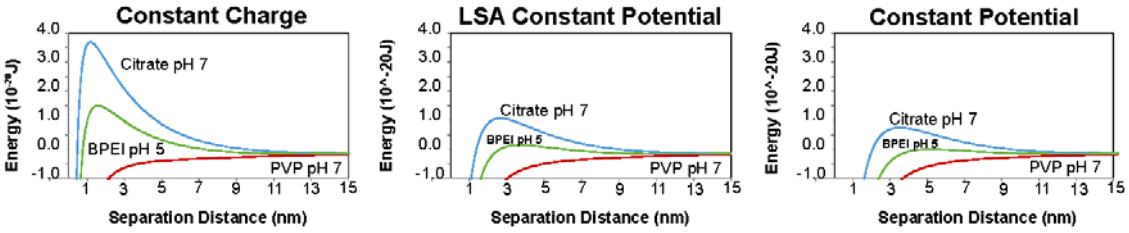

Figure 4-5: Energy Barrier Estimations Using Different EDL Approximations. Scenarios represent Ag NP and Anodisc pH values were the particle and membrane have the same sign surface potential. All NPs were modeled using a 10 nm radius.

An exception to this energy barrier order is when the 90th percentile radii and the constant charge assumption for the electrical double layer are used during DLVO calculations. For this scenario, BPEI Ag NPs at pH 5 have a higher energy barrier than citrate Ag NPs at pH 7. This result highlights the fact that a range of particle size distributions in samples may contribute to differential deposition. A much larger 90th percentile radii for the BPEI Ag NPs also highlights that aggregation occurs to a greater extent for some types of Ag NPs. Cationic polymers are frequently used in drinking water treatment as a flocculent in order to induce interparticle bridging and could be occurring for the BPEI Ag NPs as well.

The scenario of all particles at a 10 nm radius are presented in this paper, although, as with the 90th percentile results, it is recognized that differential particle sizes (both within and between particle type) can have a significant impact for BPEI Ag NPs. For example, for a 10 nm radius citrate Ag NP, the energy barrier is larger (regardless of approximation method) than a 10 nm BPEI or PVP Ag NP calculated by the same approximation method. However, if citrate Ag NPs are held constant at 10 nm, their energy barrier is surpassed when BPEI Ag NPs are at 74 nm using the LSA, 26 nm using the constant charge approximation, or never using the constant potential approximation (the difference in the surface potential of the Anodisc and particle is large enough that the approximation breaks down at short distances and always gives attraction) (Figure 4-6). On the other hand, under all approximation methods, PVP Ag NPs' energy barrier never

exceeds citrates' energy barrier since, as the particle size is increased, the van der Waals attractive energy and double layer repulsion both increase at comparable rates.

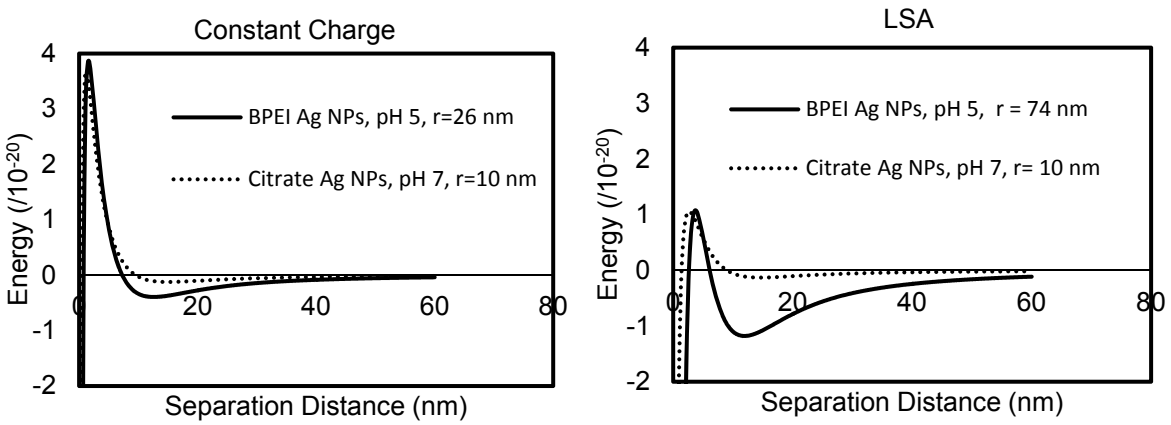

Figure 4-6: Impact of Particle Size on Energy Barrier.

Hypothesis 1 Results.

The experimental results suggest that pH conditions which promote attachment can be selected according to DLVO theory, but that the degree of difference in deposition depends on the NP stabilizing agent (Figure 4-7).

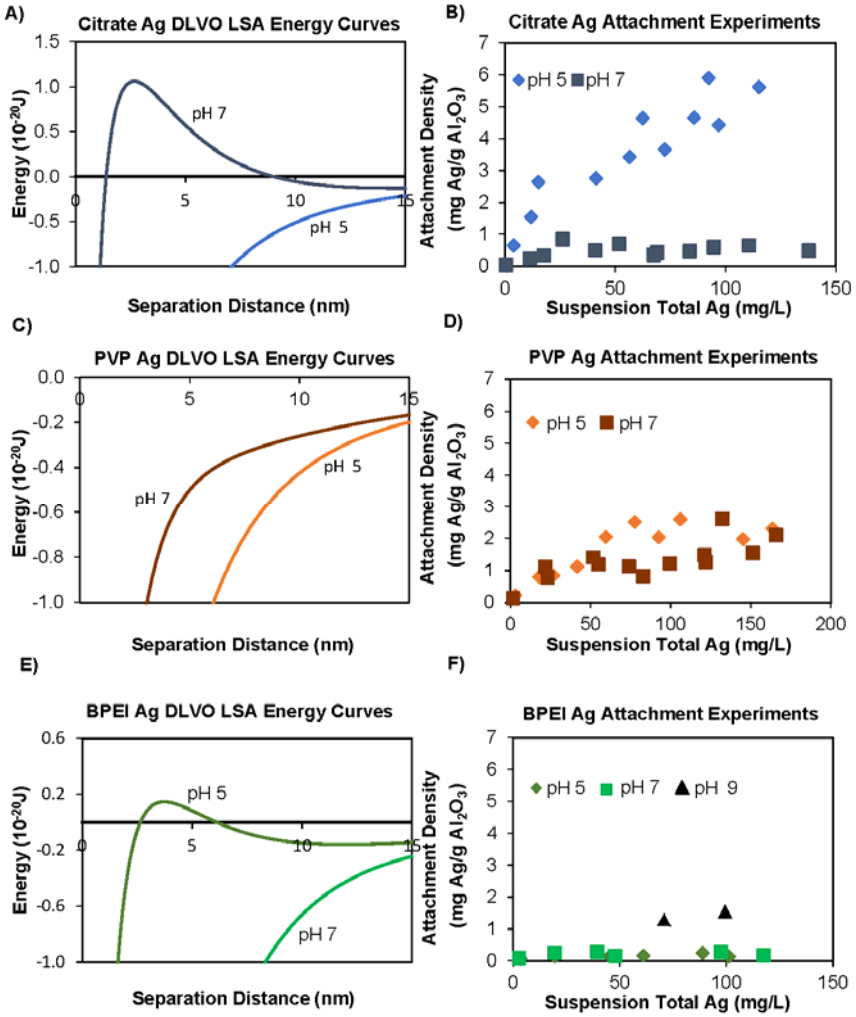

Figure 4-7: DLVO LSA Modeling and Attachment Density Experimental Results at pH 5 and 7. A) & B) Citrate Ag NPs, C) & D) PVP Ag NPs, and E) & F) BPEI Ag NPs. 10 nm particle radii.

For electrostatically stabilized citrate Ag NPs, modeling (Figure 4-7a) predicts a large energy barrier for same sign surface conditions (pH 7) vs. attraction under opposite sign

surface conditions (pH 5). The experimental results (Figure 4-7b) demonstrate this phenomenon remarkably well. On the other hand, modeling (Figure 4-7c) predicts attraction under all conditions for sterically stabilized PVP Ag NPs, with attraction starting at farther separation distances for pH 5 (opposite sign condition) than pH 7 (same sign surface potential condition). Consistent with these results, the PVP Ag NP experimental results demonstrate a less pronounced pH dependence than the citrate Ag NPs (Figure 4-6d). Some difference in the attachment at the two pH values occurs in the suspension total Ag concentration range of 50-125 mg/L, but at concentrations lower and higher there is not a separation with pH. It is possible that the deposition at low PVP Ag NP concentrations appear similar, regardless of pH, because the NPs are more spread out and do not experience strong lateral repulsive interactions among deposited and free particles. As the density of the coverage increases, the influence of the electrical double layer could play a more important role via lateral repulsive forces and thus produce slight variation with pH. At concentrations higher than 125 mg/L Ag, an inversion of the surface potential of the deposited NP can occur which can lead to multilayer deposition. Multilayer deposition of PVP Ag NPs were observed using scanning electron microscopy (SEM) (Figure 4-8).

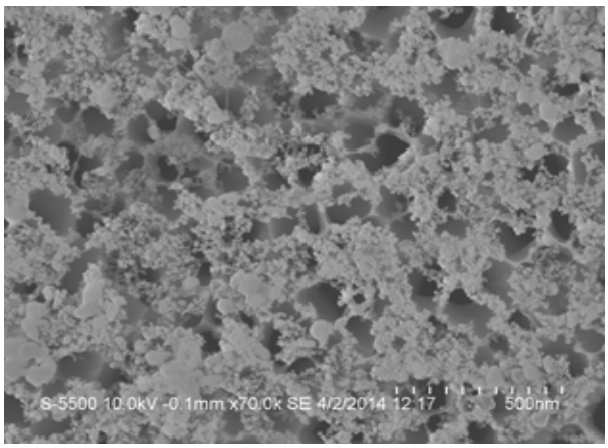

Figure 4-8: PVP Ag NPs on Anodisc Showing Multilayer Deposition. Image was obtained using a Hitachi S5500 SEM

Despite an energy barrier for like sign conditions at pH 5 (Figure 4-7e), BPEI Ag NPs (electrosterically stabilized) demonstrate little difference in deposition at pH 5 vs. pH 7 (Figure 4-7f). This insensitivity to pH indicates that the electrostatic interactions from the amine functional groups likely play a smaller role than the steric interactions between the BPEI molecule and the filter surface. If the pH of the solution is increased to pH 9, where the Anodisc surface potential is significantly lower (-40 mV, as shown in Figure 4-3), increased deposition can be induced (Figure 4-7f). DLVO modeling was also performed at pH 9 for BPEI Ag NPs and, as expected, greater attraction was observed at pH 9 than 7 for all separation distances (*e.g.*, for LSA across all separation distances there was an average of 2.1×10^{-22} J greater attraction at pH 9 versus 7). However, the magnitude of the surface potential of the Anodisc is much higher than the 25 mV constraint for using the linearized version of the Poisson Boltzmann equation, so would require numerical methods for an accurate solution to the energy curves.

Hypothesis 2 Results

The DLVO modeling results predict that the order of least deposition to most deposition is citrate pH 7, BPEI pH 5, PVP pH 7, citrate pH 5, BPEI pH 7, and PVP pH 5 (Figure 4-9a). This order remains the same regardless of which electric double layer approximation method is used. Experimental results do not agree with this predicted order (Figures 4-9b and 9c). This disagreement suggests either that electrostatic interactions are not the dominant mechanism in NP attachment to the surface of ceramic water filters or that the origin of surface charge or potential is different depending on the stabilizing agent. For conditions of same sign surface potential of the filter and NP, BPEI Ag NPs were predicted to have a lower energy barrier than citrate Ag NPs; however, they show less deposition. This disagreement could be due to several different physical phenomena. Steric

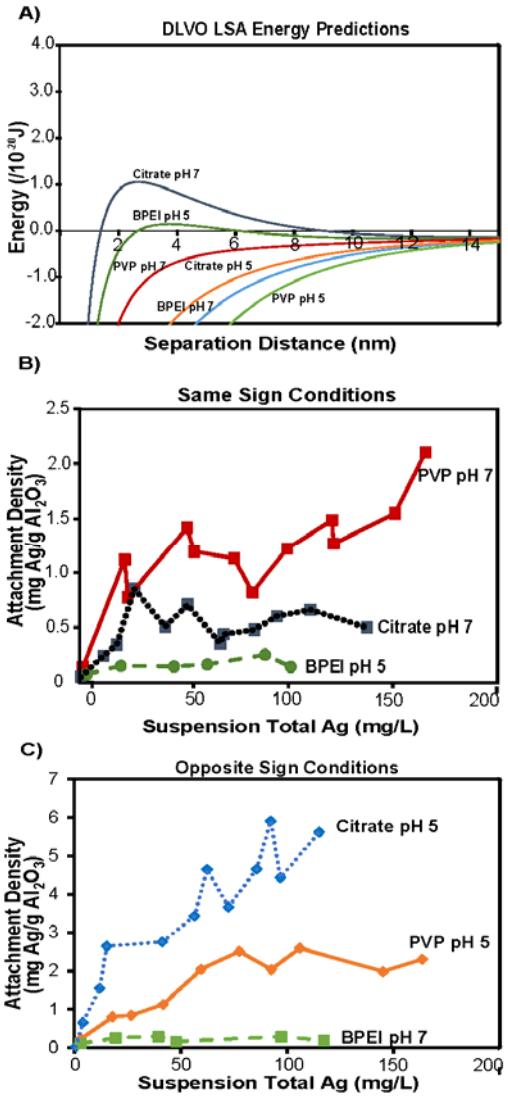

Figure 4-9: Theoretical and Experimental Ag NP Deposition Order. A) DLVO energy predictions calculated using LSA for the double layer energy. B) Experimental results for Ag NPs having the same sign surface potential as the membrane and C) experimental deposition results for conditions where Ag NPs have the opposite sign as the surface potential of the membrane.

interactions of the BPEI molecule or aggregation of BPEI Ag NPs over the course of the experiment could both cause less deposition of BPEI Ag NPs than citrate. One way that the experimental deposition orders can be explained is by using different assumptions based on the type of stabilizing molecule. Interestingly, if the constant charge approximation method is selected to calculate the energy barrier for BPEI Ag NPs, but LSA is used for the other NPs, the order matches experimental findings. (Note, one might wonder if the flip in energy barrier is induced by the fact that the constant charge assumption overestimates the exact solution for the energy barrier at close separation distances. However, the deviation between the exact and approximate solution is not as large as the difference in solutions for the constant charge versus constant potential assumptions. It is imaginable that counterion charges could be trapped inside the long arms of the BPEI layer and thus unable to escape in short times, lending credence to the constant charge assumption being more appropriate than LSA for estimating the energy barrier. On the other hand, PVP and citrate have been shown to form compact layers on NPs so LSA or constant potential might be more appropriate (Park 2013; Mdluli et al, 2009). For conditions of opposite sign surface potential of the filter and NP, the citrate Ag NP showed more favorable deposition than was expected in comparison to the other types of NPs. Citrate was the only electrostatically stabilized particle so it is quite reasonable to assume that other repulsive forces inhibit attachment for the particles that have steric stabilization.

CONCLUSIONS

- Stabilizing agents used in the production of Ag NPs effect attachment of Ag NPs to ceramic water filters. At similar conditions, citrate Ag NPs have the highest attachment affinity followed by PVP Ag NPs, and BPEI Ag NPs. This result has implications of differential success rates for both removal of unwanted particles from water as well as intentional adhesion to surfaces.

- DLVO Theory is effective at selecting pH conditions that promote increased deposition for citrate stabilized Ag NPs. For particles that include steric stabilization, the results are not straightforward. Better understanding of deposition of NPs on the ceramic membrane requires systematic calculations of DLVO energy along with steric energy.

- For electrostatically and electrosterically stabilized NPs, attachment to ceramic membranes is increased as the difference in opposite sign surface potential increases. This difference in surface potential leads to under (constant potential) and over (constant potential) estimations of the linearized solutions to the Poisson Boltzmann equation at short separation distances.

- The influence of Ag NP size varies depending on the stabilizing agent and approximation method used to solve for the energy of interaction. The order of the energy barriers will switch for a 10 nm citrate Ag NP when BPEI Ag NPs are in

the range of 26-74 nm. PVP and citrate Ag NPs do not switch energy barrier order as the size of the PVP Ag NPs changes.

- Future research should be conducted on various stabilizing molecules to determine if constant charge or constant potential is the most appropriate assumption for estimating double layer energy.

- DLVO theory can only make predictions for a single particle and flat plate collector. Depending on stabilizing agent, NP solutions aggregate at different rates that are magnified by increasing concentration. Since larger particles lead to increased double layer repulsion, care should be taken to select the length of time for soaking the filters in NP solutions such that the mixture of sizes does not inhibit deposition.

Chapter 5: Extended DLVO – The Role of Nontraditional Interactions in the Attachment of Silver Nanoparticles to Ceramic Water Filters

INTRODUCTION

Traditionally, the interactions between a particle and flat surface are modeled using DLVO theory. DLVO theory only considers van der Waals and electrical double layer interactions; however, it is well known that many other influential interactions exist as well. These include, but are not limited to, Lewis acid-base interactions, steric interactions, and interactions associated with the presence of other particles in suspension. Other researchers have observed the significance of these interactions. For example, Lewis acid-base interactions play a substantial role in the coagulation of hectorite suspensions (van Oss et al., 1990) and in fouling of membranes used for water treatment (Hoek and Agarwal, 2006). Steric stabilization is widely used in the synthesis of NPs to prevent aggregation. Steric forces have been observed in many AFM studies that look at the interactions between polymer coated particles and planar surfaces (Grasso et al., 2002), as well as in biological samples such as *Cryptosporiduium parvuum's* interactions with silica surfaces (Byrd et al., 2005). Natural organic matter in natural water systems is perhaps the most environmentally significant source of steric interactions.

Sungmin Youn, a PhD student in the Environmental Engineering program at UT Austin, significantly contributed to this chapter through collaborative modeling and review. Sungmin improved and converted excel spreadsheets into Matlab code found in Appendices A and B.

The objective of this chapter is to evaluate the significance of nonelectrostatic driving forces in attachment of Ag NPs to ceramic membranes. Experimental attachment density curves were presented in Chapter 4 for different Ag NPs attached to porous Al_2O_3 Anodisc membrane filters. It was concluded that the discrepancies in observed vs. predicted deposition could be attributed to the need for different boundary condition assumptions (constant potential vs. constant charge), depending on the stabilizing agents. This chapter will evaluate three additional explanations through discussion of: 1) Lewis acid-base interactions, 2) steric interactions, and 3) particle-particle interactions. The effect of filter material will also be discussed through a comparison of Ag NP attachment densities to Al_2O_3 and clay based ceramic filters.

BACKGROUND

Lewis Acid-Base Interactions

This category of non-DLVO interactions includes hydrogen bonding and solvation forces. Solvation forces are also commonly referred to as hydrophobic interactions (surface-surface attraction), or hydration pressures (surface-surface repulsion). These structural interactions are responsible for accounting for the orientation of water molecules on the surface of the material and their role in attraction or repulsion. For certain materials at small separation distances, acid-base interaction energies have been demonstrated to be 100 times as large as van der Waals energies and over ten times those of electrical double layer energies (van Oss et al., 1990)

Measurements of surface tension and contact angle have been used to quantify attractive hydrophobic Lewis acid-base energies according to a procedure outlined by van Oss et al. (1990). The procedure requires contact angles of two polar and one nonpolar liquid, in conjunction with the Young-Dupré equation to determine the acid-base free energy of interaction for a particle and a planar surface of the same material. However, in this work, the particle and the membrane are not the same material, and major analytical obstacles exist to measure the interfacial tension associated with the acid-base properties of the Ag NPs.

Direct measurement of these properties is a challenging endeavor, but the work of others can be used to evaluate the role of these interactions in the attachment of Ag NPs to ceramic membrane surfaces. Israelachvili (1992) states that, for two surfaces in water, their Lewis acid-base interactions can be mathematically described as:

$$\Delta G_{attraction} = -2\gamma_i \, e^{-s/\lambda_o} \quad (5\text{-}1a)$$

$$\Delta G_{repulsion} = +G_o e^{-s/\lambda_o} \quad (5\text{-}1b)$$

and also notes that experimentally observed values for γ_i range from 10 – 50 mJ/m^2 and 3-30 mJ/m^2 for G_o. For 1:1 electrolytes, λ_o is typically 0.6-1 nm for repulsion and 1-2 nm for attraction. At a separation distance (s) of 5 nm (a distance near to the DLVO energy barriers in this work) and a λ_o of 1 nm, these equations correspond to attractive energies of -0.001 to -0.005 (x10^{-20}) J and repulsive energies of 0.002 to 0.02 (x10^{-20}) J. Regardless of the electrical double layer approximation method, these calculated Lewis acid-base energies are not enough to contribute to changing the order of the predicted

deposition (Table 5-1). As a result, a more detailed analysis of the magnitude of acid-base interactions that can be expected for Ag NP -Al_2O_3 membrane systems is not considered further.

Table 5-1: DLVO Energies ($x10^{-20}$ J) for Different Electrical Double Layer Assumptions at 5 nm separation distance, A= $10x10^{-20}$ J

Ag NP	Constant Charge (CC)	Δ CC	LSA	Δ LSA	Constant Potential (CP)	Δ CP
Citrate pH 7	0.866		0.571		0.527	
		0.542		*0.490*		*0.523*
BPEI pH 5	0.324		0.082		0.004	
		0.242		*0.581*		*0.560*
PVP pH 7	0.082		-0.499		-0.556	

Steric Interactions

Two physical phenomena need to be considered for NPs coated with a polymer that imparts steric stabilization. An increase of polymer concentration in the overlapping region induces an increase in osmotic pressure, while the compression of the polymer chains leads to a loss of entropy (both dependent on the conformation of the polymer on the surface). Accounting for osmotic pressure and entropy losses requires detailed knowledge of many difficult to measure and related parameters, such as stabilizer thickness, degree of polymerization, the distribution of the polymer on the surface, and the curvature of the particle.

DLVO theory has been extended to include steric forces in several manners. One approach is to use Equation 5-2 developed by de Gennes (1987) in which the first term

accounts for the osmotic repulsion (stretching favored) and the second term accounts for entropy loss (stretching opposed).

$$\boldsymbol{F_{steric} \sim k_B T \emptyset^{3/2}} \left[\left(\frac{L_o}{s} \right)^{9/4} - \left(\frac{s}{L_o} \right)^{3/4} \right] \quad (5\text{-}2)$$

where k_B is Boltzmann's constant, T is absolute temperature, $\emptyset$ is the segment density distribution of the polymer, s is the distance between the sphere and the plane, and L_o is the thickness of the polymer layer. (Note, the equation has been modified from its original form both in terms of notation and to fit the geometry of a particle and a flat surface.) In Pensini et al. (2013), this model successfully explained AFM data of the attachment of iron oxide NPs, stabilized with carboxymethyl cellulose, onto various substrates in aqueous solutions. Unfortunately, this model can only be integrated using numerical methods and was developed for linear, neutral chains; therefore, will not be considered further.

Molecular theory has also been used for problems involving tethered polymer layers and explicitly takes into account size, shape, and charge distribution of every molecular species. By using this approach, Nap et al. (2013) developed a lengthy description of entropy and free energy contributions via nine different equation terms. Unlike the other models, this approach takes into account charge regulation as surfaces approach through integration of equilibrium constants. However, it also requires numerical methods that are quite complicated to implement.

Finally, a widely employed theory to describe interactions between polymer layers is based upon Flory-Kirgbaum theory. Lin and Weisner (2012) derive the

following energy expression for the osmotic contribution between a coated particle and an uncoated planer surface using this theory (the paper demonstrates that the elastic contribution is negligible). Their model was validated using AFM results reported in the literature.

$$\Delta G_{self-mixing} = k_B T \left(\frac{Vp^2}{v_s} \right) \left(\frac{1}{2} - \mathbf{X} \right) \emptyset_{s,avg,\infty}{}^2 \; V_{1,s} \left(\frac{V_{1,s}}{V_3} - 1 \right) \tag{5-3}$$

where V_p is the volume of the polymer, v_s is the volume of a solvent molecule, χ is the Flory-Huggins solvency parameter, ϕ represents the segment density distribution, and $V_{1,s}$ and V_3 represent the volume for the polymer under different compression domains (this variable includes separation distance). This relationship is probed further in this chapter and applied to the situations of interest in our experiments.

The segment density distribution plays an important role in Equation 5-3. Its value controls how the branches of the polymer come in contact with the approaching surface. Researchers have used several different models to represent this parameter. The most frequently used models are a uniform configuration of polymer chains or a pseudotails configuration (Lin and Wiesner, 2012). Pseudotails is typically represented by either a mushroom, brush or blob motif. For example, a brush segment density distribution would be a conformation where the polymer protrudes perpendicularly from the surface of the NP. The segment density distribution is highly effected by curvature. Higher curvature values decrease the amount of polymer in contact with the approaching surface. In this work, where the configuration is unknown, the model was used to

determine how high a segment density distribution is required to explain the order of experimentally obtained deposition experiments from Chapter 4.

Particle-Particle Interactions

Deposition experiments use suspensions composed of many particles. In addition to particle-filter interactions, there are also particle-particle suspension interactions. Since NPs are supposedly "stabilized" during synthesis, the literature does not consider that the energy barrier for particle-particle aggregation may be lower than the energy barrier for particle-membrane interaction. If this is the case, a lower attachment density might be induced because particles are more attracted to each other than to the membrane surface. The DLVO particle-particle interactions can be calculated in much the same way as described in Chapter 4, but without the assumption that one of the particle radii goes to infinity.

MATERIALS AND METHODS

Three types of Ag NPs (citrate, PVP, and BPEI) and two types of ceramic water filters (Al_2O_3 Anodisc membranes and clay filters) were used in this portion of the work and are thoroughly described in Chapter 3. The following research questions were evaluated using a combination of modeling and laboratory experiments: All code can be found in Appendix B.

Steric Interactions

1) *At what "threshold" polymer segment density distribution do steric interactions influence the predicted deposition order of Ag NPs?*

Stabilizer thickness, a parameter necessary for calculating the volume of the polymer on the particles in steric force calculations, was measured (very rapidly before the organics were destroyed by the beam) using a Hitachi S5500 STEM. NP solutions were mounted via drop casting onto carbon coated 400 mesh copper grids from Electron Microscopy Science. To measure the stabilizing layer thickness, dark field imaging was found more effective for PVP and Citrate Ag NP samples, and bright field imaging was used for BPEI Ag NPs.

Using an average stabilizer thickness value obtained from STEM, Matlab code was implemented to calculate the segment density distribution where the DLVO energy of interaction of citrate-Ag NPs was exceeded by BPEI Ag NPs. These calculations were completed using the Lin and Weisner model (Eqn 5-3). Chapter 4 outlines the parameter assumptions used for electrical double layer calculations using the constant charge and LSA constant potential assumptions, and the measured surface potential values used by particle type and membrane. The key values are summarized again in Table 5-2, along with additional information relevant to the steric energy calculations:

Table 5-2: Steric Modeling Parameters

Global Parameters: particle radius = 10 nm			
DLVO Parameters: Hamakar Constant = 5.2 x 10^{-20} J; I = 10 mM; λ = 100 nm			
Ag NP	**pH**	**Ag NP Surface Potential (mV)**	Anodisc Surface Potential (mV)
Citrate	5	-23.4	14.5
	7	-29.1	-24.4
PVP	5	-9.8	14.5
	7	-9.3	-24.4
BPEI	5	33.8	14.5
	7	28.4	-24.4
Steric Parameters: Flory Huggins Solvency Parameter, χ: 0.45 (χ is unknown for BPEI Ag NPs, a value of 0.45 was selected as a conservation case for a hydrophilic polymer. Lower values of χ would produce higher energy barriers (or lower segment densities) Opposite sign surface potential conditions: 5 nm separation distance for energy barrier comparisons Same sign surface potential conditions: energy maximum comparison (variable separation distance)			

Particle-Particle Suspension Interactions

2) Is the energy barrier for particle-particle suspension interaction lower than the energy barrier for particle-membrane deposition for 10 nm radii particles?

DLVO energy barriers for particle-particle energies of interaction were calculated using the LSA electrical double layer assumption. For the calculation of attractive energy the retarded form of van der Waals attraction for two spheres was used:

$$V_S = -\frac{Aa_1a_2}{6(a_1+a_2)s} \times \left[1 - \frac{bs}{\lambda}\ln\left(1+\frac{\lambda}{bs}\right)\right] \quad (5\text{-}3)$$

where A is the Hamaker constant, a_1 and a_2 are the radii of the spheres, s is the separation distance , λ is the characteristic wavelength, and b is a fitting parameter used to match exact computations. A value of 100 nm was used for λ and a value of 5.32 was used for b (Gregory, 1981). A range of Hamaker constants of 10×10^{-20} - 40×10^{-20} J are cited in the literature for Ag (Parsegian and Weiss,1981) so several values were investigated using Matlab and will be discussed.

Al_2O_3 Membrane-Clay Filter Attachment Comparison

3) How does membrane material effect attachment density of Ag NPs?

Since Ag NPs are currently applied to ceramic water filters used in developing countries, experiments were also conducted to understand the applicability of this work to clay based ceramics. Approximately 10 mg pieces of filters were soaked in 100 mg/L NP solutions. The filters were then analyzed for suspension phase and attached phase Ag content according to procedures outlined in Chapter 3. As the results will demonstrate, attachment conditions were unfavorable under all conditions for the clay filters. Therefore an experiment was also conducted with silica NPs (radii = 10 nm) to test the hypothesis that an electrostatically charged particle with a positive surface charge would exhibit higher levels of attachment. Two commercially available types of electrostatically stabilized silica NPs were purchased from nanoCompsix. The standard particle has a negative surface charge at pH 7 and the aminated has a positive surface charge at pH 7. These particles were selected to give a negative and positive surface charge comparison where steric interactions are not a factor.

RESULTS

Steric Interactions

From analyzing multiple STEM images using NIH's ImageJ software, BPEI stabilized Ag NPs were found to have an average stabilizer coating thickness of 10 nm. Representative particles are displayed in Figure 5-1. PVP Ag NPs had an average coating thickness of 3 nm and citrate Ag NPs had an average thickness of 2 nm. Since the DLVO energy barriers occur at separation distances larger than the interpenetration distance for the thickness layers of citrate and PVP, steric interactions were only calculated for BPEI nanoparticles.

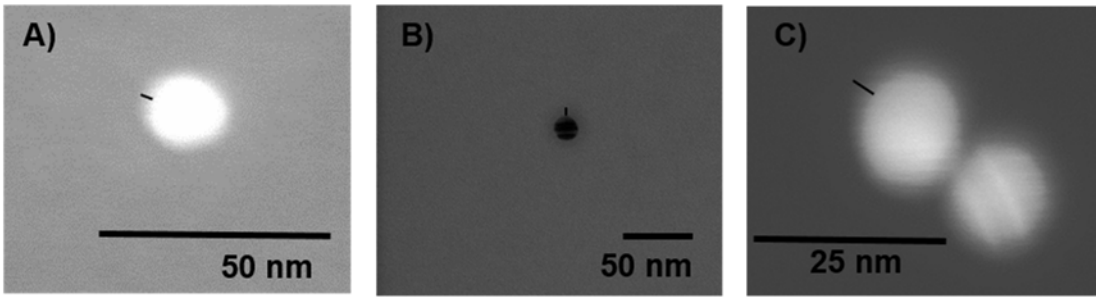

Figure 5-1: STEM Stabilizer Thickness Measurements A) PVP Ag NP (accelerating voltage 30.0 kV, stage -0.2 mm, magnification x600k), B) BPEI Ag NP (30.0 kV, -0.2 mm, x189k), C) Citrate Ag NP (30.0kV, -0.2 mm, x1000k). Stabilizer thickness focused and measured in approximate 30 seconds and notated with black line.

Assuming a uniform 10 nm layer of BPEI on the Ag NPs, the segment density distribution was varied in Equation 5-3. As more segments of BPEI are attached to the Ag core, the energy barrier (DLVO + sterics) increases until it reaches an energy value larger than the DLVO only energy barrier for citrate Ag NPs at pH 7 (Figure 5-2).

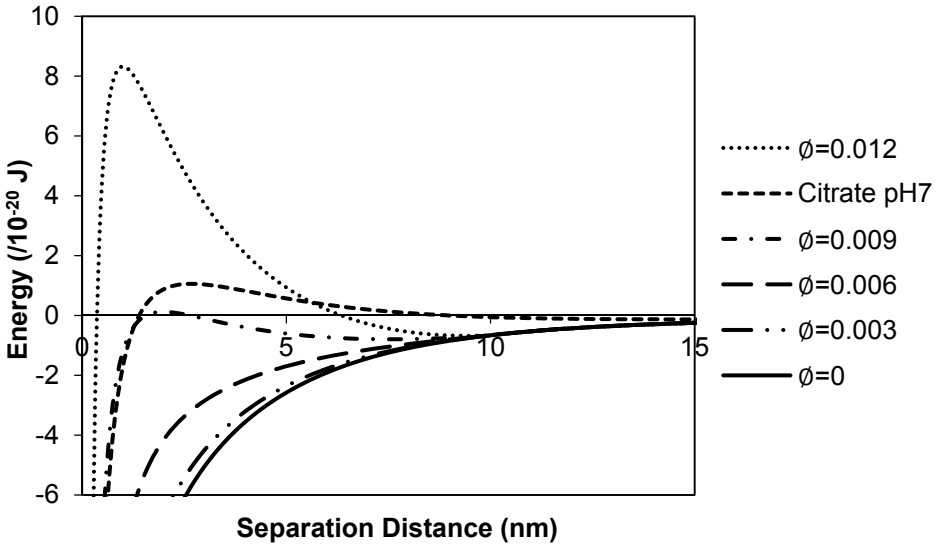

Figure 5-2: Effect of Segment Density Distribution (nm^{-3}) on energies of interaction for BPEI Ag NPs at pH 7 conditions and using LSA approximations for the electrical double layer.

The values of the segment density distribution that cause less favorable deposition of BPEI Ag NPs than citrate Ag NPs at pH 7 (the highest DLVO estimated energy barrier) are contained in Table 5-3. These values are on the same order of magnitude regardless of the combination of boundary condition assumptions for the electrical double layer portion of the total interaction energy. Adding steric interactions essentially renders the boundary condition assumption irrelevant. BPEI Ag NPs at pH 7 require more segments than pH 5 because pH 7 is where the membrane and particle have opposite sign surface potential. Therefore, at pH 7, more electrostatic attraction must be overcome with steric interactions before unfavorable attachment conditions relative to citrate Ag NPs pH 7 are observed. The values of the segment density distribution represent the number of polymer segments that must be attached uniformly to the volume surrounding the core of

the NP, and they are not large values. For perspective, approximately 113 hydrogen atoms will fit in a 1 nm^2 area and could form multiple layers around a sphere. The values summarized in Table 5-3 indicate a very small amount of BPEI is capable of providing substantial steric repulsion and explain the experimental deposition order observed in Chapter 4 (least to most deposition: citrate pH 7, BPEI pH 5, PVP pH 7, citrate pH 5, BPEI pH 7, and PVP pH 5).

Table 5-3: Threshold Segment Density Distributions

EDL Estimation Method		**Segment Density Distribution** Φ (nm^{-3})	
BPEI	*Citrate*	pH 5	pH 7
LSA	LSA	0.0045	0.0114
CC	CC	0.0048	0.0118
LSA	CC	0.0057	0.0119

Particle-Particle Suspension Interactions

A comparison of particle-particle to particle-membrane interactions highlights the integral role of the Hamakar constant, A, in predicting which interaction is favored. The Hamaker constant is a material specific interaction constant derived by pairwise summation of intermolecular interactions (Visser, 1972). Ag-Ag Hamaker constants obtained from different specroscopic studies in water range from 10-40 x 10^{-20} J (Parsegian and Weiss, 1981). At values over approximately 18 x 10^{-20} J, particle-particle aggregation is always more favorable than deposition (Figure 5-3). On the other hand, if a value of 10 x 10^{-20} J (or less) is used for the Hamaker constant, different Ag NP-pH combinations result in different particle or membrane preferences (Figure 5-4). Aggregation experiments with Ag NPs have calculated values of A for citrate Ag NPs to be 3.7 x 10^{-20} J, so these different interactions are likely to play a real role in deposition (Huynh and Chen, 2011). Figure 5-4 also contains a line representing the particle-filter interactions after particles have deposited on the surface of the Anodiscs. This scenario was modeled using a spherical Ag geometry interaction with a flat surface of Ag.

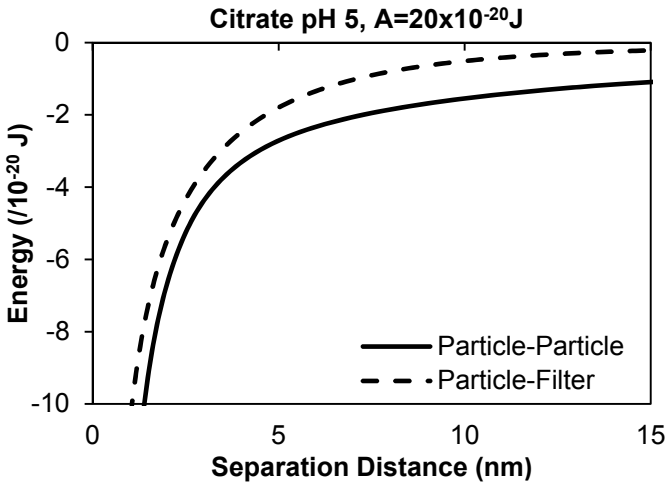

Figure 5-3: Example of More Favorable Particle-Particle DLVO Interaction Energies Compared to Particle-Membrane Interaction Energies. Citrate Ag NPs, r = 10 nm, pH 5, LSA double layer condition, and A = 20 x 10^{-20} J for Ag-Ag & 5.2 x 10^{-20} J for Ag-Filter. The top line is particle-membrane and bottom line particle-particle.

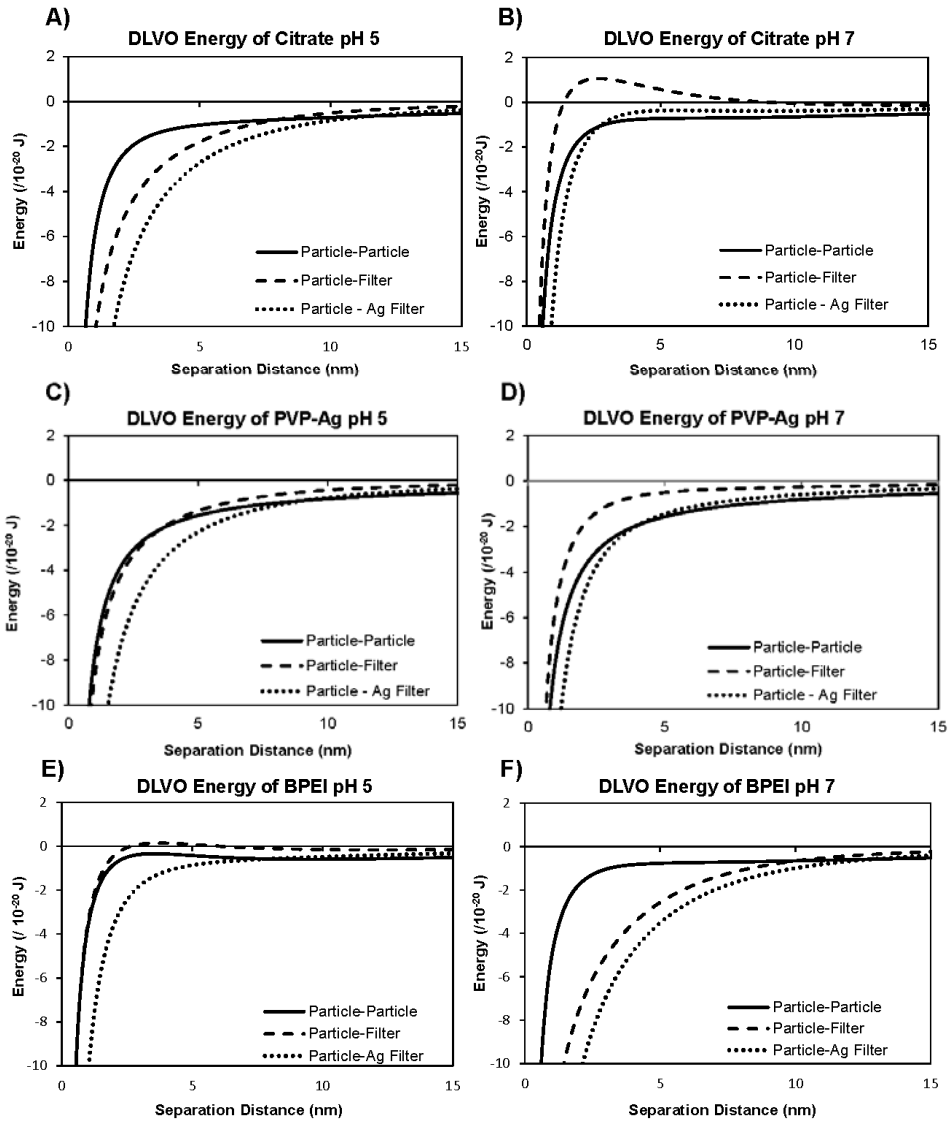

Figure 5-4: Low Hamakar Constant Particle-Particle DLVO Interaction Energies Compared to Particle-Membrane Interaction Energies. LSA double layer condition, r=10 nm, and A = 10 x 10^{-20} J for Particle-Particle and Particle-Ag Filter and A = 10 x 10^{-20} J for Particle-Filter.

.

DLVO theory predicts that both citrate and PVP Ag NPs will prefer the membrane at pH 5 whereas they prefer another particle at pH 7 at short separation distances, but at larger separation difference particle-particle aggregation is favorable. A greater difference in the energy curves exists both between pH values and between the particle and membrane curves for citrate vs. PVP Ag NPs. This result agrees with experimentally observed attachment densities presented in Chapter 4. PVP attachment densities were quite similar, perhaps in part because the "tug" towards aggregation and the membrane was more similar under both pH conditions whereas citrate is more disparate. BPEI Ag NPs are predicted to prefer the membrane at pH 7 instead of 5 because of the opposite sign of the particle and the filter.

The stronger attraction between particle-particle interactions versus particle-membrane interactions may also explain the "patchy" distribution of NPs that were observed from the deposition experiments (Figure 5-5). Figure 5-5a is the condition where the citrate Ag NPs have the same sign charge as the Anodisc membrane and Figure 5-5b is when they have the opposite sign charge. Figure 5-5c is of PVP Ag NPs under opposite sign particle-membrane conditions.

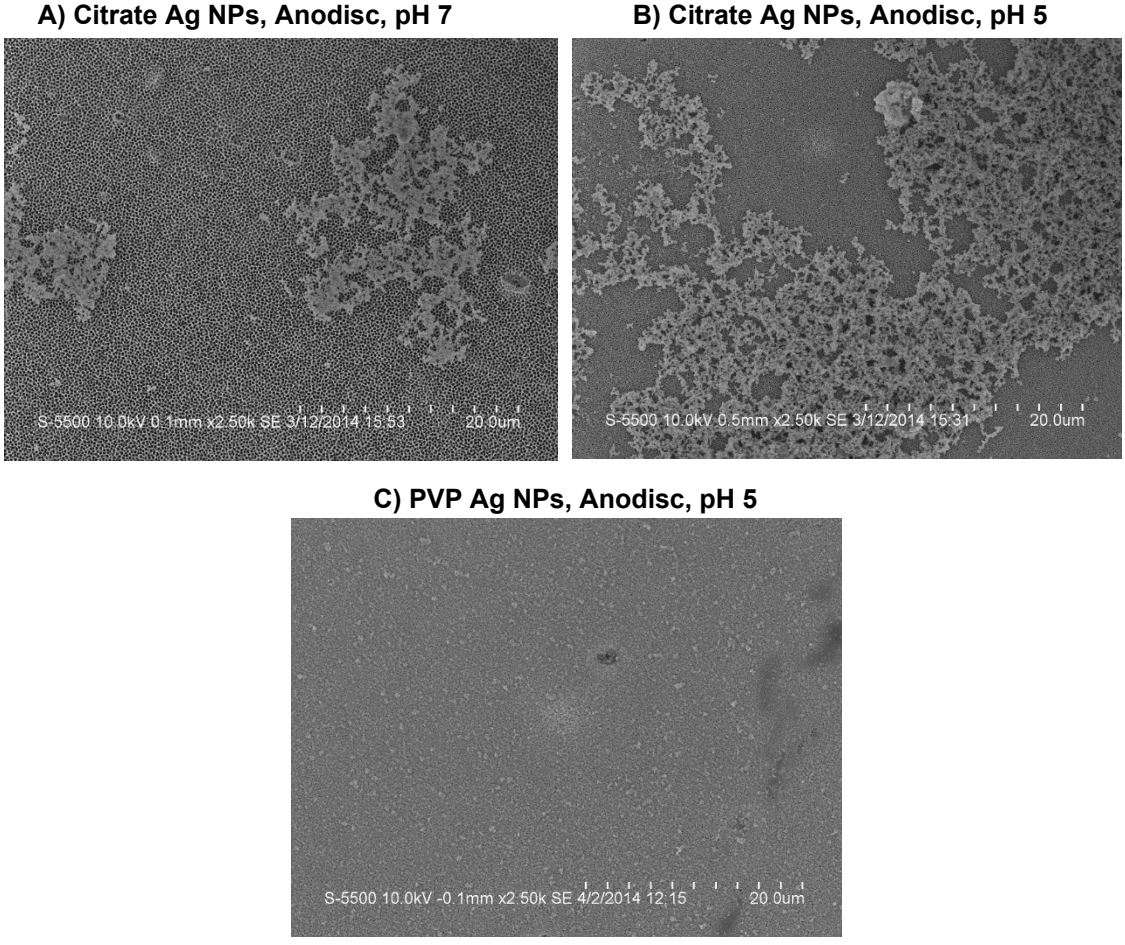

Figure 5-5: Ag NP-Anodisc "Patchy" Coatings. Deposition Conditions: $Ag_{initial}$ = 50 mg/L, I = 10 mM as KNO_3. Imaging on a SEM on a Hitachi S-5500 A) Citrate pH 7, B) Citrate pH 5, and PVP pH 5

When particle and membrane surface are oppositely charged the images show larger areas of coverage. In agreement with the particle-Ag Filter modeling results in Figure 5-4, particles are also attracted to each other so multilevel deposition is evident.

Al_2O_3 Membrane-Clay Filter Attachment Comparison

Clay-based filters experienced similar affinity trends as the Anodisc membranes. Under similar starting concentrations, citrate Ag NPs demonstrated the highest attachment, followed by PVP Ag NPs, and then BPEI Ag NPs (Figure 5-6).

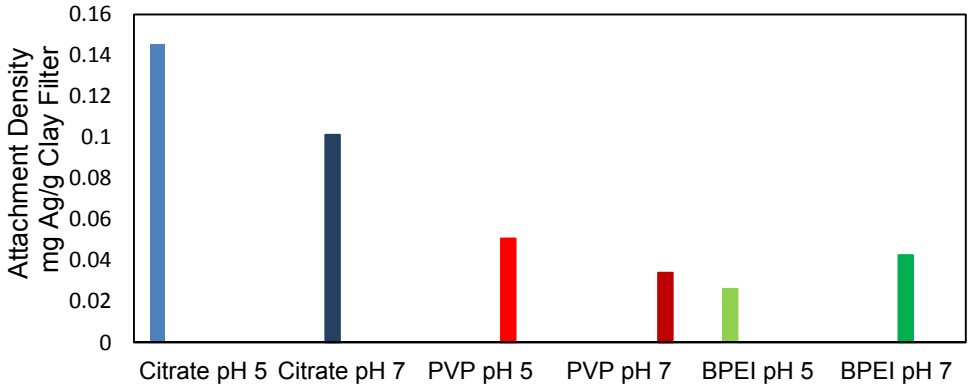

Figure 5-6: Attachment Density of Differently Stabilized Ag NPs to Clay Based Ceramic Water Filters (100 mg/L start Ag concentration).

Slight variations with pH were also observed according to surface potential magnitude differences. However, when compared to Anodiscs' deposition at the same final suspension phase Ag concentrations, the clay filters had substantially less attachment for all types of Ag NPs (Figure 5-7).

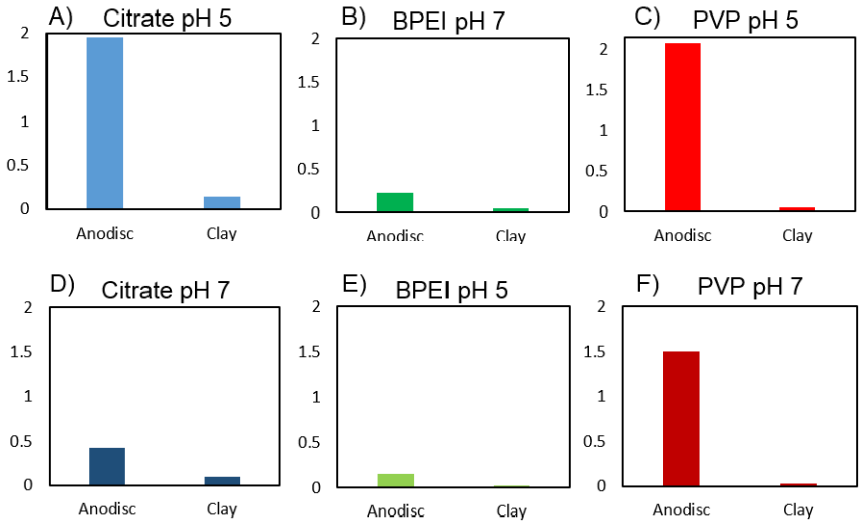

Figure 5-7: Comparison of Anodisc and Clay Based Filter Ag Attachment Densities (mg Ag/g filter)for comparable final suspension phase Ag concentrations.

The drastic difference in Ag attachment is, in part, due to the point of zero charge of the clay filters being much lower than that of the Anodiscs. As a result, at both pH 5 and 7, the clay filter has a negative surface charge where the Anodisc was positive at pH 5 and negative at pH 7. The only conditions where the clay filter and particles have opposite sign surface potentials is for BPEI Ag NPs. However, either due to different boundary condition assumptions and/or steric interactions, it has been demonstrated that BPEI is unfavorable for attachment regardless of the sign of the charge on the filter. The clay filters are also more chemically complex. They contain many more elemental constituents than the Al_2O_3 membranes (Table 2-1) that alter the structure of the surface and effect the configuration of available Ag NP deposition sites and surface roughness.

The steric effect of the BPEI Ag NP is not the only explanation for lack of affinity to the clay water filters. A test using positively charged silica NPs was conducted where the silica NPs were stabilized using amine groups grafted to the surface that do not impart steric stabilization. When compared to negatively charged silica NPs, the amine stabilized silica had an attachment density over twice as large (Figure 5-8). However, compared to the attachment of Ag NPs to the Anodiscs, the values were still very low.

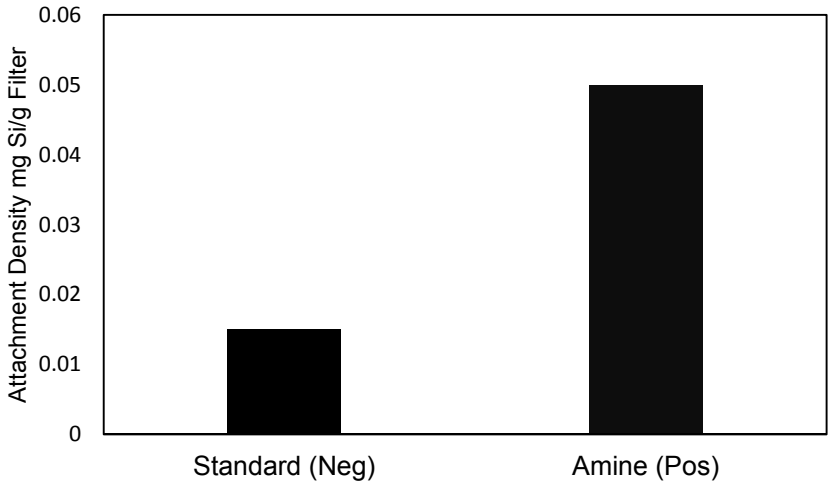

Figure 5-8: Comparison of Negatively Charged and Positively Charged (no sterics) Si NP Attachment Densities for Clay Filters.

CONCLUSIONS

- Typical Lewis acid-base interaction energies are not likely to be large enough in magnitude to effect the deposition of Ag NPs to ceramic water filters. This conclusion was reached on the basis of data from the literature, and so no effort to directly measure these interaction energies was made in this research, but would be interesting to obtain in the future.

- Steric interactions are a reasonable explanation for the BPEI Ag NPs repulsion from the membranes. At a measured stabilizer thickness of 10 nm, very few segments of BPEI need to be attached to the surface to render the energy barrier the highest out of all the Ag NPs tested.
- The value selected for the Ag-Ag Hamakar constant plays a significant role in predicting if particles are more attracted to each other or the membrane. For values of the Hamakar constant less than 18×10^{-20} J, the particles are attracted to each other more favorably than the membrane for when the particle and membrane have the same sign surface charge. This "competition" diminishes the attachment density on the membrane and magnifies differences in deposition between same sign particle-filter and opposite sign particle-filter interactions.
- Membrane material was found to play a substantial role in the deposition of all types of Ag NPs. Future work should investigate the relationship between membrane properties such as surface roughness and surface area to the attachment capacity of Ag NPs.
- To improve the attachment of Ag NPs to clay based filters future work could also investigate the effectiveness of coupling the nanoparticle to the ceramic through use of (3-Aminopropyl)triethoxysilane (APTES). APTES is commonly used to silanate microscope coverslips (Curry et al., 2005). Lv et al. (2009) demonstrated that it is possible for the nitrogen in APTES to coordinate with Ag, while the other end attaches to ceramic via Si-O-Si bonds.

Chapter 6: Multilevel Modeling of Retention and Disinfection Efficacy of Silver Nanoparticles on Ceramic Water Filters

INTRODUCTION

The objective of this research is to understand how variations in synthesis methods of Ag NPs affect both the release of Ag from ceramic water filters (CWFs) and disinfection efficacy. This study links experimental data collected at a CWF factory with multilevel statistical modeling to answer if there is a significant difference in the: a) rate of Ag lost, b) initial amount of Ag lost, c) Ag lost for rainwater vs. dugout water (a local surface water source), and d) total coliform removal. Compared to other statistical analysis techniques, multilevel models are adaptable to a wider range of datasets. For several reasons, including expense of sample analysis, faulty instrumentation, time constraints, and/or quality control measures, the number of data points in drinking water quality research can be relatively small, collected at irregular intervals, and have missing data points. To draw meaningful conclusions from the data when confronted with these challenges, it is necessary to move beyond traditional statistical techniques used in environmental engineering to more robust methods pioneered in other disciplines.

CERAMIC WATER FILTERS

Large-scale efforts to provide global access to clean drinking water have been an international priority since the Millennium Development Goals were established in 2000 (Millennium Project, 2006).

Dr. Paola Passalacqua advised the statistical portion of the work performed in this chapter.

One household water quality intervention that has been particularly well received for its ease of use, cultural acceptance, and effectiveness is CWFs. After Hurricane Mitch hit Honduras in 1998, the organization Potters for Peace began widespread distribution of the CWF technology. Potters for Peace estimates that 46 independent organizations (in 18 different countries) produce variations of their CWF design (Potters for Peace, 2015).

Filters are made from local earthenware clays and a combustible material, such as sawdust or rice husks, which is burned out during the firing process, thereby leaving a porous structure. CWFs, which typically hold approximately 10 L of water in the pot, filter water at average rates of 1-5 L/h when the filter is clean and the feed water is not highly turbid. Water is then stored in an encased plastic receptacle with a tap until used (Figure 6-1).

Figure 6-1: Typical Ceramic Water Filter. Pure Home Water 2014 AfriClay Filter and Safe Storage Container.

Researchers (Ren et al., 2013) have found CWFs are 3-6 times more cost-effective at reducing waterborne diarrheal illness than centralized water treatment

systems. In the same study, they also found CWFs positively impact human health because they contribute lower particulate matter emissions over the course of their lifecycle than centralized water treatment and distribution systems. Through a meta-analysis focused on cost and aversion of disability adjusted life years (DALYs), CWFs have also been shown to yield a larger health impact (reduction of diarrhea) over lower cost household water treatment interventions such as chlorination and solar disinfection (Clasen and Haller, 2008).

Many CWF factories paint or dip the filters in Ag NPs solutions to provide disinfection. Numerous researchers have demonstrated that Ag is effective at inactivating bacteria in solution (AshaRani et al., 2009; Auffan et al., 2009; Carlson et al.,2008; Eckhardt et al. 2013; El Badawy et al., 2011). Previous studies have also established that filters painted with Ag NPs provide increased bacterial removal versus bare filters (Bielefeldt et al. 2009; Oyanedel-Craver and Smith, 2008; PATH, 2012). However, some of these studies found a rapid loss of the Ag resulting in reduced disinfection efficacy after multiple batches of dirty water. Previous studies that focused on the Ag applied to CWFs did not consider the synthesis method for the Ag NPs, despite there being a wide variety of techniques/molecules used to control the NPs' shape and size and research suggesting toxicity is related to the surface charge of the Ag NPs (El Badawy et al., 2011). It is unknown how different stabilizing molecules used in the production of Ag NPs affect attachment and detachment of the Ag to the ceramic, and as a result the effectiveness and lifespan of the water filter. This study is the first of its kind to

investigate the effect of molecular stabilizing agents on Ag retention and disinfection efficacy on CWFs.

MATERIALS AND METHODS

The data used for this work were collected during field work at Pure Home Water (PHW), a filter factory located in Tamale, Ghana. Filtration experiments were performed on 15 filters divided into five different treatment scenarios (three filters each for four different types of Ag NPs and three filters without Ag as a control for the bacterial portion of the work). To quantify filter effectiveness and lifespan, bacterial removal and total Ag concentrations (nanoparticle and soluble Ag in the same measurement) were monitored in the filtered water at 4-6 different time points (volumes of filtered water). Further, the experiments were performed using two different water sources: stored rainwater and water from a local surface water source called a dugout.

NPs Synthesis & Characterization

Four types of Ag NPs were used in this study. Polyvinylpyrrolidone (PVP), branched polyethylenimine (BPEI), and citrate stabilized Ag NPs were synthesized at The University of Texas at Austin (USA) and transported to PHW. The fourth type was purchased by PHW from Argenol Laboratories (Zaragoza, Spain). The colloidal Ag from Argenol is routinely applied by PHW to the filters prior to distribution. It is stabilized by a casein molecule. Transmission electron microscope (TEM) images of the various particles were taken to confirm that the different particle types were of a similar size (Figure 6-2). Analysis of multiple images using the software ImageJ found the average diameters for BPEI, Citrate, PVP, and PHW NPs were 10, 8, 8, and 7 nm and the

standard deviations were 5, 6, 5, and 4 nm, respectively. The molecular structures of the stabilizing molecules for the particles used in these experiments are also provided in Figure 6-2.

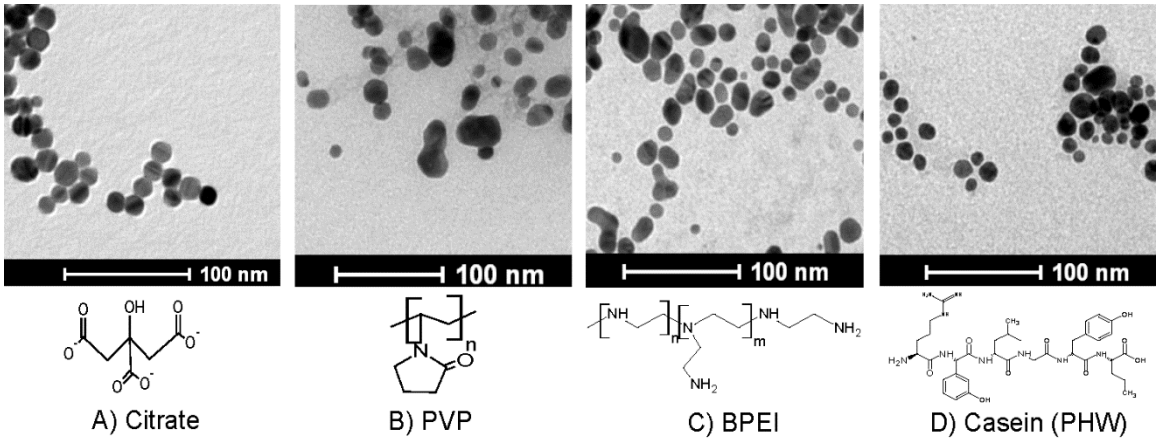

Figure 6-2: TEM Images of Ag NPs and Molecular Structure of Stabilizing Agents taken shortly after synthesis at UT Austin (A-C) and of PHW's purchased Ag NPs (D) after return from field work.

The PVP and BPEI-stabilized Ag NPs were synthesized by adding an equal volume of 3 mM Ag nitrate ($AgNO_3$) dropwise into an iced, stirred 6 mM sodium borohydride ($NaBH_4$) solution. After the full contents of the $AgNO_3$ were integrated, either 40K PVP was added to make a 0.2% PVP solution, or 1,800 Dalton BPEI was added such that the final concentration of BPEI was 0.5 g/L. Subsequently, the solutions were centrifuged and decanted multiple times to clean and concentrate the NPs. The citrate-stabilized Ag NPs were synthesized according to Gorham et al. (2012) with several modifications. The prescribed synthesis method specifies bringing 400 mL of water to a rapid boil, adding 1.69 mL of a 58.8 mM $AgNO_3$ solution with 2.92 mL of a 34 mM sodium citrate solution, and dropwise addition of 2 mL of a 100 mM $NaBH_4$. Instead of these specific volumes,

all quantities were multiplied by 10. The original method also prescribes stirring for 30 minutes at a slow boil, turning off the hot plate, and allowing to cool until room temperature, but for this work the solution was boiled rapidly over 10 hours in order to concentrate the solution before cooling to room temperature.

Citrate, PVP, and BPEI were selected intentionally due to their differences in stabilization mechanism/molecular functional groups. The citrate molecule stabilizes the Ag NPs via electrostatic interactions with hydroxyl groups, whereas PVP stabilizes the Ag NPs via repulsive steric forces imparted by the polymer chains. BPEI combines electrostatic stabilization via the charged amine functional groups with steric stabilization. Citrate and PVP are also the most widespread stabilizing agents reported in the literature (Tolymat et al., 2010). Further, the surface charge at natural water conditions (pH 7-9) for all of these particles vary (Figure 6-3). The zeta potential measurements were made using particles synthesized in our laboratory and a Malvern Zetasizer; for these measements, the ionic strength was held constant at 10 mM and pH varied using concentrated HNO_3 and NaOH. PVP and citrate are negative (and differ in magnitude by

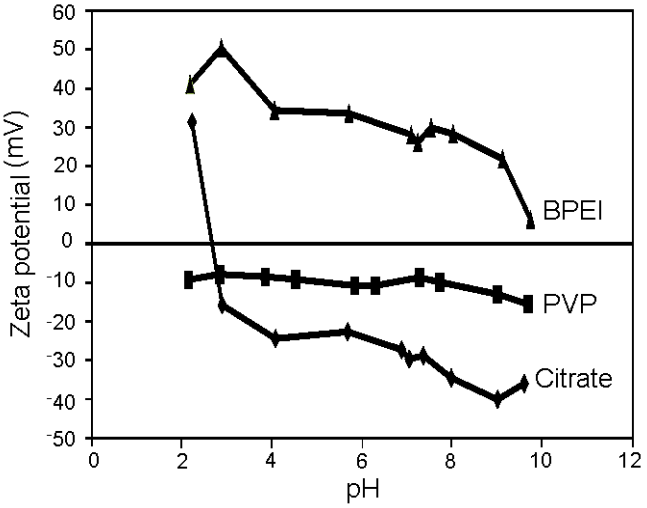

Figure 6-3: Effect of Stabilizing Molecule on Ag NP surface charge for Ag NPs synthesized at UT Austin. Zeta potential measurements were made using a Malvern Zetasizer. Ionic strength was held constant at 10 mM using KNO_3 and pH varied using concentrated HNO_3 and NaOH.

up to 4.5 times), whereas BPEI has a positive charge. The surface of the clay filter is expected to be negatively charged throughout the pH range investigated.

Ag Application

The Ceramics Manufacturing Working Group (2011), an organization of filter researchers and manufacturers assembled by the US Centers for Disease Control, recommends that 64 mg of Ag be applied to each filter by brushing on 302 mL of a 211 mg/L solution. A follow-up study commissioned by PATH (2012) applied 0.003 mg/g, 0.03 mg/g, and 0.3 mg/g (mass of Ag per mass of filter disks). This study found no significant difference in bacterial inactivation for the filters with 0.003 mg/g or 0.03 mg/g applied, but a significant difference in bacterial inactivation between the 0.003 mg/g and 0.3 mg/g filters. In the study reported herein, the filters' mass at PHW ranged from 2.6 to 3.4 kg and 0.018 mg of Ag were applied per g of filter. This amount was selected to balance both practice (Ceramics Working Group, 2011), new recommendations (PATH, 2012), and practical constraints (transporting solutions from the US). The Ag NPs were applied via brushing where two thirds of the solution volume was painted on the interior surface of the filter and the remaining volume was applied to the exterior surface of the filter. After painting, the filters were allowed to dry for one day before the filtration experiments.

Filtration Experiments

Prior to Ag application, the 15 filters were tested for flowrate and baseline total coliform removal with 3 filters for each Ag NPs treatment (Figure 6-4). Flowrates ranged from 3.1 L/hour to 4.1 L/hour when tested with rainwater. Rainwater was used throughout the course of the study for five of the filters (one in each Ag treatment group). The rainwater contained very low levels of coliforms so that, prior to Ag application, the filtered water experienced a slight increase in coliforms in some filters. The other ten filters were fed surface water from a nearby dugout.

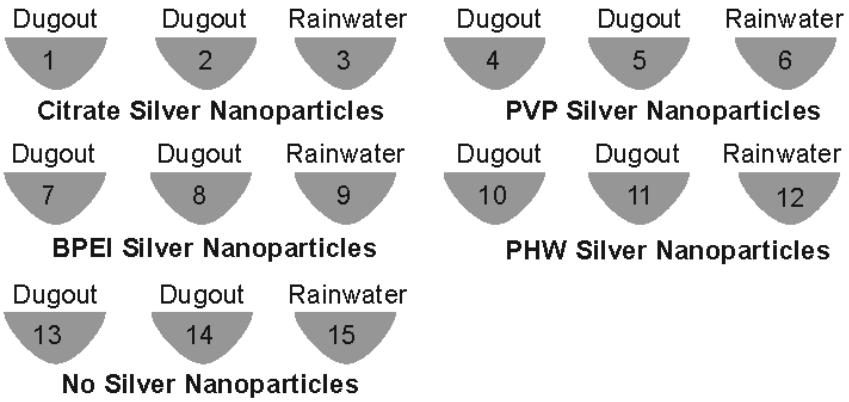

Figure 6-4: Filtration Experimental Setup. Experimental division of filters by water type and Ag type

The dugout water filters achieved an average total coliform removal of 93% prior to Ag application and 99% removal of total coliforms after Ag application. After the filters were painted with the different Ag NPs solutions, water samples were collected at 1, 3, 10, and 30 liters (L). Flowrates were substantially reduced for these filters because of the large particle loading in the dugout water (roughly reduced to 0.5 L/hour for turbid water). As a result contact times between the Ag and the water were variable in these experiments. Filters tested using rainwater had a shorter contact time than filters tested

using rainwater. Since a constant flowrate could not be maintained, the water loaded into the CWFs was tracked to collect samples at distinct volumes of water filtered. The fifth and sixth data points were at somewhat different volumes depending on the flowrate of each particular filter, but were typically near 50 and 100 L. Filtered water samples were collected in triplicate for each sampling volume. One of the samples was run in triplicate for coliforms. The total coliform counts were determined using 3M coliform/*E. coli* petrifilms and stored in an incubator at 35 ˚C. Coliform counts were performed after 24 hours and *E.coli* after 48 hours of plating the samples. The remaining water samples were kept protected from light and transported back to UT-Austin for Ag analysis where they were measured in triplicate using an Agilent ICP-OES. Low concentration samples were measured on an Agilent 7500ce Quadrupole ICP-MS.

Multilevel Model

Multilevel statistical models (also commonly referred to as hierarchical, random-coefficient, covariance component models, or mixed effects models) are pervasive in the social sciences. Over the last two decades, multilevel models have been used in educational research to better estimate parameters and perform significance testing for data structures that exhibit nesting. In addition to the education sector, fields such as demography, physical therapy, and epidemiology have made use of multilevel analysis for simultaneous examination of the effects of group-level and individual-level variables (Raudenbush, and Bryk 2002; Kwok et al., 2008, Diez-Roux, 2000, Entwisle et al, 1986).

During drinking water treatment studies, such as filtration research, data for particular parameters are repeatedly collected over some period of time (*i.e.*, longitudinal

data). The classic method for analyzing longitudinal data, a repeated measures ANOVA, requires the time points to be identical for all subjects, cannot handle missing data, and makes unrealistic assumptions about the residual covariance matrix. As a result, Type I errors (false positives) are often inflated and the power to detect treatment or covariance effects is diminished. Another traditional method used to examine longitudinal data, time series analysis, requires long strings of observations (Box et al., 2013). Multilevel modeling is a necessary tool for answering the research questions in this study because the data set is small/has missing data points, is clustered by Ag treatment, and measured longitudinally (therefore exhibiting dependence between time points).

The standard approach to multilevel modeling involves first fitting an unconditional model and then a conditional model. Since dependence is often observed between time points for longitudinally measured data, the unconditional model has an explanatory variable in level one that accounts for time (in this study volume of water filtered), but does not contain any explanatory variables in the second level. The unconditional model establishes baseline statistics used for evaluating "improvement" of subsequent level two models that do integrate explanatory variables to explain variation. As such, inclusion of one or more explanatory variables at level two is then referred to as the conditional model. The conditional model explores whether variation in intercepts and slopes of individual subjects is related to the explanatory variables (in this study, Ag type and water type). In the social sciences, this approach of including time in level one of the unconditional model is typically referred to as "growth curve modeling." Since Ag is removed from the filters in this study, growth terminology is avoided during

descriptions but maintained in defining the equations and reporting the results to keep the signs of estimates consistent with conventions in the literature. The following models were defined to assess the differences in Ag and water type on the retention of the Ag and the effectiveness at removing the bacteria (removal simultaneously referring to straining due to the filter pores and inactivation due to the Ag):

Unconditional Model

Level 1: $Ag_{ij} = \beta_{0j} + \beta_{1j}Volume_{ij} + r_{ij}$ (6-1)

Level 2: $\beta_{0j} = \gamma_{00} + u_{oj}$ (6-2)

$\beta_{1j} = \gamma_{10} + u_{1j}$ (6-3)

Reduced: $Ag_{ij} = (\gamma_{00} + \gamma_{10} Volume_{ij}) + (u_{oj} + u_{1j}Volume_{ij}) + r_{ij}$ (6-4)

Conditional Model

Level 1: $Ag_{ij} = \beta_{0j} + \beta_{1j}Volume_{ij} + r_{ij}$ (6-5)

Level 2: $\beta_{0j} = \gamma_{00} + \gamma_{01} AgType_j + \gamma_{02}WaterType_j + u_{oj}$ (6-6)

$\beta_{1j} = \gamma_{10} + \gamma_{11} AgType_j + \gamma_{12}WaterType_j + u_{1j}$ (6-7)

Reduced:

$Ag_{ij} = (\gamma_{00}+\gamma_{01} AgType_j + \gamma_{02}WaterType_j + \gamma_{10} Volume_{ij} + \gamma_{11} AgType_jVolume_{ij}$

$+\gamma_{12}WaterType_jVolume_{ij}) + (u_{oj} + u_{1j}Volume_{ij}) + r_{ij}$ (6-8)

Ag represents the natural log of the Ag concentration in μg/L (and represents log base 10 reduction values for the bacterial removal analysis), Volume is the natural log of liters of water filtered, AgType refers to four different treatment scenarios for the Ag lifespan

tests (BPEI-Ag, PVP-Ag, Citrate-Ag, and PHW-Ag) and five different scenarios for the bacterial removal tests (BPEI-Ag, PVP-Ag, Citrate-Ag, and PHW-Ag, plus a control of no Ag). Note, it is conventional to use the word "rate" when referring to the slope terms in the model. Since flowrate was not held constant during the course of the experiments, volume was used as the independent variable. However, the conventional terminology of rate is still utilized throughout the discussion with the recognition that volume corresponds to a length of time of usage of the filters. The *proc mixed* function in the commercial software package SAS version 9.2 was used for this analysis and restricted maximum likelihood was used as the parameter estimation method. Sample code is found in Appendix C. Several statistical computing programs are capable of fitting this type of model including, but not limited to, HLM and MLWIN and can be selected according to interface preference and availability.

Bacterial removal is commonly assessed in two different ways: percent removal and log reduction values (LRV). LRV are the log (base 10) of the ratio of the number concentration of coliforms before filtration to the number concentration of coliforms after treatment. "No growth" on the petrifilm media is reported as <1 colony forming unit (CFU) per mL. The model requires numerical inputs so zero was used for the "no growth" condition. However, the log of zero is undefined so, if the filters remove all of the coliforms (to the detection limit of 1 CFU/mL), then the LRVs cannot be determined. For these situations, LRV were assigned to be the total value of the influent coliforms (since it removed all of the coliforms). Influent concentrations varied based on the day that the water was collected from the dugout, so a low LRV does not necessarily mean

worse treatment. Both percent removal and LRV were investigated in the model, but the assumptions (discussed in the next section) were violated for the percent removal case, so ultimately LRVs were used for evaluating bacterial removal. Although not the case for all filters, the majority of filters had similar influent values for each sample of filtered water. This similarity allows us to compare bacterial removal effectiveness in relation to the different NPs coatings on the filters.

Assumptions

Multilevel modeling assumes several key data characteristics (Raudenbush and Bryk, 2002), including the following:

- Level one residuals are independent, homoscedastic, and normally distributed with mean 0 and variance σ^2.
- Level two random effects are independent over level two units, homoscedastic, and multivariate normally distributed with mean 0 and covariance matrix T (i.e., random effects are independent across level two units but can be correlated within a level 2 unit).
- Level one residuals are uncorrelated with level two random effects and vice versa, and level one and level two predictors are uncorrelated with level one residuals and level two random effects (independent).

Not all of these assumptions can be empirically evaluated. The data set was evaluated using scatter plots to test linearity, histograms and quantile-quantile (QQ) plots to examine normality, and bivariate plots of residuals by predictors to test for homoscedasticity, as shown in the following sections.

Linearity

Graphical procedures were used to test for linearity. Due to observed exponential decay, a natural log transformation was performed on all of the Ag concentration and volume of filtered water data in order to produce a linear decay trend necessary for the model assumptions (Figure 6-5).

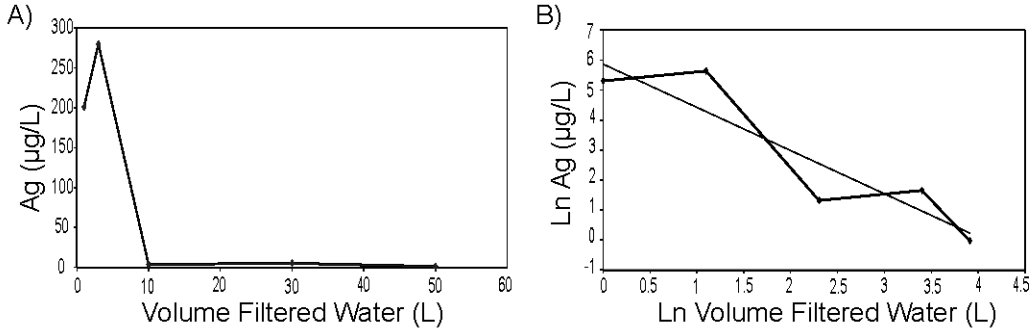

Figure 6-5: Typical Ag Release and Linearization: Example with Filter 10 PHW Ag, Dugout Water. Raw data are in Figure 6-5A and Ln transformation of the data and how it is used in the model are in Figure 6-5B.

In general, percent coliform removal values for all the filters yielded a flat line (Figure 6-6a). LRVs varied more, sometimes increasing and sometimes decreasing, depending heavily on the influent water characteristics on the day of testing (Figure 6-6b).

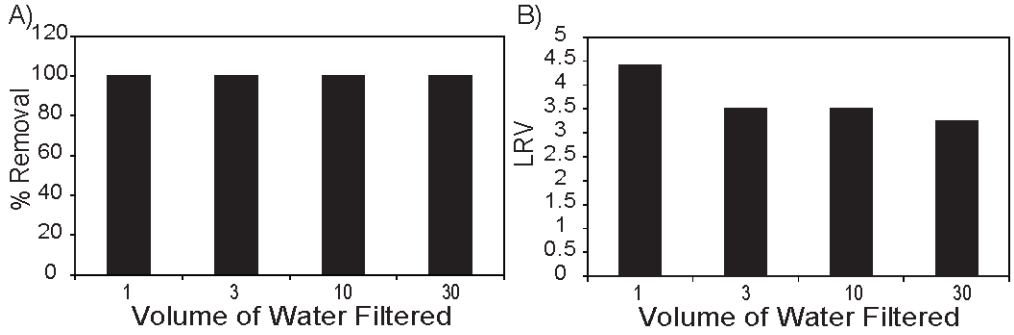

Figure 6-6: Example Total % and LRV Coliform Removal: Filter 7 with BPEI Ag, Dugout Water. Figure 6-6A and 6-6B show the same coliform results, but A is presented in terms of percentage removal and B in terms of log reduction values (LRV)

Normality

Histograms and QQ plots were examined for both levels of the models. A probability plot correlation coefficient (PPCC) test for normality was also conducted for each scenario (Filliben, 1975). For the Ag model, the critical values for a 0.05 significance level were 0.980 for level one (n=62) and 0.926 for level two (n=12). With a PPCC equaling 0.996 for level one, and PPCC values equaling 0.977 (slopes) and 0.962 (intercepts) for level two, the Ag model upheld the normality assumption (Figure 6-7).

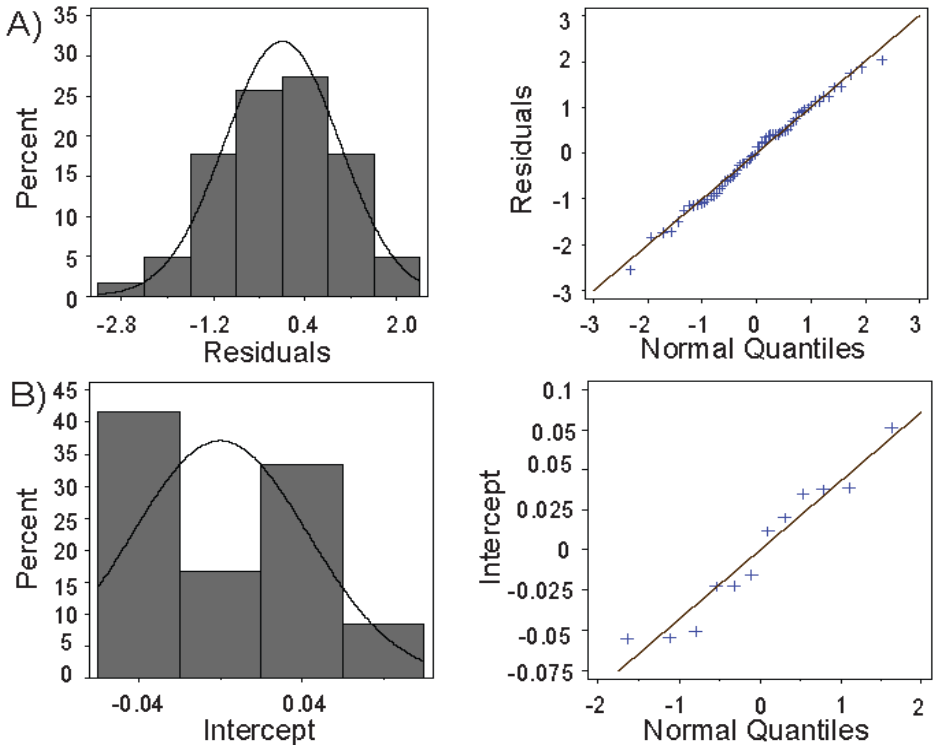

Figure 6-7: Ag Conditional Model: Level One and Level Two Normality Tests. Part A, the top graphs, show histograms and qq plots for level one residuals. Part B, the bottom graphs, shows an example histogram and qq plot for the level two residuals. These graphs correspond to the random portion of the intercepts (u_{oj} in equation 6-6)

Similar plots were produced for the bacterial removal model using both percent total coliform removal and LRVs as indicators of treatment effectiveness.

For the bacterial model, the critical values for a 0.05 significance level were 0.978 for level one (n=56) and 0.937 for level two (n=15). For percent removal, the QQ plots strayed substantially from a 45 degree line (Figure 6-8a) at level one and had a PPCC value of 0.664, and at level two a PPCC value of 0.929 (slopes) and 0.919 (intercepts). When LRVs were used, the PPCC value improved substantially at level one and was 0.990 (Figure 6-8b). Using LRVs, the level two PPCC values were 0.681 (slopes) and 0.971 (intercepts). Ultimately, LRVs were used for the bacterial analysis instead of percent removal values with recognition that, in the small data set, the slope values at level two do not perfectly adhere to the assumption normality assumption. A larger data set would be necessary to confirm the actual trend in the population.

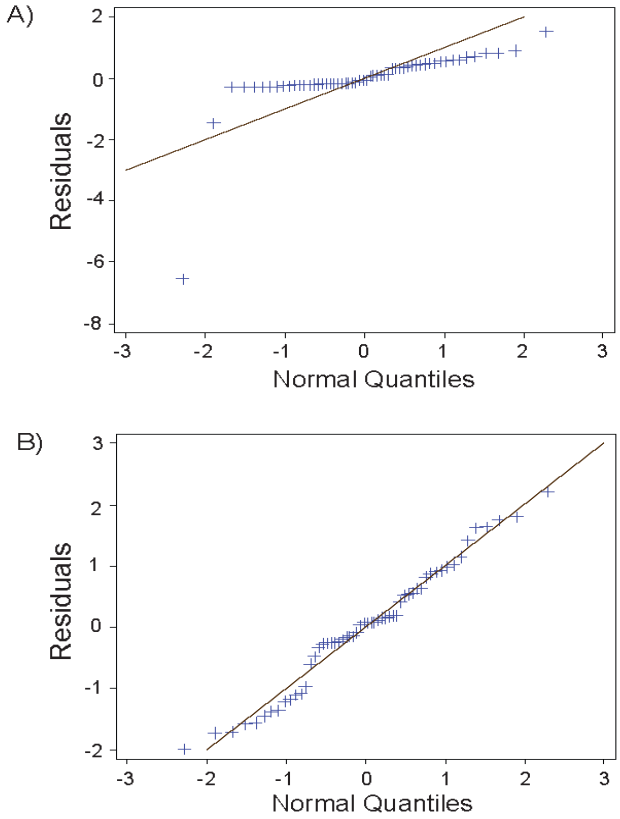

Figure 6-8: Total Coliform Percent Removal and Log Reduction Value QQ Plots of Level One Residuals. Part A, the top graph, visually demonstrates how percent removal of total coliforms fails the assumption of normality. By adhering more closely to a straight line, part B, the bottom graph, shows how log reduction values better fit a normal distribution.

Independence

Scatter plots of the residuals by explanatory variable were examined for the Ag and bacteria models at both levels. Example Ag level one plots are shown in Figure 6-9. The graphs containing predicted values and filter number on the abscissa did not contain a discernible pattern of residuals and had equal scatter above and below zero (Figure 6- 9 a and b). This result indicates that the independence assumption held. The plots containing LnVolume on the abscissa are banded, indicating that the residuals are time

dependent (Figure 6-9c). An observed banded trend, in both the conditional and unconditional models, reinforces the utility of using a multilevel model where independence of the repeated measure is not a prerequisite.

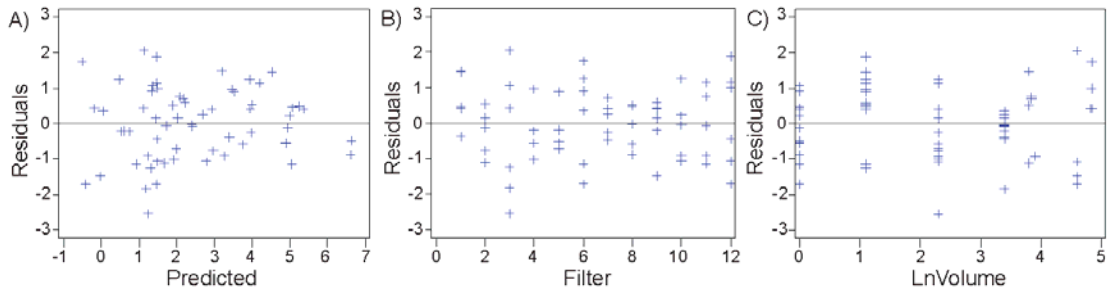

Figure 6-9: Ag Conditional Modal Bivariate Scatter Plots. Example plots of visual test for independence. Part A contains the residuals for the Ag conditional model associated with level one and parts B and C contain the residuals associated with level two of the Ag conditional model.

RESULTS

The coefficient estimates, standard error, and hypothesis test results for the unconditional Ag model (no explanatory variables at level two) are presented in Table 6-1. In the fixed effects portion of the table, the standard error terms for both initial status and mean growth rate are very small, resulting in large t ratios and low p values (<0.001). These results indicate that, on average, neither the initial Ag released nor the rate of release are zero in the population. That is, Ag is coming off the filter. Since the first volume of water was coded as zero in the data set, the estimates tell us that on average 62 µg/L of Ag were initially removed from the filters ($e^{4.14}$) and the rate of loss was 2.03 µg/L ($e^{0.71}$). In the random effects portion of the results table, the variance component in the initial status, 2.84, indicates that the initial amount of Ag released is fairly variable between filters as compared to the rate of loss of Ag, which was not as variable at 0.11.

The level one error term, 2.55, represents the average unexplained variation within the repeated measures of a particular filter, and the p-value indicates there is significant variation that cannot be explained even after controlling for the effect of volume of water filtered. Typically, continuation to a conditional model (explanatory variables at level two) is pursued when a significant amount of variation in the random effects is unexplained. The rule of thumb is to consider a p-value that is <0.05 as signifying that the variance component is statistically significantly different than zero. Based on the results of the unconditional model for this data set, we do not expect that the inclusion of explanatory variables (i.e., Ag type and water type) at level two will explain the variation in the rate of Ag loss (u_{1i}) (because there is not a large amount left to explain), but might reduce the variance for the initial status and level one error.

Table 6-1. Ag Unconditional Model Estimates

Fixed Effects	*Estimate*	*Standard Error*	*t Ratio*	*p Value*
Mean initial status, γ_{00}	4.14	0.60	6.85	<0.001
Mean growth rate, γ_{10}	-0.71	0.16	-4.42	<0.001
Random Effects	*Variance Component*	*Standard Error*	*Z Value*	*Pr Z*
Initial Status, u_{oi}	2.84	1.87	1.52	0.06
Growth rate, u_{1i}	0.11	0.12	0.87	0.19
Level-1 error, r_{1i}	2.55	0.57	4.46	<0.001

The model results for the conditional Ag model (Ag type and water type as explanatory variables at level two) are summarized in Table 6-2. It displays parameter estimates and significance values much in the same manner of Table 6-1, but in this table the estimates are made according to each type of Ag and water. It is important to note

that the coefficient estimates will change depending on the particle or water type coded as the baseline for comparison. In this case, the PHW Ag NPs and rainwater scenarios were selected as the zero reference since core research questions were if the factory should consider using a different type of Ag NPs (one that is retained longer) or if the dugout water affects retention. These choices allow the p values for the other Ag and water types to be interpreted as being significantly different, or not, from the currently used scenario. F statistics for fixed effects are also contained in Table 6-2. This parameter and corresponding significance test is for the explanatory variables as a whole. It tells if Ag type or water type has an effect on the initial status and rate of Ag loss, but does not indicate which type of Ag or water is responsible. The standard errors are larger than the estimates for most of the different types of Ag, indicating that there is no statistically significant relationship between initial Ag release and Ag type or between the continued loss of Ag and Ag type (this is also reflected in the large p-values). On the other hand, the p-values and related parameters in Table 6-2 indicate a significant effect of water type.

Table 6-2. Ag Conditional Model Estimates

Fixed Effects	*Estimate*	*Standard Error*	*t Ratio*	*p Value*
Model for initial status, β_{0i}				
INTRCPT2, γ_{00}	1.42 (w=1.77; s= 3.78)	0.85 (w=0.58; s=1.31)	1.72 (w=3.04; s=2.89)	0.13 (w=0.01; s=0.02)
AgType,γ_{01}			*F-Value: 1.38*	*Pr>F: 0.3249*
BPEI	1.56	0.97	1.61	0.15
Citrate	-0.04	0.97	-0.04	0.97
PVP	-0.12	0.98	-0.12	0.90
PHW	0	-	-	-
WaterType, β_{02}			*F-Value: 25.31*	*Pr>F: 0.0015*
Dugout	3.62	0.72	5.03	0.0015
Rainwater	0	-	-	-
Model for growth rate, β_{1i}			*F-Value: 20.06*	*Pr>F: <0.0001*
INTRCPT2,γ_{10}	-0.08	0.32	-0.26	0.7950
AgType,γ_{11}			*F-Value: 0.97*	*Pr>F: 0.41*
BPEI	-0.44	0.39	-1.12	0.27
Citrate	0.11	0.39	0.28	0.78
PVP	-0.40	0.41	-0.98	0.33
PHW	0	-	-	-
Water Type, γ_{12}			*F-Value: 6.79*	*Pr>F: 0.01*
Dugout	-0.74	0.29	-2.61	0.01
Rainwater	0	-	-	-
Random Effect	*Variance Component*	*Standard Error*	*Z Value*	*Pr Z*
INTRCPT2, u_0	0 (w=0; s=3.61)	- (w= -; s=2.58)	- (w= -; s=1.40)	- (w= - ;s=0.08)
Volume slope, u_1	0.05 (w=0.03;s= 0.14)	0.13 (w=0.09;s=0.17)	0.34 (w=0.37; s=0.81)	0.37 (w=0.36; s=0.21)
Level-1, r	2.34 (w=2.43; s = 2.53)	0.49 (w=0.51; s=0.58)	4.76 (w=4.79; s=4.40)	<0.0001 (w & s =<0.0001)

The conditional model defined in Equation (6-8) contains both water type and Ag type as explanatory variables. However, the model was also run in SAS separately using water type and Ag type individually as level two explanatory variables. The results for the fixed effects led to similar conclusions as the combined model except for the significance testing of initial status, INTRCPT2, γ_{00}, and the random effects results. These values have been included in parenthesis in Table 6-2 to aid in the discussion of the proportion of variance accounted for by each variable individually. The "w" notation indicates the results for water type and the "s" notation for Ag type when run as the only explanatory variable at level two.

The LRV bacterial unconditional model (the only explanatory variable is volume at level one) is summarized in Table 6-3.

Table 6-3. LRV Total Coliform Unconditional Model Estimates

Fixed Effects	*Estimate*	*Standard Error*	*t Ratio*	*p Value*
Mean initial status, γ_{00}	1.95	0.53	3.66	0.0026
Mean growth rate, γ_{10}	-0.21	0.16	-1.33	0.19
Random Effects	*Variance Component*	*Standard Error*	*Z Value*	*Pr Z*
Initial Status, u_{oi}	2.45	1.58	1.55	0.06
Growth rate, u_{1i}	$2.8* 10^{-18}$	-	-	-
Level-1 error, r_{1i}	2.34	0.51	4.49	<0.0001

The mean initial status tells us that, when considering all filters, on average the filters had a 1.9 LRV. The variance component for initial status (2.45) under the random effects portion alludes to variation between filters. The fixed effects results indicate a significant difference in initial bacteria removal, but not in their rate of removal with time. Logically, the variation in growth rates is very small as good removal is expected after Ag application.

The results of the LRV bacterial conditional model (water type and Ag type as explanatory variables at level 2) are contained in Table 6-4. As with the Ag release model, water type is significant (p-value for dugout water compared to rainwater is 0.0025). As a whole, the estimates for Ag types do not indicate a significant difference in bacterial deactivation when compared with the no Ag control, except in the case of one type of Ag, BPEI-Ag. It has a p-value = 0.04 when being compared to LRV of the filters without Ag. Like Table 6-2, Table 6-4 includes results in parenthesis in the random effects section that report values when the model was run with one explanatory variable at a time in level two.

Table 6-4. LRV Bacteria Conditional Model Estimates

Fixed Effects	*Estimate*	*Standard Error*	*t Ratio*	*p Value*
Model for initial status, β_{0i}				
INTRCPT2, γ_{00}	-1.71	0.86	-1.98	0.08
AgType,γ_{01}			*F-Value: 1.73*	*Pr>F: 0.23*
BPEI	2.73	1.12	2.43	0.04
Citrate	1.50	1.03	1.45	0.18
PVP	2.00	1.14	1.76	0.11
PHW	0.89	1.03	0.87	0.41
noAg	0	-	-	-
WaterType, β_{02}			*F-Value: 17.28*	*Pr>F:0.0025*
Dugout	3.31	0.80	4.16	0.0025
Rainwater	0	-	-	-
Model for growth rate, β_{1i}			*F-Value: 1.04*	*Pr>F: 0.31*
INTRCPT2,γ_{10}	-0.26	0.33	-0.77	0.45
AgType,γ_{11}			*F-Value: 0.75*	*Pr>F: 0.56*
BPEI	0.07	0.49	0.14	0.89
Citrate	0.62	0.46	1.34	0.19
PVP	-0.22	0.55	-0.40	0.69
PHW	0.38	0.46	0.84	0.41
noAg	0	-	-	-
Water Type, γ_{12}			*F-Value: 0.32*	*Pr>F: 0.5762*
Dugout	-0.20	0.35	-0.56	0.58
Rainwater	0	-	-	-
Random Effect	*Variance Component*	*Standard Error*	*Z Value*	*Pr Z*
INTRCPT2, u_0	$3.08* 10^{-34}$ (w=$2.66*10^{-34}$; s=2.93)	- (w= - ; s=2.36)	- (w= - ; s=1.24)	- *(w = - ; s=0.11)*
Volume slope, u_1	0 (w = $2.286 *10^{-53}$; s= 0)	-	-	-
Level-1, r	2.38 (w=2.29 ; s = 2.37)	0.56 (w=0.48;s= 0.56)	4.25 (w=4.81;s= 4.24)	<0.0001 (w & s =<0.0001)

DISCUSSION

Silver

The results indicate that Ag type is not a factor in the initial and sustained loss of Ag from the ceramic filters, but water type plays a large role. Dugout water removed significantly more Ag as compared to a baseline of rainwater (p-values = 0.0015 and 0.012 for intercept and slopes, respectively). Initially 37.46 μg/L ($e^{3.62}$) more Ag comes off a filter when treating dugout water, and the sustained release is on average 1.09 μg/L ($e^{0.08}$) more when using dugout water versus rainwater.

Limited water quality characteristics were measured during the fieldwork. The average pH of the dugout water was 6.8 versus 7.5 for the rainwater. The average total dissolved solids (TDS) of the dugout water was 19 mg/L versus 60 mg/L for the rainwater. The dugout water was visually substantially more turbid than the rainwater. Alkalinity and hardness were measured using an idip, which is essentially a photometer and so is inappropriate for turbid water samples. The rainwater had an average value of 3.75 mg/L as $CaCO_3$ for hardness and 21.75 mg/L as $CaCO_3$ for alkalinity. Since chloride complexes with Ag, chloride concentrations were measured in ten water samples from different days (five dugout and five rainwater) using ion chromatography. The results for the dugout water were 1.25, <1.00 (three samples), and 1.03 mg/L chloride. The results for the rainwater were 1.31, 1.34, 1.37, 2.36, and 1.39 mg/L chloride. Chloride concentrations were low compared to typical surface waters, but had a higher molar concentration than silver (~70 times higher). However, since the chloride concentrations were similar in magnitude for both types of water, but water type made a significant

impact on Ag removal, Ag-Cl complexation is not expected to be a driving force in Ag NP removal. It is likely that the dugout water was harder than the rainwater and higher in NOM, leading to complexes between the Ag and the multivalent cations and/or NOM and thus removing the Ag from the filter at a greater rate for the dugout water than the rainwater.

Comparison of the random effects results in Tables 6-1 and 6-2 show that the addition of explanatory variables at level two reduces the variation, both between filters and within an individual filter. When both water type and Ag type are controlled for, variation between filters decreased from 2.84 to 0 (100% reduction), the variation between the slopes went from 0.11 to 0.05 (56%) and the variation within a filter run still unaccounted for went from 2.55 to 2.34 (8%). When only water type is considered the between variation of intercepts is reduced by 100%, slopes by 70%, and within 5%, whereas for Ag the intercept variation is increased by 27%, increased slopes by 32%, and reduced within by 1%. Due to the increases in variation when Ag is used as an explanatory variable, and its lack of significance in the estimate testing, the final conditional model should only include water type as an explanatory variable.

Bacteria

The model for LRVs of bacteria was coded to compare water type and Ag type differences to filters without any Ag on them. The unconditional model results in Table 3 indicate that the rate of bacterial removal over multiple batches of dirty water for the filters was not significantly different, but the initial removal values ("initial status," or the intercepts) were significantly different. The results for the conditional model (Table 6-4),

which uses water type or Ag type as explanatory variables, agree with the unconditional model showing neither the slope nor intercept parameters are significant factors in the LRV trend over time. However, for the initial removal, BPEI is significantly different than the filters without Ag (p-value = 0.04), albeit only slightly. BPEI was the only stabilizing agent with a positive surface charge. Bacteria (Poortinga et al., 2002) and the filter material both have a negative surface charge at the pH values of the dirty water. This charge difference would contribute to a better initial attraction between the BPEI-Ag and the bacteria and filter. After a substantial volume of water has passed through the filter, there might not be a surface attraction effect because the Ag is coated with natural organic matter (presumably with negative surface charge (Zheng et. al, 2009) found in the feed water.

Several challenges with the LRV model should be appreciated. First, only a very small amount of data was used for this model (56 observations).

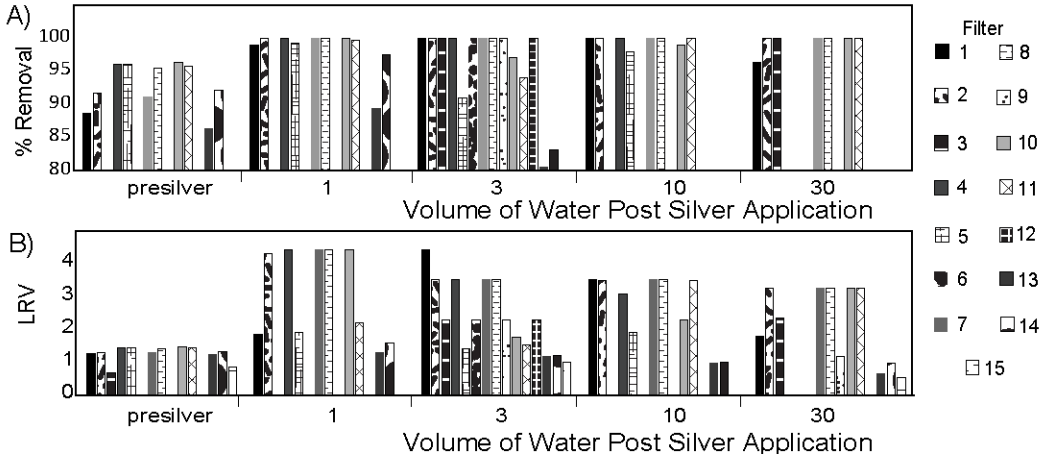

Figure 6-10: Total Coliform Removal by Filter. Part A is in terms of percentage removal and part B is in log reduction value. The filter numbers increase sequentially from left to right within each volume category. Blank spaces represent either missing data or a lack of influent coliforms (common for filters where rainwater was used).

Secondly, the model indicates no significant difference in LRV for filters coated with Ag and those without Ag. Other researchers have found that a certain percentage of filters are less effective at disinfection despite being coated with Ag (Brown, 2007, Lantagne, 2001), so this result is certainly a possibility. Histograms by filter for LRV and percent removal of total coliforms (refer to Figure 6-4 for a key to water and Ag type for each filter number) are shown in Figure 6-10.

Included in these figures are data from filtration test runs on each filter prior to Ag application to determine a baseline removal in total coliforms (not included in the SAS model). Note, every filter is not included at each volume point for several different reasons. First, the influent rainwater samples did not always contain coliforms to remove. Secondly, some of the filters increased the coliform counts, and finally several data points did not conform to analytical standards (too numerous to count) so were not included in the figure. However, the figure gives a strong visual trend that the LRV increased after Ag application. The influent coliform values for the pre Ag test were higher than the influent for the other tests, so low starting values are not the cause of this trend.

CONCLUSIONS

Multilevel modeling using the SAS *proc mixed* function was a useful tool for assessing differences in Ag release from the filters. The model assumptions of linearity, normality, and independence were observed after a natural log transformation of the data for Ag concentration and bacterial removal. The model estimates indicate that Ag type

does not have a significant effect on initial amount released or release rate, but water type does significantly affect the loss of Ag.

Interpretation of the bacterial removal effectiveness was substantially more challenging using this procedure. The assumptions did not hold for the percent removal of total coliforms so LRVs were used. Even using LRVs, linearity for all the filters was questionable for some of the individual filters as well as normality at level two for the slopes. The multilevel model did highlight an initial, significant difference in initial bacterial removal for BPEI-Ag coated filters versus filters without any Ag on them; this distinction was not clear when the data were clustered together. However, this result needs to be confirmed with a larger dataset. The challenges of this analysis highlight the need to develop a standardized field bacteria testing protocol in which influent bacteria levels do not vary across the period of the test. Future work should be done to link the Ag release data to the bacterial removal rates to determine if disinfection occurs in the plastic storage container (via released Ag) or within the filter (via attached Ag).

The findings of this work reveal three practical recommendations for ceramic pot filter factories. First, it should be emphasized during filter distribution that households should not drink the first 10L of water that are filtered because the Ag concentration is likely to exceed the World Health Organization safe limit for Ag. Secondly, in this study the type of Ag NP did not have an effect on its attachment to the filter, so continuing to purchase Ag NPs from industrial suppliers, is a good option. Finally, to aid in future research of the lifespan of the Ag coatings on the filters, it would be useful to analyze and document the pH and hardness of the water source in each community where filters are

distributed. This information could be used to simulate realistic Ag removal conditions on laboratory scale filters that can be highly controlled and monitored.

Due to missing data values, irregular time intervals, and a small data set, significance testing would not have been possible using traditional statistical methods. This study demonstrates the value of multilevel modeling in drinking water treatment research, particularly in the development of new materials.

Chapter 7: The Effects of Water Chemistry on the Desorption and Dissolution of Silver from Ceramic Water Filters

INTRODUCTION

The objective of this chapter is to gain a deeper understanding of how specific water characteristics affect the lifespan of ceramic water filters with different types of Ag NPs adhered to the surface. Data in Chapter 6 indicates that water type has a significant impact on initial and sustained release of Ag NPs from ceramic water filters. However, the water at Pure Home Water was not thoroughly characterized due to the challenging field conditions. This chapter analyzes filtration experiments that replicate field work in Ghana, but were performed in a controlled laboratory setting where select water characteristics could be maintained.

Several others have studied the influence of water characteristics on release rates of NPs and many of their conclusions agree. Quevedo and Tufenkji (2009) found that monovalent salts had a higher propensity to remove carboxyl terminated quantum dots, whereas the release rates with divalent salts were slower. Stewart (2010) used a quartz crystal microbalance with dissipation monitoring to study the release of casein stabilized Ag NPs from silicon wafers. The Ag NPs were purchased from the same company used by many filter factories, including Pure Home Water in Ghana. Stewart found that the ionic strength (I) (150 mM as $NaNO_3$ and 150 mM as $Ca(NO_3)_2$), turbidity (51 NTU Kaolin particles), and pH (4.8 and 9.3) had very little effect on the removal of the Ag NPs from the surface of the silicon wafer. On the other hand, high release rates were observed in the presence of high concentrations of organic compounds (tryptic soy broth) and in

the presence of sodium hypochlorite (8.8 mg/L sodium hypochlorite (8.0 mg/L as Cl_2) removed 90% of silver from the surface of the silica wafer). More recently, Rayner et al. (2013) investigated how three water chemistry conditions (150 mg/L NaCl, 150 mg/L $CaCl_2$, and 5 mg/L TOC as Humic Acid) effected the bacterial removal performance of ceramic water filters using the same Ag NPs. They found that differences in water chemistries did not have a significant effect. In granular media filtration research, Kim (2014) observed that significant detachment of captured Ag NPs occurred by lowering ionic strength from 100 mM to 0.025 for monovalent salts, but that detachment was insignificant when lowering ionic strength from 10 mM to 0.025 mM $Ca(NO_3)_2$. He also observed that the presence of NOM enhanced detachment. From these studies, it is expected that hard water will cause lower initial, but longer release rates of Ag NPs and that NOM will enhance detachment. To the author's knowledge, the detachment of Ag NPs with different stabilizing agents from ceramic water filters has never been investigated.

MATERIALS AND METHODS

Membrane Preparation

Citrate, PVP, and BPEI stabilized Ag NPs were prepared according to procedures outlined in Chapters 3 and 6. Anodisc membranes were used for this portion of the work, rather than the clay filters, because very low attachment densities occurred when the clay filters were soaked in all of the different types of Ag NP suspensions. Although many properties of the clay and Anodisc filters are different, the pH values of the waters were below the point of zero charge for the Anodiscs. As such, the surface charge of the clay

filters in Ghana were likely similar to the Anodiscs during these experiments. The Anodisc ceramic membranes were prepared for filtration tests by soaking the filters in 100 mg/L Ag NP suspensions for 3 hours (a detailed procedure is outlined in Chapter 3) and at pH values that promoted deposition (pH 5 for Citrate and PVP, and pH 7 for BPEI). After soaking, the membranes were allowed to dry overnight. Filters were carefully inserted into 13 mm polypropylene Swinnex filter holders (EDM Millipore). Use of flat silicone gaskets on either side of the Anodiscs and zip ties on all tubing connections was essential for preventing leakage during filtration or cracking the filter upon tightening the holders.

Filtration

Two base test waters were used in these experiments. Water A represents a relatively hard water, as found in many places in the central U.S. (including Austin), with a hardness (added as magnesium nitrate salt) of approximately 200 mg/L as $CaCO_3$ (i.e., 4 meq/L), alkalinity of approximately 200 mg/L as $CaCO_3$ (added as $NaHCO_3$), and a pH of 8.3 (adjusted using KOH when necessary). Water B represents water, similar to those found in the northeast U.S. This water had no hardness but an ionic strength of 10 mM (added as $NaNO_3$), an alkalinity of approximately 50 mg/L as $CaCO_3$ (added as $NaHCO_3$), and a pH of 6.5 (adjusted using concentrated HNO_3). NOM was also added to these base water recipes during experiments with filters covered with citrate Ag NPs. For this portion of the work, waters A and B were spiked with 5 mg/L Humic Acid (equivalent to 2.6 mg/L as DOC) to represent typical NOM in water systems. Suwannee

River Humic Acid from the International Humic Substances Society was used. Table 7-1 summarizes the filtration experiments that were performed.

During filtration, the water was stored in covered beakers and a multichannel peristaltic pump was used to flow water through multiple filters at a flow rate of 0.5 mL/min. Samples were collected until silver stopped, or nearly stopped, detaching/dissolving from the filters.

Table 7-1: Summary of Filtration Experimental Factors

Filters		**Test Waters**	
Membrane Material	***Ag NPs***	***Base Recipe***	***Additions***
Al_2O_3	Citrate BPEI PVP	Water A (Hardness = 200 mg/L $CaCO_3$ as $Mg(NO_3)_2 \cdot 6H_2O$ Alk = 200 mg/L $CaCO_3$ as $NaHCO_2$) Water B (I = 10 mM as $NaNO_3$ Alk = 50 mg/L $CaCO_3$ as $NaHCO_2$)	NOM (5 mg/L Humic Acid) *Only tested for Citrate-Ag NPs

Multilevel Model

A multilevel model was built according to the procedures detailed in Chapter 6, but with one difference. The model in this chapter controls for interactions between silver type and water type because these interactions were found to be significant. Also, of note, in Chapter 6 because the first sample was taken at 1L and, since ln 1 is equal to zero, this allowed for interpretation of the intercept data as being the average Ag concentration in the first sample. For the work presented in this chapter, the initial sample volume was either 5 mL or 10 mL (1 mL could not be used due to sample volume constraints for the ICP Ag concentration analysis). As a result, intercept values should be

interpreted as a theoretical "back" estimate to instantaneous release from the filter, not as a concentration that was ever measured.

Development of the final conditional model involved stepwise addition of explanatory variables at level two. The model was run multiple times to evaluate the amount of variation explained through use of the following four factor combinations: 1) water type, 2) Ag type, 3) water type and Ag type (with and without interactions) 4) water type, Ag type, and amount of Ag remaining on the filter. NOM was not included as a water type in the analysis because not all types of Ag NPs were tested with NOM. A separate analysis of the significance of NOM with citrate Ag NPs covered membranes was performed.

Verification of Assumptions

The assumptions of linearity, normality, and independence were evaluated to assure a multilevel model was appropriate for this data set. Graphical procedures were used to test for linearity. Figure 7-1 demonstrates that linearity holds after a ln- ln transformation. The raw values for total Ag in the effluent of the filtered water are contained in Appendix D, along with graphs of the data grouped by silver and water type. To test for normality, histograms and QQ plots were examined for both levels of the model and the normality assumption

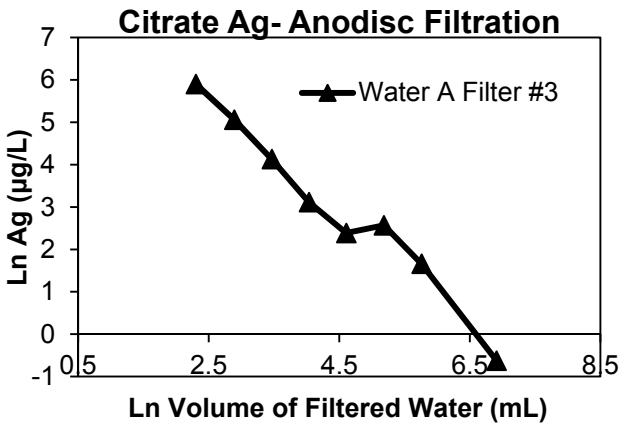

Figure 7-1: Example of Linearity of the Ag Detachment from Anodisc with Citrate-Ag NPs Deposited.

upheld for this model. To test for independence, scatter plots of the residuals by explanatory variable were examined. For example, the graph containing predicted values by filter number on the abscissa did not contain a discernible pattern of residuals and had equal scatter above and below zero, indicating that the independence assumption also holds for this model (Figure 7-2).

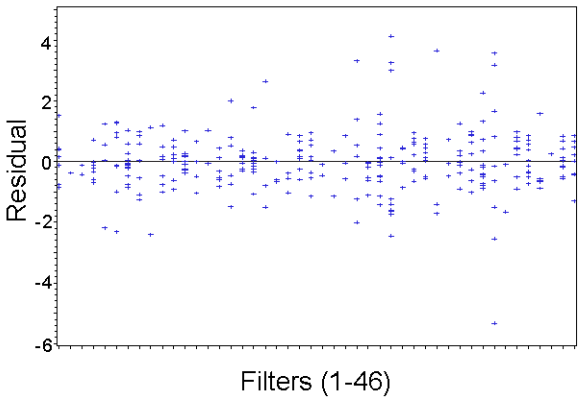

Figure 7-2: Example of Residuals by Predicted Values Scatter Plot to Test Independence

RESULTS

Ag Detachment

The measured concentration of Ag released from the filters, as a function of volume of water filtered, is displayed in Figure 7-3. From the graphs alone it is difficult to discern significance differences in Ag release. Note, only filters that did not crack during the experiments were plotted and used during the statistical analysis. As a result, the numbering of the filter data in Figure 7-3 is not sequential for all water conditions.

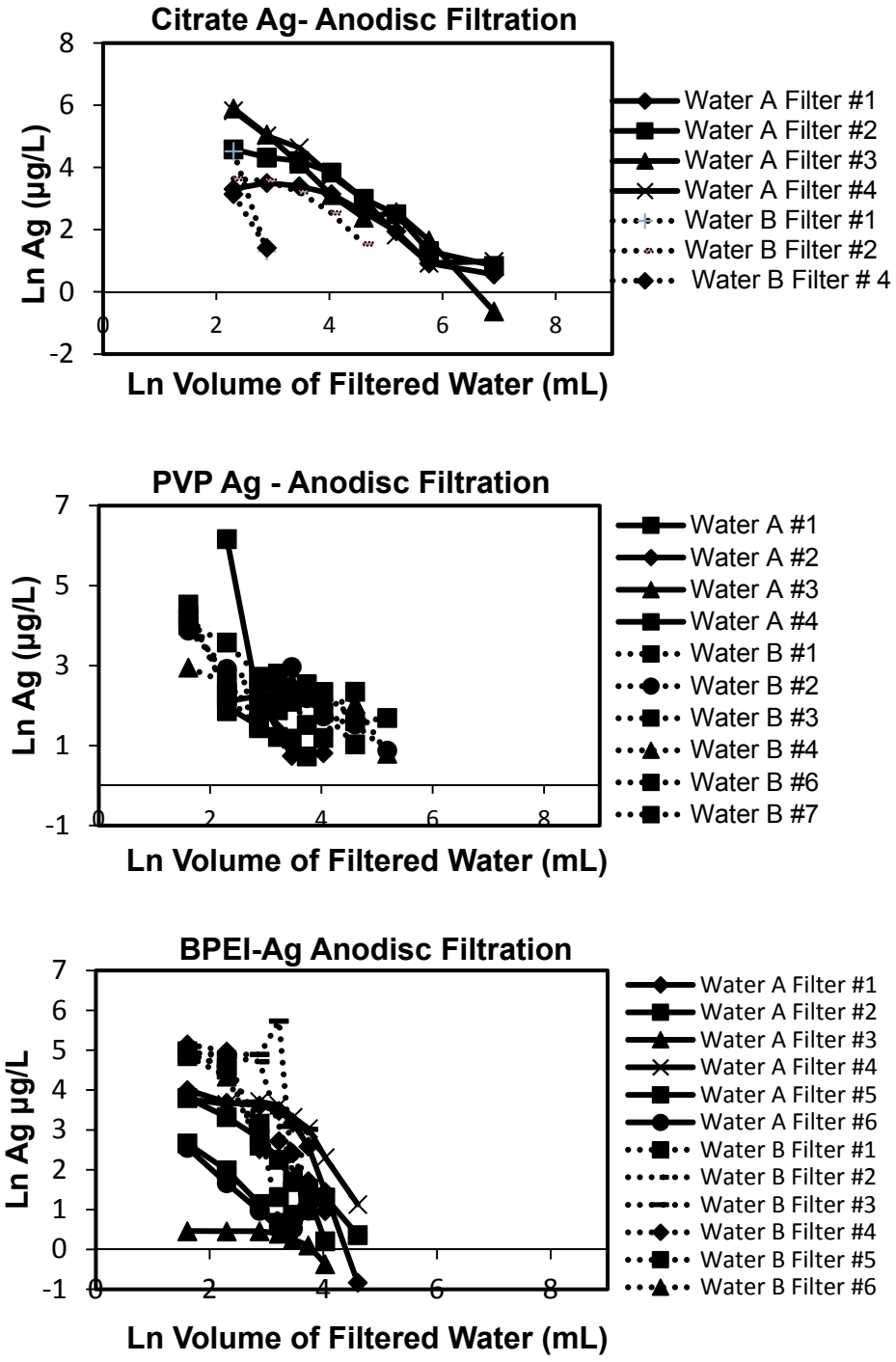

Figure 7-3: Ag Detachment from Anodiscs

Unconditional Model

The resulting coefficient estimates, standard error, and hypothesis tests for the unconditional model are presented in Table 7-2. The p values of less than 0.05 in the fixed effects portion of the table indicate that Ag is coming off the filter and the estimates tell us that the average "initial" amount is 360 μg/L and average rate of loss is 2.85 μg/L, ignoring Ag or water type groupings. The results also indicate that, prior to the addition of explanatory variables at level two, a significant amount of unexplained variation is present. This variation is larger for the "initial" release of Ag between filters (variance of 3.67 with p-value 0.0025), but is also significant for the rate of loss of the Ag (variance of 0.22 with p-value of 0.0014) and for the unexplained variation with the repeated measures of a particular filter (0.73 with a p-value of <0.0001).

Table 7-2. Unconditional Model

Fixed Effects	*Estimate*	*Standard Error*	*t Ratio*	*p Value*
Mean initial status, γ_{00}	5.89	0.39	15.27	<0.0001
Mean growth rate, γ_{10}	-1.05	0.10	-10.01	<0.0001
Random Effects	*Variance Component*	*Standard Error*	*Z Value*	*Pr Z*
Initial Status, u_{oi}	3.67	1.31	2.80	0.0025
Growth rate, u_{1i}	0.21	0.09	2.28	0.0014
Level-1 error, r_{1i}	0.73	0.08	8.70	<0.0001

Conditional Model

The goal of including explanatory variables at level two is to reduce the variance components associated with differences between filters ("initial" release and Ag loss with volume of water filtered). In this work, four different parameters were evaluated for their

role in explaining differences in the release of Ag NPs. Table 7-3 summarizes how variation is accounted for as specific variables are added to the model. Table 7-3 also notes, in the "Significant Fixed Effects" column, which variables, as a group, are considered significant for explaining how Ag releases from the filters (a F test < 0.05 was used for the significance criteria). Inclusion of only water or only Ag does not indicate significance of either factor. However, when both Ag and water are added, the model identifies that it is important to include Ag type. Finally, through the inclusion of the interaction term in the model, the role for water type is identified as an important parameter. As a whole, F tests for fixed effects indicate that if we fail to control for both of the factors at the same time, their individual significance is missed.

Table 7-3. Explanatory Variable Effect on Variance

Parameter	***Random Effects***		***Z Value***	***Pr Z***	***Significant Fixed Effects***
	Variance Component	***Standard Error***			
1) Water Only					
Initial Status, u_{oi}	3.66	1.30	2.80	0.0026	LnVol
Growth rate, u_{1i}	0.21	0.09	2.26	0.0120	
2) Silver Only					
Initial Status, u_{oi}	3.36	1.28	2.62	0.0044	LnVol
Growth rate, u_{1i}	0.21	0.10	2.21	0.013	
3a) Water and Silver					
Initial Status, u_{oi}	2.79	1.17	2.39	0.0085	AgType, LnVol
Growth rate, u_{1i}	0.17	0.09	1.93	0.027	
3b) Water and Silver with Interaction					
Initial Status, u_{oi}	2.42	1.075	2.25	0.012	AgType, LnVol, WaterType*AgType
Growth rate, u_{1i}	0.16	0.093	1.91	0.028	

A fourth scenario, not displayed in the table, was also run to evaluate the impact of variations that stem from membrane preparation, since different types of Ag NPs deposit more or less favorably on the Anodiscs. For this case, the amount of Ag left on the filter was measured using ICP-OES at the end of the filtration run. Since none of the filters come close to losing all of the deposited Ag NPs (on average 79% of silver was estimated to remain on the filters, σ=16%), and the loss rates are within the same order of magnitude, larger final amounts of Ag NPs on the filter should correlate to greater deposition during the membrane preparation process. Estimates of the initial Ag using two alternative methods: a) calculated using final suspension phase concentrations from the application of the Ag NPs to the membrane, in conjunction with the deposition curves presented in Chapter 4 and b) integration of the Ag release curve added to the final amount of Ag on the filter were also considered as explanatory variables for membrane preparation. Not surprisingly, these small values of Ag calculated using methods a) and b) were inconsistent with each other. On average, the BPEI Ag NP method (a) estimated 55% (σ=19%) less initial Ag on the membrane than method (b). For citrate Ag NPs, method (a) estimated an average initial amount of Ag on the membrane that was 11% (σ=52%) larger than method (b). For PVP Ag NPs method (a) gave an initial amount 21% (σ=31%) larger than method (b). The discrepancies in these values likely stems from the Ag sampling resolution from the filtration tests and scatter in the deposition data in Chapter 4. Regardless, the parameter estimates for a model that controls for membrane preparation are not included in the table because they failed to significantly reduce variation between slopes, intercepts of different filter runs or within the data of one filter

run. This result seems reasonable since Ag was not completely removed from any of the filters.

Final Conditional Model

The conditional model that provided the most reduction in variance of the slopes (25%) and intercepts (34%) includes both Ag type and water type at level two and a term to account for different interactions between the water and type of Ag NP. The final reduced form of this model is:

$$\begin{aligned} LnAg_{ij} = (&\gamma_{00}+\gamma_{01}\,SilverType_j+\gamma_{02}WaterType_j+\gamma_{03}SilverType_jWaterType_j \\ &+\gamma_{10}\,LnVolume_{ij}+\gamma_{11}\,SilverType_jLnVolume_{ij} \\ &+\gamma_{12}WaterType_jLnVolume_{ij})+(u_{oj}+u_{1j}LnVolume_{ij})+r_{ij} \end{aligned} \quad (7\text{-}1)$$

This model allows for significance testing of how Ag type, water type, and their interactions, influence the detachment of Ag from the filters. It provides equations that can be used to predict Ag release for particular types of Ag when a particular water is being filtered. A summary of the parameter estimates and significance tests discussed in this section can be found in Appendix E.

Silver Type

Ag type was a significant factor in predicting how much Ag was "initially" removed from the membranes, but not in predicting its loss rate over time (intercept F value significance =0.033, slope intercept F value significance = 0.20). Citrate Ag NPs compared to BPEI Ag NPs, and PVP Ag NPs compared to BPEI Ag NPs do not behave significantly differently in terms of initial release for either water type. However, Citrate and PVP Ag NPs behave significantly different in water A (p-value = 0.0014) (Figure 7-

4). A much higher amount of Ag is initially removed from filters containing Citrate Ag NPs than filter containing PVP Ag NPs.

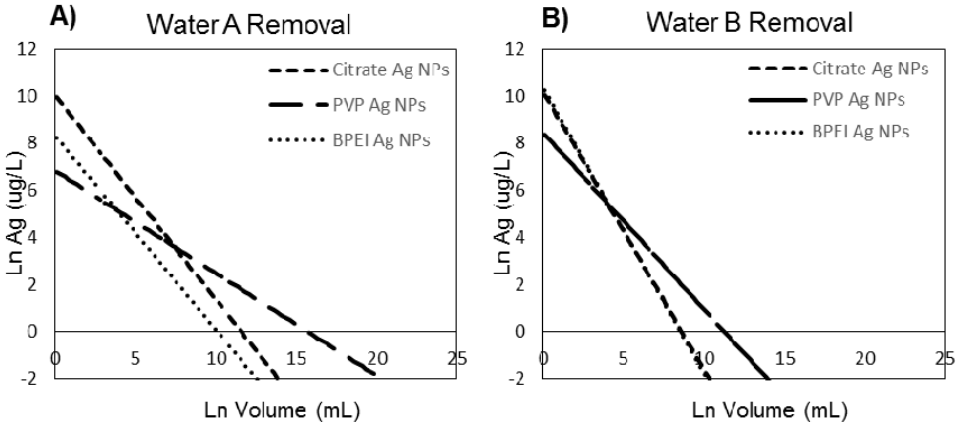

Figure 7-4: Model Estimates Demonstrating the Influence of Ag NP Type on Silver Lost for a) hard water and b) not hard water

Water Type

Water type alone is not a significant factor in predicting how much Ag is "initially" removed from the membranes (F test 0.094) or its rate of loss over time (F test 0.16). However, each type of NP does interact differently with each type of water (F test 0.012), which changes the way that the Ag is removed from the filters. Figure 7-5 visually demonstrates the different interactions with water A and B when controlling for

Ag NP type. For all of the cases, the hard water removes the Ag from the filters for longer periods of time. In Figure 7-5a, it is evident that water type does not influence the initial release of Citrate Ag NPs, whereas it does for PVP (Figure 7-5b) and BPEI (Figure 7-5c). These observations are consistent with the significance testing documented in Appendix E. For PVP and BPEI Ag NPs, during the first few hundred mL the samples have higher Ag concentrations for the water that lacks hardness. Later, samples contain higher levels of Ag for the hard water. This is consistent with the raw data (Appendix D) and reflects a "start-up" period for detachment before the constitutes in the hard water have an impact on Ag removal.

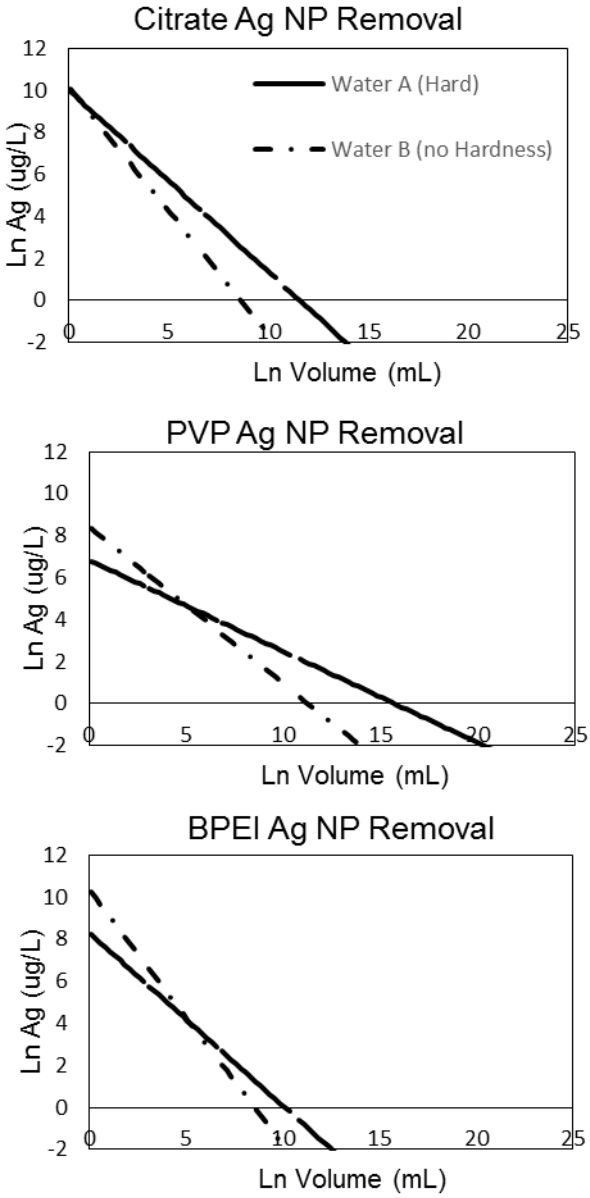

Figure 7-5: Model Estimates Demonstrating the Influence of Water Type on Ag Lost for A) citrate Ag NPs, B) PVp Ag NPs, and C) BPEI Ag NPs

Predicting Silver Release

The utility of multilevevl modeling is that it can produce a set of equations that allow for the estimation of effluent Ag concentrations for particular types of silver and influent water conditions for any sample

volume. These equations were used to create Figures 7-4 and 7-5 and are summarized in Table 7-4. They were developed by substituting the parameter estimates into Equation 7-1. It is important to remember that parameter estimates vary depending on which values are selected for the baselines. Appendix E contains the parameter estimates for all of the different water Ag NP combinations, which were necessary for developing the equations in Table 7-4. Using these equations one can solve for ln values of silver release for either water A or B for each type of Ag NP (volume should be in terms of mL). The equations capture differences in release rate of Ag, with the hard water removed the Ag for longer periods of time, and differently by particle type.

Table 7-4: Model Equations to Predict Ag NP Removal from Anodiscs at Different Water Qualities

Silver Type	Water Type	Ln Ag (µg/L)
Citrate	A	10.03LnVolume-0.87
Citrate	B	10.17LnVolume-1.18
PVP	A	6.83LnVolume-0.43
PVP	B	8.42LnVolume-0.75
BPEI	A	8.31LnVolume-0.82
BPEI	B	10.36LnVolume-1.21

NOM

The effect of water type on Citrate Ag NP detachment was tested using SAS. NOM was found to have a significant impact on the rate of release, but not the "initial" release. There is not a significant difference between the slopes for water A with NOM and water B with NOM (p-value = 0.89), but there is a significant difference between water A and the waters that contain NOM (ANOM p-value = 0.014, BNOM p-value = 0.02). There is also a significant difference between water B and the waters that contain NOM (ANOM p-value =0.006, BNOM p-value = 0.0067). Figure 7-6 contains experimental data of representative filters tested under each water condition. The NOM-containing water removes Ag for a longer period of time than the waters without NOM.

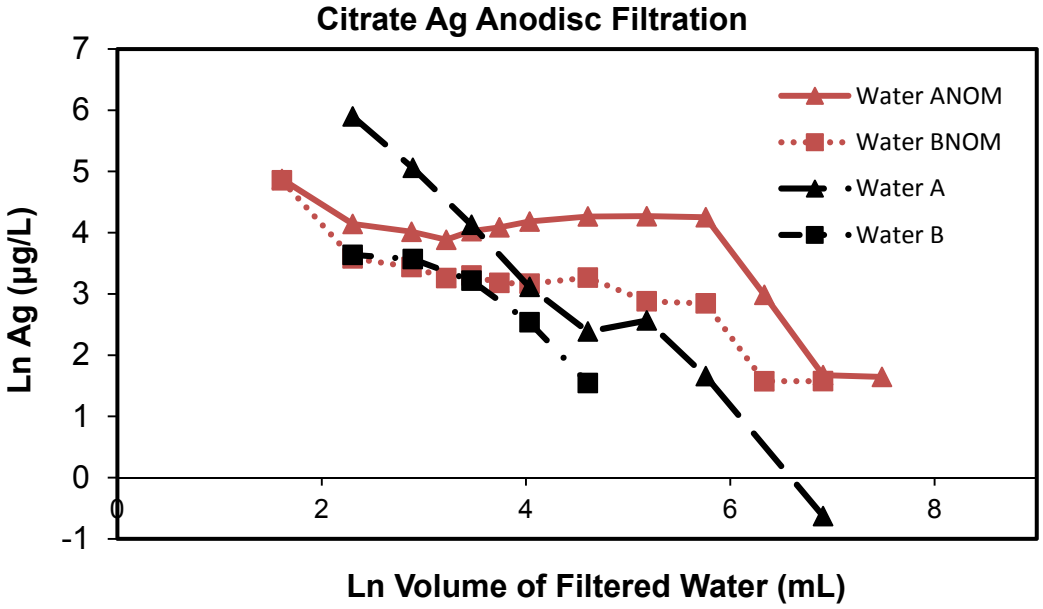

Figure 7-6: Influence of NOM on Citrate Ag NP detachment from Anodiscs

Zeta Potential

Chapter 4 highlights the significant role that the electrical double layer plays in attachment of Ag NPs to Anodiscs. It is hypothesized that differential changes to the electrical double layer, according to Ag NP type, occur due to the presence of filtration water conditions that are different than when the Ag NPs were deposited on the filter. As a result, these differential changes to the electrical double layer cause the differences in release. Table 7-5 contains zeta potential values measured by the author for the Ag NPs suspended in the same water compositions used during the filtration tests. Originally, citrate Ag NPs have a zeta potential of -23.4 mV, PVP Ag NPs -9.8 mV, and BPEI Ag NPs 33.8 mV under deposition conditions. NOM tends to produce a more negative zeta potential value for BPEI (the sign even becomes negative in water A with NOM), regardless of whether the water contains hardness. NOM produces a slightly more positive surface for both PVP and citrate Ag NPs regardless of water type. The hard water (A) produces a slightly more positive value for both PVP and citrate Ag NPs, but reduces the zeta potential for BPEI Ag NPs compared to the original deposition conditions. However, NOM plays a different role with PVP and Citrate Ag NPs. NOM increases the zeta potential when added to PVP Ag NPs and water B for citrate, but it decreases the zeta potential when added to citrate Ag NPs added to water A. This might explain why the slope of water A is significantly different for PVP Ag NPs. Differences between water A and B are likely due to the magnesium in water A providing different degrees of charge neutralization effects for PVP and citrate Ag NPs. The carbonate added in the alkalinity could also be providing some charge neutralization for the BPEI Ag NPs.

Since the Ag NPs rest on top of the Anodiscs, it is expected that the change in the Ag zeta potentials would control the initial release of Ag. However, the Ag NPs deposited do not completely cover the surface of the membrane, so it is likely that changes to the Anodisc surface potential also impact the release of Ag NPs. The membrane has a positive surface potential of 14.5 mV for citrate and PVP Ag NP deposition conditions and -24.4 mV for BPEI Ag NP deposition. Although the zeta potential of the membrane was not measured under the different water conditions, at the pH values of both water conditions, it is expected that the Anodisc will have a negative surface potential. This charge difference should lead to a greater release of citrate and PVP Ag NPs than BPEI Ag NPs because the signs of the particles and the filters switch from being opposite signs to like signs. This expectation is consistent with observations.

Table 7-5: Ag NP Zeta Potential at Filtration Water Conditions

Nanoparticle-Water	Zeta Potential (mV)
Citrate-Ag Water A NOM	-19.5
Citrate-Ag Water A	-20.1
Citrate-Ag Water B NOM	-23.0
Citrate-Ag Water B	-19.4
PVP-Ag Water A NOM	-5.1
PVP-Ag Water A	-3.8
PVP-Ag Water B NOM	-7.6
PVP-Ag Water B	-5.1
BPEI-Ag Water A NOM	-4.9
BPEI-Ag Water A	24.4
BPEI-Ag Water B NOM	10.1
BPEI-Ag Water B	19.8

CONCLUSIONS

- A multilevel model is an effective tool to estimate the release of Ag NPs from ceramic filters as a function of volume of water filtered. Equations were developed to predict the amount of Ag released for three types of Ag NPs experiencing "hard" and "not hard" water conditions each.
- Both water type (via the interaction term) and Ag type (i.e., the stabilizing chemical attached to the Ag NPs) were significant explanatory variables in explaining the release of Ag from ceramic membranes. Ag type was found to influence the initial amount released, but not the rate of Ag loss. Water Type (via the interaction term) effects both the initial release and the rate of loss over time (or volume filtered). Results agree with previous research findings that hardness and NOM prolong the release of silver over time, but have a lower initial amounts released.
- The current model should not be applied to PVP or BPEI Ag NPs for water with NOM because the only data used in creation of the NOM estimates were for citrate Ag NPs.
- Despite lower initial amounts of PVP and BPEI Ag NPs deposited on the membranes than Citrate Ag NPs the test waters without NOM did not remove all the Ag. Future work could expand the data set to include NOM for PVP and BPEI Ag NP membranes.
- Even with the inclusion of Ag type and water type, there is still a significant amount of unexplained variation in the proposed multilevel model. Future work

should focus on including more factors to level two until this variation is insignificant. Adding NOM for all types of Ag NP filters, isolating the effects of hardness and pH, and/or including a term that captures the zeta potential of the Ag and of the filter with changing water conditions are all reasonable next steps.

Chapter 8: Conclusions and Recommendations

This dissertation examined the influence of three common stabilizing agents (citrate, polyvinylpyrrolidone (PVP), and branched polyethylenimine (BPEI)) on attachment affinity of Ag NPs to ceramic water filters. Ag NPs are added to water filters to provide disinfection. The main findings and recommendations are discussed according to the three initial objectives.

1) Characterize the attachment density of Ag NPs on porous ceramic filters.

Stabilizers substantially influence the attachment of Ag NPs to ceramic water filters. Citrate-stabilized Ag NPs were found to have the highest attachment affinity to both Al_2O_3 (under conditions in which the surface potential was of opposite sign to the filter) and clay-based ceramic filters. BPEI-stabilized Ag NPs were the least favorable under all conditions. The mechanisms behind these findings are thoroughly described under objective two's conclusions, but are primarily due to an interplay between particle size, electrical double layer, and steric interactions. Attachment density can be controlled to some extent with pH, with the most drastic influence for particles that are electrostatically stabilized. The clay-based ceramic water filters experienced substantially less Ag NP deposition than the Al_2O_3 membranes. Future work should examine how filter properties, such as surface area and roughness, affect the magnitude of Ag NP deposition relative to other materials.

2) Identify the dominant interaction energies involved in Ag NP-ceramic deposition.

Chapter 4 demonstrated that the interaction between the electrical double layers plays a critical role in the attachment of NPs to flat surfaces and, in particular, that predictions of double layer interactions are sensitive to boundary condition assumptions (constant charge vs. constant potential). Experimental deposition results can be explained when using different boundary condition assumptions for different stabilizing molecules, but not when the same assumption was assumed for all three types of particles. Particle size was also demonstrated to have a varied effect on predicted deposition for BPEI stabilized particles, but not for PVP, when solely considering DLVO interactions between the particle and the membrane.

Unfavorable attachment of BPEI Ag NPs can also be explained due to steric interactions as shown in Chapter 5. Using a measured thickness layer of 10 nm BPEI, segment density distributions were calculated under different conditions. All scenarios indicated that very little BPEI needs to be attached to the surface to induce repulsion from the filter. Also, when steric forces were included, the differences between electrical double layer boundary assumptions were rendered negligible. The discussion in Chapter 5 also details how attachment density might be reduced due to particle-particle aggregation being more favorable than particle-membrane deposition. The value of the Hamaker constant used for the Ag-Ag interactions is the controlling factor. Future work should focus on how particle size changes throughout the course of deposition experiments. Particle size distributions hold the potential to provide insights into how the interplay of sterics, electrical double layer, and particle-particle interactions dominate the

deposition process at different points in time. A deeper understanding of the effects of particle size and size distribution will provide better insights into how long to soak filters for Ag NP application.

3) Describe how water chemistry affects the detachment and dissolution of Ag from ceramics.

A multilevel statistical model was built to evaluate if there was a significant difference in: a) rate of Ag lost, b) initial amount of Ag lost, c) Ag lost for water of different quality, and d) total coliform removal. For experiments performed on location at Pure Home Water, a CWF factory in Tamale, Ghana. The model results indicate that Ag type does not have a significant effect on initial amount released or sustained release rate; however, water type does significantly affect the loss of Ag. Bacterial removal effectiveness was more challenging to evaluate, but some data suggest that the BPEI Ag NPs provided improved bacterial removal.

The work in Chapter 7 at UT Austin with highly controlled water characteristics, reinforces the idea that dugout water likely contained higher levels of hardness and natural organic matter than the rainwater, which caused the Ag to release to a greater degree for dugout water. The experiments in Chapter 7 found that type of Ag NP only has a significant impact on the initial amount of PVP vs. Citrate Ag NPs lost from the filter and that the rate of Ag removal is dominated by the interactions of Ag type with water type. These interactions were observed through changes in the zeta potentials of the Ag NPs when introduced to the different water types. Changes in surface potentials result in changes to the energies of interactions describes in detail in Chapters 4 and 5.

The findings also support the recommendation to filter manufacturers that Ag type is not as important as tracking what type of water is put through the filter when estimating how much silver remains on the filter. The results of this work also suggest that Ag release diminishes before the consumption of the Ag on the filter. This trend means that any decrease in bacterial removal over the lifespan of the filter element is likely due to the Ag being inaccessible for contact with the bacteria, not due to a lack of Ag on the filter. Future work should strive to correlate lifespan to "availability" and not only Ag release and expand the data set to include more types of water and NOM for all types of Ag NPs.

The Anodiscs used in this work also represent membranes that are used for municipal treatment in developed countries. The volumes of water filtered represent approximately 14 hours (waters A and B) to over 18 days (water with NOM) of operation for a membrane unit with 25 m^2 of surface area operated at 170 L/m^2-hr. Initially, the filters release Ag at concentrations higher than the World Health Standard of 0.1 mg/L. For the water that did not contain NOM, the released silver reduces to be within regulations within the first day; however, for waters containing NOM, this excessive Ag release is an issue for some time. Other concerns for this system that were not investigated in this work, but are critical to the effectiveness of this technology are practical issues such as the loss of Ag during backwashing and cleaning procedures and loss of disinfection due to unavailability from fouling (although the Ag NPs might help reduce fouling as well). Future work should strive to understand the interplay of these critical parameters.

In conclusion, not all Ag NPs are created equal. There are many interacting and dynamic parameters that govern the attachment of Ag NPs to ceramic water filters. However, if the greatest amount of particle deposition and retention is desired, the following choices lead to the highest chances of success: a) smallest particles resistant to aggregation, b) electrostatically stabilized, c) pH value where the filter and particle have opposite sign surface potentials, d) soft water, and e) no NOM.

Appendices

APPENDIX A: DLVO MATLAB CODE

```
%This program was written by Sungmin Youn to find the size of silver nanoparticles
%stabilized by different organic ligands that provides a greater DLVO energy barrier
%than the maximum DLVO energy barrier of a 10nm(radius) citrate stabilized silver
%nanoparticle.

function [size,energy]=plotresult()
global ap zetaf zetap A
ap=0.010;          %Initial radius of silver nanoparticle BPEI in units of micro meter
zetap=0.0338;     %Measured zeta potential of particle in units of Volt
zetaf=0.0145;      %Measured zeta potential of flat plate in units of Volt
A=(5.2*10^-20);   %Hamacker constant in J
control=1;
%User can decide what assumption to use for the maximum energy barrier of the
%silver nanoparticles 1=constant charge, 2=LSA, 3=constant potential
%The program uses precalculated maximum energy barriers for each boundary condition
%assumption for citrate silver nanoparticles to compare various sizes of differently
%stabilized silver %nanoparticles. (input measured zeta values for capping agent of
%interest above)
if control==1
   cutoff=3.69E-20; %CC energy barrier of 10nm citrate Ag at pH 7
elseif control==2
   cutoff=1.06E-20; %LSA energy barrier of 10nm citrate Ag at pH 7
elseif control==3
   cutoff=7.48E-21; %CP energy barrier of 10nm Citrate Ag at pH 7
end

last=1000;      %maximum iteration

for k=1:last
   count=1;    %count
   for i=0.0001:0.0001:0.025 %separation distance in micro meter (begin:step:final)
      %this for-loop calculates DLVO energy at separation distances from 0.1nm to 25nm
      [vdw(count), edlcp(count), edlcc(count), edllsa(count)] = edlvospf(i);
      %using subroutine calculates van der Waals energy, and EDLs
      dist(count)=i;
      count=count+1;
   end
   s=dist(:)*1000; %converting separation distance to be in terms of nanometer
   %the previously selected boundary condition assumption is being used to calculate the
DLVO energy
```

```
   %value for the target condition
   if control==1
      DLVOE=vdw(:)+edlcc(:);
   elseif control==2
      DLVOE=vdw(:)+edllsa(:);
   elseif control==3
      DLVOE=vdw(:)+edlcp(:);
   end

   %checking process if the maximum energy is found
   if max(DLVOE) > 0
      if max(DLVOE) >= cutoff
         found=['The maximum energy barrier at the radius of ', num2str(ap*1000), 'nm is
', num2str(max(DLVOE)),'J, which is greater than 10nm Citrate energy barrier at pH 7'];
         disp(found)
         size=ap;
         energy=max(DLVOE);
         break
      else
         notfound=['the maximum energy barrier is still lower than the 10nm citrate
silvernanoparticles. Iteration= ', num2str(k)];
         disp(notfound)
      end
   elseif max(DLVOE) <= 0
      att=['it is always attractive at all separation, Iteration= ', num2str(k)];
      disp(att)
   end

   if k==last
      disp('not able to find the size that exceeds the citrate maximum energy barrier within
the given size range.')
      size=0;
      energy=0;
   end

   ap=ap+0.002;
   %for every cycle of the for-loop, the program increases the radius of particle by 2nm.
end
end

function [vdw,edlcp,edlcc,edllsa]=edlvospf(s)

global ap zetaf zetap A
```

```
%-------------------------defining constants-----------------------------
e=1.602*10^-19;         %in units of Coulomb
temp=298;               %in units of Kelvin
Kb=1.3806*10^-23;       %Boltzmann const in units of (m^2*kg/s^2-K)
conc=0.010;             %concentration of electrolytes in mole/L
avogadro=6.02*10^23;    %1/mol
z=1;                    %monovalent ions
er=78.5;                %relative permittivity of water
e0=8.85*10^-12;         %permittivity in vacuum in units of C^2/(J-m)
lambda=0.1; %retarded van der waals lambda=100nm;
%-------------------------------------------------------------------------

%---------------------kappa calculation-----------------------------------
kappa=sqrt((2*conc*1000*avogadro*e^2*z^2)/(er*e0*Kb*temp))/(10^9);
% above equation resulting values in units of nm^-1
kappa=kappa*1000;   % converting units to um^-1
%-------------------------------------------------------------------------

%--------zeta measurements -> surface potential -> charge-----------------
sd=0.5; %distance to the slipping plane from the surface in units of nm
%Rearranged Gouy-chapman model to solve surface potential from the measured zeta
potential values
phif=((4.*Kb.*temp)./(z.*e)).*atanh(tanh((z.*e.*zetaf)./(4.*Kb.*temp))/exp(-
kappa.*sd./1000));
phip=((4.*Kb.*temp)./(z.*e)).*atanh(tanh((z.*e.*zetap)./(4.*Kb.*temp))/exp(-
kappa.*sd./1000));
y1=z*e*phip/(Kb*temp);  %charge of particle
y2=z*e*phif/(Kb*temp);  %charge of flat pate
%-------------------------------------------------------------------------

%--------Retarded van der waals attractive force--------------------------
Evdw=((-A.*ap)./(6*s))./(1+(14.*s)./lambda);
%unit=energy (J)
%Benjamin and Lawler, 2013 (eqn 11-12)
%-------------------------------------------------------------------------

%-----------------electric double layer (constant potential)---------------
Eedlcp=(10^-6).*(pi().*e0.*er.*ap).*(2.*phif.*phip.*log((1+exp(-kappa.*s))./(1-exp(-
kappa.*s)))+(phif.^2+phip.^2).*log(1-exp(-2.*kappa.*s)));
%unit =energy (J)
%-------------------------------------------------------------------------
```

```
%-----------------electric double layer (constant charge)---------------
Eedlcc=(10^-
15).*((2.*pi().*ap.*Kb.*temp.*conc.*avogadro)./(kappa.^2)).*(y1.^2+y2.^2).*(((2.*y1.*
y2)/(y1.^2+y2.^2))*log((1+exp(-kappa.*s))./(1-exp(-kappa.*s)))-log(1-exp(-
2.*kappa.*s)));
%unit =energy (J)
%-------------------------------------------------------------------------

%-----------------electric double layer (LSA)---------------
gamma1=tanh(y1/4);
gamma2=tanh(y2/4);
Eedllsa=(10^-
15).*((128.*pi().*ap.*conc.*avogadro.*Kb.*temp)./(kappa.^2)).*gamma1.*gamma2.*ex
p(-kappa.*s);
%unit =energy (J)
%-------------------------------------------------------------------------

vdw=Evdw;          %return van der Waals interaction energy
edlcp=Eedlcp;      %return electric double layer energy(constant potential)
edlcc=Eedlcc;      %return electric double layer energy(constant charge)
edllsa=Eedllsa;    %return electric double layer energy(LSA)
end
```

APPENDIX B: EXTENDED DLVO MATLAB CODE

%This program was written by Sungmin Youn to calculate the threshold segment %density distribution required for steric forces to induce an energy barrier higher %than an energy of interest.

```
function [vdw,edlcp,edlcc,edllsa,str]=edlvospf(s)

global ap zetaf zetap Aspf phi

%-------------------------defining constant-----------------------------
e=1.602*10^-19;         %in units of Coulomb
temp=298;               %in units of Kelvin
Kb=1.3806*10^-23;       %Boltzmann const in units of (m^2*kg/s^2-K)
conc=0.010;             %concentration of electrolytes in mole/L
avogadro=6.02*10^23;    %1/mol
z=1;                    %monovalent ions
er=78.5;                %relative permittivity of water
e0=8.85*10^-12;         %permittivity in vacuum in units of C^2/(J-m)
lambda=0.1; %retarded van der waals lambda=100nm;
%-------------------------------------------------------------------------

%---------------------kappa calculation-----------------------------------
kappa=sqrt((2*conc*1000*avogadro*e^2*z^2)/(er*e0*Kb*temp))/(10^9);
% above euqation resulting values in units of nm^-1
kappa=kappa*1000;   % converting it to um^-1
%-------------------------------------------------------------------------

%--------zeta measurements -> surface potential -> charge-----------------
sd=0.5; %distance to the slipping plane from the surface in units of nm
%Rearranged the Gouy-chapman model to solve surface potential from the
%measured zeta potential values
phif=((4.*Kb.*temp)./(z.*e)).*atanh(tanh((z.*e.*zetaf)./(4.*Kb.*temp))/exp(-
kappa.*sd./1000));
phip=((4.*Kb.*temp)./(z.*e)).*atanh(tanh((z.*e.*zetap)./(4.*Kb.*temp))/exp(-
kappa.*sd./1000));
y1=z*e*phip/(Kb*temp);  %charge of particle
y2=z*e*phif/(Kb*temp);  %charge of flat pate
%-------------------------------------------------------------------------

%--------Retarded van der waals attractive force-------------------------
Evdw=((-Aspf.*ap)./(6*s))./(1+(14.*s)./lambda);
%unit=energy (J)
%Benjamin and Lawler, 2013 (eqn 11-12)
```

```
%-------------------------------------------------------------------------

%-----------------electric double layer (constant potential)---------------
Eedlcp=(10^-6).*(pi().*e0.*er.*ap).*(2.*phif.*phip.*log((1+exp(-kappa.*s))./(1-exp(-
kappa.*s)))+(phif.^2+phip.^2).*log(1-exp(-2.*kappa.*s)));
%unit =energy (J)
%-------------------------------------------------------------------------

%-----------------electric double layer (constant charge)---------------
Eedlcc=(10^-
15).*((2.*pi().*ap.*Kb.*temp.*conc.*avogadro)./(kappa.^2)).*(y1.^2+y2.^2).*(((2.*y1.*
y2)/(y1.^2+y2.^2))*log((1+exp(-kappa.*s))./(1-exp(-kappa.*s)))-log(1-exp(-
2.*kappa.*s)));
%unit =energy (J)
%-------------------------------------------------------------------------

%-----------------electric double layer (LSA)---------------
gamma1=tanh(y1/4);
gamma2=tanh(y2/4);
Eedllsa=(10^-
15).*((128.*pi().*ap.*conc.*avogadro.*Kb.*temp)./(kappa.^2)).*gamma1.*gamma2.*ex
p(-kappa.*s);
%unit =energy (J)
%-------------------------------------------------------------------------

%-------------------------------steric energy-----------------------------
%steric happend when the separation distance is between 0 and coating
%thickness
%H is the particle surface to the flate plate, which is same as s.

a=ap*1000;  %convering the given micron particle size into nanometer
delta=10;   %coating thickness (nm)
H=s*1000;   %converting the given micron separation size into nanometer

Vp=2.9;     %volume of polymer in nm^3
Vs=0.03;    %volume of solvent (water) in nm^3
kai=0.45;   %flory-huggins parameter
%phi=0.1;    %segment density distribution

if H >= delta
   Esteric=0;
   %unit=energy(J)
else
```

```
   V1=(2*pi()/3)*(1-a^3/((a+delta)^3))*((a+delta)^2)*(delta-H);
   V3=(pi()/3)*(delta-H)*(-2*delta^2+delta*H+H^2+3*a*(delta+H));
   const=Kb*temp*((Vp^2)/Vs)*(0.5-kai)*(phi^2);
   Esteric=const*V1*(V1/V3-1);
end
%-------------------------------------------------------------------------

str=Esteric;       %return steric energy
vdw=Evdw;          %return vad der Waals interaction energy
edlcp=Eedlcp;      %return electric double layer energy(constan potential)
edlcc=Eedlcc;      %return electric double layer energy(constan charge)
edllsa=Eedllsa;    %return electric double layer energy(LSA)

end

function []=plotresult()

global ap zetaf zetap Aspf phi
phi=0;    %segment density distribution initial
ap=0.01;
%Initial radius of silver nanoparticle in units of micro meter

zetap=0.0284;          %measured zeta potential of particle in units of Volt
zetaf=-0.0244;         %measured zeta potential of flat plate in units of Volt
Aspf=(5.2*10^-20);     %hamaker constant in units of Joule

[citvdw(1), citedlcp(1), citedlcc(1), citedllsa(1), citstr(1)] = edlvospf(0.005);

citcontrol=3;
%citrate pH7 at different assumption to use for energy at separation 5nm
%1=constant charge, 2=LSA, and 3=constant potential
if citcontrol == 1
   cit=-1.0196E-20+1.8856E-20;
elseif citcontrol == 2
   cit=-1.0196E-20+1.5910E-20;
elseif citcontrol == 3
   cit=-1.0196E-20+1.5465E-20;
end

last=1000;
for k=1:last

   [vdw(k), edlcp(k), edlcc(k), edllsa(k), str(k)] = edlvospf(0.005);
```

```
   tarcontrol=3;
   if tarcontrol==1
      DLVOE=vdw(k)+edlcc(k)+str(k);
   elseif tarcontrol==2
      DLVOE=vdw(k)+edllsa(k)+str(k);
   elseif tarcontrol==3
      DLVOE=vdw(k)+edlcp(k)+str(k);
   end

   if cit <= DLVOE
      found=['When segment density is ', num2str(phi), 'nm^-3, DLVO energy for BPEI
pH5  at 5nm (', num2str(DLVOE),'J) is greater than Citrate pH 7'];
      disp(found)
      break
   else
      notfound=['DLVO energy is still lower. Iteration= ', num2str(k)];
      notfound1=['DVLO energy for Citrate pH7  ', num2str(cit), ', and for BPEI at pH5 is
', num2str(DLVOE), 'at phi ', num2str(phi)];
      disp(notfound)
      disp(notfound1)
   end

   phi=phi+0.0001;

   end
end
```

%This program was written by Sungmin Youn to compare DLVO energies of %interactions of two particles with a particle and a flat plate

%particle and particle:

```
function [vdw,edlcp,edlcc,edllsa]=edlvoss(s)

global ap zetap Ass

%-------------------------defining constant------------------------------
e=1.602*10^-19;         %in units of Coulomb
temp=298;               %in units of Kelvin
Kb=1.3806*10^-23;       %Boltzmann const in units of (m^2*kg/s^2-K)
conc=0.010;             %concentration of electrolytes in mole/L
avogadro=6.02*10^23;    %1/mol
z=1;                    %monovalent ions
```

```
er=78.5;                %relative permittivity of water
e0=8.85*10^-12;         %permittivity in vacuum in units of C^2/(J-m)
lambda=0.1; %retarded van der waals lambda=100nm;
%-------------------------------------------------------------------------

%--------------------kappa calculation-----------------------------------
kappa=sqrt((2*conc*1000*avogadro*e^2*z^2)/(er*e0*Kb*temp))/(10^9);
% above euqation resulting values in units of nm^-1
kappa=kappa*1000;   % converting it to um^-1
%-------------------------------------------------------------------------

%--------zeta measurements -> surface potential -> charge-----------------
sd=0.5; %distance to the slipping plane from the surface in units of nm
%Rearranged the Gouy-chapman model to solve surface potential from the
%measured zeta potential values
phip=((4.*Kb.*temp)./(z.*e)).*atanh(tanh((z.*e.*zetap)./(4.*Kb.*temp))/exp(-
kappa.*sd./1000));
y1=z*e*phip/(Kb*temp);  %charge of particle
%-------------------------------------------------------------------------

%-----------------van der waals attractive force--------------------------
Evdw=(-Ass.*ap)./(12.*s);
%unit=energy (J)
%-------------------------------------------------------------------------

%-----------------electric double layer (constant potential)--------------
Eedlcp=(1/2).*(10^-6).*(pi().*e0.*er.*ap).*(2.*phip.*phip.*log((1+exp(-kappa.*s))./(1-
exp(-kappa.*s)))+(phip.^2+phip.^2).*log(1-exp(-2.*kappa.*s)));
%unit =energy (J)
%-------------------------------------------------------------------------

%-----------------electric double layer (constant charge)-----------------
Eedlcc=(10^-
15).*(1/2).*((2.*pi().*ap.*Kb.*temp.*conc.*avogadro)./(kappa.^2)).*(y1.^2+y1.^2).*(((2
.*y1.*y1)/(y1.^2+y1.^2))*log((1+exp(-kappa.*s))./(1-exp(-kappa.*s)))-log(1-exp(-
2.*kappa.*s)));
%unit =energy (J)
%-------------------------------------------------------------------------

%-----------------electric double layer (LSA)-----------------------------
gamma1=tanh(y1/4);
```

```
Eedllsa=(10^-
15).*(1/2).*((128.*pi().*ap.*conc.*avogadro.*Kb.*temp)./(kappa.^2)).*gamma1.*gamm
a1.*exp(-kappa.*s);
%unit =energy (J)
%--------------------------------------------------------------------------


vdw=Evdw;          %return vad der Waals interaction energy
edlcp=Eedlcp;      %return electric double layer energy(constan potential)
edlcc=Eedlcc;      %return electric double layer energy(constan charge)
edllsa=Eedllsa;    %return electric double layer energy(LSA)

end
```

APPENDIX C: EXAMPLE SAS CODE – LRV CONDITIONAL MODEL

```
/*Model*/
        proc mixed data=WORK.AnneGhanaLn covtest noclprint;
                class SilverType WaterType Filter;
                model LRVTC = SilverType WaterType LnVolume
                SilverType*LnVolume
                        WaterType*LnVolume/solution ddfm=bw outpred=pred;
                random intercept LnVolume/subject=Filter type=un  gcorr solution;
                ods output solutionr=randomeffects;
                run;
/*Level 1 Assumption Testing*/
        proc print data=pred;
                var Filter LnVolume pred resid;
                run;
        proc standard data=pred mean=0 std=1 out=standard;
                var resid;
                run;
        proc means data=standard
                var resid;
                run;
        proc univariate data=standard;
                var resid;
                histogram/cfill=DimGray normal(color=black w=2);
                qqplot/normal (mu=est sigma=est);
                run;
        proc gplot data=standard;
                plot resid*(pred Filter LnVolume)/vref=0;
                run;
/*Level 2 Assumption Testing*/
        proc print data=randomeffects;
                run;
        proc transpose data=randomeffects out=random;
                by Filter;
                var estimate;
                id effect;
                run;
        proc print data=random;
                run;
        proc univariate data=random;
                var intercept LnVolume;
                histogram/cfill=DimGray normal (color=black w=2);
                qqplot/normal (mu=est sigma=est);
                run;
```

```
proc gplot data=random;
        plot LnVolume*intercept;
        symbol v=dot w=0.5 h=0.5 i=rl l=2 c=black;


                run;
```

APPENDIX D: FILTRATION TESTS RAW DATA

Filter	SilverType	WaterType	Volume_mL	Ag_ugL	SolAg_mgL	FilterAg_mg_final	Filter_mg
Filter1Sept19	Citrate	A	10	27.3	121.7	0.045	10.6
Filter1Sept19	Citrate	A	18	33.2	121.7	0.045	10.6
Filter1Sept19	Citrate	A	32	30.1	121.7	0.045	10.6
Filter1Sept19	Citrate	A	56.5	23.2	121.7	0.045	10.6
Filter1Sept19	Citrate	A	100	13.0	121.7	0.045	10.6
Filter1Sept19	Citrate	A	178	7.0	121.7	0.045	10.6
Filter1Sept19	Citrate	A	317	2.5	121.7	0.045	10.6
Filter1Sept19	Citrate	A	1000	1.8	121.7	0.045	10.6
Filter2Sept19	Citrate	A	10	98.2	131.3	0.049	10.8
Filter2Sept19	Citrate	A	18	75.3	131.3	0.049	10.8
Filter2Sept19	Citrate	A	32	67.3	131.3	0.049	10.8
Filter2Sept19	Citrate	A	56.5	46.5	131.3	0.049	10.8
Filter2Sept19	Citrate	A	100	20.0	131.3	0.049	10.8
Filter2Sept19	Citrate	A	178	12.2	131.3	0.049	10.8
Filter2Sept19	Citrate	A	317	3.7	131.3	0.049	10.8
Filter2Sept19	Citrate	A	1000	2.3	131.3	0.049	10.8
Filter3Sept19	Citrate	A	10	364.5	78.3	0.025	10.8
Filter3Sept19	Citrate	A	18	157.4	78.3	0.025	10.8
Filter3Sept19	Citrate	A	32	62.1	78.3	0.025	10.8
Filter3Sept19	Citrate	A	56.5	22.5	78.3	0.025	10.8
Filter3Sept19	Citrate	A	100	10.9	78.3	0.025	10.8
Filter3Sept19	Citrate	A	178	13.0	78.3	0.025	10.8
Filter3Sept19	Citrate	A	317	5.3	78.3	0.025	10.8
Filter3Sept19	Citrate	A	1000	0.5	78.3	0.025	10.8
Filter4Sept19	Citrate	A	10	338.6	83.6	0.018	10.7
Filter4Sept19	Citrate	A	18	151.3	83.6	0.018	10.7
Filter4Sept19	Citrate	A	32	103.1	83.6	0.018	10.7
Filter4Sept19	Citrate	A	56.5	41.8	83.6	0.018	10.7
Filter4Sept19	Citrate	A	100	19.8	83.6	0.018	10.7
Filter4Sept19	Citrate	A	178	6.2	83.6	0.018	10.7
Filter4Sept19	Citrate	A	317	2.5	83.6	0.018	10.7
Filter4Sept19	Citrate	A	1000	2.7	83.6	0.018	10.7
Filter1Oct27	Citrate	A	10	53.5		0.045	10.62
Filter1Oct27	Citrate	A	18	16.7		0.045	10.62
Filter1Oct27	Citrate	A	32	15.5		0.045	10.62
Filter1Oct27	Citrate	A	56.5	4.6		0.045	10.62
Filter1Oct27	Citrate	A	100	6.6		0.045	10.62
Filter1Oct27	Citrate	A	178	2.1		0.045	10.62
Filter1Oct27	Citrate	A	317	5.2		0.045	10.62
Filter2Oct27	Citrate	A	10	76.9		0.041	10.9
Filter2Oct27	Citrate	A	18	16.2		0.041	10.9
Filter2Oct27	Citrate	A	32	7.5		0.041	10.9
Filter2Oct27	Citrate	A	56.5	2.9		0.041	10.9
Filter1Nov5	Citrate	B	10	92.2	94.2046	0.05	11.1
Filter1Nov5	Citrate	B	18	3.7	94.2046	0.05	11.1
Filter2Nov5	Citrate	B	10	23.8	101.841	0.055	11
Filter2Nov5	Citrate	B	18	18.3	101.841	0.055	11
Filter2Nov5	Citrate	B	32	5.9	101.841	0.055	11
Filter3Nov5	Citrate	B	10	38.1	52.9571	0.046	11
Filter3Nov5	Citrate	B	18	35.5	52.9571	0.046	11
Filter3Nov5	Citrate	B	32	25.0	52.9571	0.046	11
Filter3Nov5	Citrate	B	56.5	12.7	52.9571	0.046	11
Filter3Nov5	Citrate	B	100	4.7	52.9571	0.046	11
Filter4Nov5	Citrate	B	10	23.3	83.5914	0.044	11.2

Filter	SilverType	WaterType	Volume_mL	Ag_ugL	SolAg_mgL	FilterAg_mg_final	Filter_mg
Filter4Nov5	Citrate	B	18	4.1	83.5914	0.044	11.2
Filter3Nov12	Citrate	B	5	854.8	102.521	0.039	10.9
Filter3Nov12	Citrate	B	10	9.1	102.521	0.039	10.9
Filter3Nov12	Citrate	B	17.8	10.6	102.521	0.039	10.9
Filter3Nov12	Citrate	B	25	7.9	102.521	0.039	10.9
Filter3Nov12	Citrate	B	32	7.6	102.521	0.039	10.9
Filter3Nov12	Citrate	B	42	297.1	102.521	0.039	10.9
Filter3Nov12	Citrate	B	56.5	5.5	102.521	0.039	10.9
Filter3Nov12	Citrate	B	100	2.5	102.521	0.039	10.9
Filter3Nov12	Citrate	B	178	5.8	102.521	0.039	10.9
Filter3Nov12	Citrate	B	314.5	28.0	102.521	0.039	10.9
Filter4Nov12	Citrate	B	5	9540.0	91.1053	0.045	10.89
Filter4Nov12	Citrate	B	10	36.7	91.1053	0.045	10.89
Filter4Nov12	Citrate	B	17.8	21.2	91.1053	0.045	10.89
Filter4Nov12	Citrate	B	25	18.2	91.1053	0.045	10.89
Filter4Nov12	Citrate	B	32	14.7	91.1053	0.045	10.89
Filter4Nov12	Citrate	B	42	15.9	91.1053	0.045	10.89
Filter4Nov12	Citrate	B	56.5	14.7	91.1053	0.045	10.89
Filter4Nov12	Citrate	B	100	15.8	91.1053	0.045	10.89
Filter4Nov12	Citrate	B	178	0.0	91.1053	0.045	10.89
Filter1Nov12	Citrate	A	10	49.8	103.137	0.025	11.01
Filter1Nov12	Citrate	A	17.8	21.9	103.137	0.025	11.01
Filter1Nov12	Citrate	A	32	9.3	103.137	0.025	11.01
Filter1Nov12	Citrate	A	56.5	3.7	103.137	0.025	11.01
Filter1Nov12	Citrate	A	100	2.7	103.137	0.025	11.01
Filter1Nov12	Citrate	A	178	7.4	103.137	0.025	11.01
Filter1Nov12	Citrate	A	317	4.3	103.137	0.025	11.01
Filter2Nov12	Citrate	A	10	878.1	99.1537	0.05	10.96
Filter2Nov12	Citrate	A	17.8	21.5	99.1537	0.05	10.96
Filter2Nov12	Citrate	A	32	29.1	99.1537	0.05	10.96
Filter2Nov12	Citrate	A	56.5	7.0	99.1537	0.05	10.96
Filter1Dec4	PVP	A	10	6.4	98.13	0.02	10.91
Filter2Dec4	PVP	A	10	8.2	83.44	0.01	10.9
Filter2Dec4	PVP	A	17.8	9.4	83.44	0.01	10.9
Filter2Dec4	PVP	A	32	2.1	83.44	0.01	10.9
Filter2Dec4	PVP	A	56.5	2.2	83.44	0.01	10.9
Filter3Dec4	PVP	A	10	7.2	72.63	0.02	11.01
Filter3Dec4	PVP	A	17.8	4.4	72.63	0.02	11.01
Filter1Dec7	PVP	A	10	5.3	104.22	0.019	10.96
Filter1Dec7	PVP	A	17.8	5.4	104.22	0.019	10.96
Filter2Dec7	PVP	A	10	22.7	93.98	0.021	10.86
Filter2Dec7	PVP	A	17.8	33.9	93.98	0.021	10.86
Filter3Dec7	PVP	A	10	8.4	126.43	0.023	10.99
Filter3Dec7	PVP	A	17.8	2.4	126.43	0.023	10.99
Filter4Dec7	PVP	A	10	474.3	105.84	0.022	11.01
Filter4Dec7	PVP	A	17.8	7.5	105.84	0.022	11.01
Filter4Dec7	PVP	A	32	3.2	105.84	0.022	11.01
Filter1Dec10	PVP	B	5	55.1	100.93	0.014	10.87
Filter1Dec10	PVP	B	10	35.7	100.93	0.014	10.87
Filter1Dec10	PVP	B	17.8	15.2	100.93	0.014	10.87
Filter1Dec10	PVP	B	25	16.5	100.93	0.014	10.87
Filter1Dec10	PVP	B	32	8.9	100.93	0.014	10.87
Filter1Dec10	PVP	B	42	4.6	100.93	0.014	10.87
Filter1Dec10	PVP	B	56.5	3.3	100.93	0.014	10.87

Filter	SilverType	WaterType	Volume_mL	Ag_ugL	SolAg_mgL	FilterAg_mg_final	Filter_mg
Filter1Dec10	PVP	B	100	10.4	100.93	0.014	10.87
Filter2Dec10	PVP	B	5	48.2	87.96	0.017	11.05
Filter2Dec10	PVP	B	10	18.6	87.96	0.017	11.05
Filter2Dec10	PVP	B	17.8	12.9	87.96	0.017	11.05
Filter2Dec10	PVP	B	25	9.5	87.96	0.017	11.05
Filter2Dec10	PVP	B	32	19.4	87.96	0.017	11.05
Filter2Dec10	PVP	B	42	8.9	87.96	0.017	11.05
Filter2Dec10	PVP	B	56.5	5.6	87.96	0.017	11.05
Filter2Dec10	PVP	B	100	4.6	87.96	0.017	11.05
Filter2Dec10	PVP	B	178	2.4	87.96	0.017	11.05
Filter3Dec10	PVP	B	5	70.7	104.67	0.021	10.96
Filter3Dec10	PVP	B	10	10.4	104.67	0.021	10.96
Filter3Dec10	PVP	B	17.8	10.7	104.67	0.021	10.96
Filter3Dec10	PVP	B	25	13.7	104.67	0.021	10.96
Filter3Dec10	PVP	B	32	8.1	104.67	0.021	10.96
Filter3Dec10	PVP	B	42	12.6	104.67	0.021	10.96
Filter3Dec10	PVP	B	56.5	10.4	104.67	0.021	10.96
Filter3Dec10	PVP	B	100	5.0	104.67	0.021	10.96
Filter3Dec10	PVP	B	178	5.4	104.67	0.021	10.96
Filter4Dec10	PVP	B	5	19.0	88.34	0.022	10.92
Filter4Dec10	PVP	B	10	13.1	88.34	0.022	10.92
Filter4Dec10	PVP	B	17.8	13.3	88.34	0.022	10.92
Filter4Dec10	PVP	B	25	11.6	88.34	0.022	10.92
Filter4Dec10	PVP	B	32	13.4	88.34	0.022	10.92
Filter4Dec10	PVP	B	42	9.4	88.34	0.022	10.92
Filter4Dec10	PVP	B	56.5	8.7	88.34	0.022	10.92
Filter4Dec10	PVP	B	100	7.7	88.34	0.022	10.92
Filter4Dec10	PVP	B	178	2.2	88.34	0.022	10.92
Filter6Dec10	PVP	B	5	92.4	130.61	0.018	10.99
Filter6Dec10	PVP	B	10	9.3	130.61	0.018	10.99
Filter6Dec10	PVP	B	17.8	4.2	130.61	0.018	10.99
Filter6Dec10	PVP	B	25	3.4	130.61	0.018	10.99
Filter6Dec10	PVP	B	42	2.1	130.61	0.018	10.99
Filter7Dec10	PVP	B	5	62.8	111.2	0.018	11.01
Filter7Dec10	PVP	B	10	14.5	111.2	0.018	11.01
Filter7Dec10	PVP	B	17.8	4.8	111.2	0.018	11.01
Filter7Dec10	PVP	B	25	6.6	111.2	0.018	11.01
Filter7Dec10	PVP	B	32	8.5	111.2	0.018	11.01
Filter7Dec10	PVP	B	42	9.2	111.2	0.018	11.01
Filter7Dec10	PVP	B	56.5	6.2	111.2	0.018	11.01
Filter7Dec10	PVP	B	100	2.8	111.2	0.018	11.01
Filter1Jan23	BPEI	A	5	54.8	79.1207	0.006	10.95
Filter1Jan23	BPEI	A	10	39.9	79.1207	0.006	10.95
Filter1Jan23	BPEI	A	17.8	37.1	79.1207	0.006	10.95
Filter1Jan23	BPEI	A	25	32.5	79.1207	0.006	10.95
Filter1Jan23	BPEI	A	32	24.1	79.1207	0.006	10.95
Filter1Jan23	BPEI	A	42	13.3	79.1207	0.006	10.95
Filter1Jan23	BPEI	A	56.5	4.2	79.1207	0.006	10.95
Filter1Jan23	BPEI	A	100	0.4	79.1207	0.006	10.95
Filter2Jan23	BPEI	A	5	44.9	105.789	0.011	10.97
Filter2Jan23	BPEI	A	10	27.8	105.789	0.011	10.97
Filter2Jan23	BPEI	A	17.8	16.2	105.789	0.011	10.97
Filter2Jan23	BPEI	A	25	9.5	105.789	0.011	10.97
Filter2Jan23	BPEI	A	32	5.5	105.789	0.011	10.97

Filter	SilverType	WaterType	Volume_mL	Ag_ugL	SolAg_mgL	FilterAg_mg_final	Filter_mg
Filter2Jan23	BPEI	A	42	4.6	105.789	0.011	10.97
Filter2Jan23	BPEI	A	56.5	3.7	105.789	0.011	10.97
Filter2Jan23	BPEI	A	100	1.4	105.789	0.011	10.97
Filter3Jan23	BPEI	A	5	1.6	96.4914		11
Filter3Jan23	BPEI	A	10	1.6	96.4914		11
Filter3Jan23	BPEI	A	17.8	1.6	96.4914		11
Filter3Jan23	BPEI	A	25	1.5	96.4914		11
Filter3Jan23	BPEI	A	32	1.3	96.4914		11
Filter3Jan23	BPEI	A	42	1.1	96.4914		11
Filter3Jan23	BPEI	A	56.5	0.7	96.4914		11
Filter4Jan23	BPEI	A	5	44.1	100.417	0.007	10.93
Filter4Jan23	BPEI	A	10	38.2	100.417	0.007	10.93
Filter4Jan23	BPEI	A	17.8	40.9	100.417	0.007	10.93
Filter4Jan23	BPEI	A	25	37.2	100.417	0.007	10.93
Filter4Jan23	BPEI	A	32	27.6	100.417	0.007	10.93
Filter4Jan23	BPEI	A	42	20.8	100.417	0.007	10.93
Filter4Jan23	BPEI	A	56.5	10.1	100.417	0.007	10.93
Filter4Jan23	BPEI	A	100	3.1	100.417	0.007	10.93
Filter1Feb5	BPEI	A	5	14.3	84.0376	0.006	10.9
Filter1Feb5	BPEI	A	10	7.3	84.0376	0.006	10.9
Filter1Feb5	BPEI	A	17.8	3.1	84.0376	0.006	10.9
Filter1Feb5	BPEI	A	25	3.7	84.0376	0.006	10.9
Filter1Feb5	BPEI	A	32	2.4	84.0376	0.006	10.9
Filter1Feb5	BPEI	A	42	3.9	84.0376	0.006	10.9
Filter1Feb5	BPEI	A	56.5	1.2	84.0376	0.006	10.9
Filter2Feb5	BPEI	A	5	12.8	88.403	0.003	11
Filter2Feb5	BPEI	A	10	5.3	88.403	0.003	11
Filter2Feb5	BPEI	A	17.8	2.6	88.403	0.003	11
Filter2Feb5	BPEI	A	25	1.7	88.403	0.003	11
Filter2Feb5	BPEI	A	32	1.7	88.403	0.003	11
Filter2Feb5	BPEI	A	42	2.6	88.403	0.003	11
Filter3Feb5	BPEI	B	5	145.6	79.8495	0.003	11
Filter3Feb5	BPEI	B	10	91.8	79.8495	0.003	11
Filter3Feb5	BPEI	B	17.8	13.6	79.8495	0.003	11
Filter4Feb5	BPEI	B	5	128.7	91.2935	0.002	11
Filter4Feb5	BPEI	B	10	76.8	91.2935	0.002	11
Filter4Feb5	BPEI	B	17.8	13.6	91.2935	0.002	11
Filter1Feb6	BPEI	B	5	135.8	81.147	0.003	11.08
Filter1Feb6	BPEI	B	10	99.4	81.147	0.003	11.08
Filter1Feb6	BPEI	B	17.8	23.6	81.147	0.003	11.08
Filter1Feb6	BPEI	B	25	2.0	81.147	0.003	11.08
Filter2Feb6	BPEI	B	5	141.6	83.293	0.003	10.83
Filter2Feb6	BPEI	B	10	126.7	83.293	0.003	10.83
Filter2Feb6	BPEI	B	17.8	111.4	83.293	0.003	10.83
Filter2Feb6	BPEI	B	25	22.0	83.293	0.003	10.83
Filter2Feb6	BPEI	B	32	7.3	83.293	0.003	10.83
Filter2Feb6	BPEI	B	42	2.2	83.293	0.003	10.83
Filter3Feb6	BPEI	B	5	139.8	83.1698	0.005	11
Filter3Feb6	BPEI	B	10	134.2	83.1698	0.005	11
Filter3Feb6	BPEI	B	17.8	133.3	83.1698	0.005	11
Filter3Feb6	BPEI	B	25	308.3	83.1698	0.005	11
Filter3Feb6	BPEI	B	32	5.1	83.1698	0.005	11
Filter3Feb6	BPEI	B	42	20.4	83.1698	0.005	11
Filter4Feb6	BPEI	B	5	172.5	95.3963	0.004	10.96

Filter	SilverType	WaterType	Volume_mL	Ag_ugL	SolAg_mgL	FilterAg_mg_final	Filter_mg
Filter4Feb6	BPEI	B	10	144.3	95.3963	0.004	10.96
Filter4Feb6	BPEI	B	17.8	12.4	95.3963	0.004	10.96
Filter4Feb6	BPEI	B	25	15.2	95.3963	0.004	10.96
Filter4Feb6	BPEI	B	32	11.2	95.3963	0.004	10.96
Filter4Feb6	BPEI	B	42	5.6	95.3963	0.004	10.96
Filter4Feb6	BPEI	B	56.5	2.6	95.3963	0.004	10.96
Filter1May8	Citrate	ANOM	5	89.2	54.31	0.062	10.8
Filter1May8	Citrate	ANOM	10	67.6	54.31	0.062	10.8
Filter1May8	Citrate	ANOM	17.8	55.8	54.31	0.062	10.8
Filter1May8	Citrate	ANOM	25	46.6	54.31	0.062	10.8
Filter1May8	Citrate	ANOM	32	41.8	54.31	0.062	10.8
Filter1May8	Citrate	ANOM	42	40.3	54.31	0.062	10.8
Filter1May8	Citrate	ANOM	56.5	41.4	54.31	0.062	10.8
Filter1May8	Citrate	ANOM	100	39.5	54.31	0.062	10.8
Filter1May8	Citrate	ANOM	178	40.1	54.31	0.062	10.8
Filter1May8	Citrate	ANOM	317	45.0	54.31	0.062	10.8
Filter1May8	Citrate	ANOM	562	12.8	54.31	0.062	10.8
Filter1May8	Citrate	ANOM	1000	8.1	54.31	0.062	10.8
Filter1May8	Citrate	ANOM	1778	7.1	54.31	0.062	10.8
Filter1May8	Citrate	ANOM	2778	15.6	54.31	0.062	10.8
Filter2May8	Citrate	ANOM	5	67.5	38.54		11.2
Filter2May8	Citrate	ANOM	10	55.3	38.54		11.2
Filter2May8	Citrate	ANOM	17.8	48.8	38.54		11.2
Filter2May8	Citrate	ANOM	25	52.8	38.54		11.2
Filter2May8	Citrate	ANOM	32	59.7	38.54		11.2
Filter2May8	Citrate	ANOM	42	60.5	38.54		11.2
Filter2May8	Citrate	ANOM	56.5	65.4	38.54		11.2
Filter2May8	Citrate	ANOM	100	78.5	38.54		11.2
Filter2May8	Citrate	ANOM	178	68.2	38.54		11.2
Filter2May8	Citrate	ANOM	317	223.0	38.54		11.2
Filter2May8	Citrate	ANOM	562	30.5	30.53		11.2
Filter3May8	Citrate	ANOM	5	131.2	57.86		11.1
Filter3May8	Citrate	ANOM	10	63.0	57.86		11.1
Filter3May8	Citrate	ANOM	17.8	55.4	57.86		11.1
Filter3May8	Citrate	ANOM	25	48.7	57.86		11.1
Filter3May8	Citrate	ANOM	32	56.0	57.86		11.1
Filter3May8	Citrate	ANOM	42	59.6	57.86		11.1
Filter3May8	Citrate	ANOM	56.5	65.6	57.86		11.1
Filter3May8	Citrate	ANOM	100	71.1	57.86		11.1
Filter3May8	Citrate	ANOM	178	71.4	57.86		11.1
Filter3May8	Citrate	ANOM	317	70.3	57.86		11.1
Filter3May8	Citrate	ANOM	562	19.8	57.86		11.1
Filter3May8	Citrate	ANOM	1000	5.3	57.86		11.1
Filter3May8	Citrate	ANOM	1778	5.2	57.86		11.1
Filter4May8	Citrate	BNOM	5	157.0	46.69	0.056	11
Filter4May8	Citrate	BNOM	10	16.2	46.69	0.056	11
Filter4May8	Citrate	BNOM	17.8	14.3	46.69	0.056	11
Filter4May8	Citrate	BNOM	25	20.6	46.69	0.056	11
Filter4May8	Citrate	BNOM	32	16.5	46.69	0.056	11
Filter4May8	Citrate	BNOM	42	27.1	46.69	0.056	11
Filter4May8	Citrate	BNOM	56.5	12.1	46.69	0.056	11
Filter4May8	Citrate	BNOM	100	12.5	46.69	0.056	11
Filter4May8	Citrate	BNOM	178	14.9	46.69	0.056	11
Filter4May8	Citrate	BNOM	317	12.6	46.69	0.056	11

Filter	SilverType	WaterType	Volume_mL	Ag_ugL	SolAg_mgL	FilterAg_mg_final	Filter_mg
Filter4May8	Citrate	BNOM	562	6.9	46.69	0.056	11
Filter4May8	Citrate	BNOM	1000	8.6	46.69	0.056	11
Filter4May8	Citrate	BNOM	1778	17.0	46.69	0.056	11
Filter4May8	Citrate	BNOM	2778	23.9	46.69	0.056	11
Filter5May8	Citrate	BNOM	5	128.4	54.89		10.9
Filter5May8	Citrate	BNOM	10	36.0	54.89		10.9
Filter5May8	Citrate	BNOM	17.8	31.2	54.89		10.9
Filter5May8	Citrate	BNOM	25	26.1	54.89		10.9
Filter5May8	Citrate	BNOM	32	27.1	54.89		10.9
Filter5May8	Citrate	BNOM	42	24.1	54.89		10.9
Filter5May8	Citrate	BNOM	56.5	23.8	54.89		10.9
Filter5May8	Citrate	BNOM	100	26.2	54.89		10.9
Filter5May8	Citrate	BNOM	178	17.8	54.89		10.9
Filter5May8	Citrate	BNOM	317	17.2	54.89		10.9
Filter5May8	Citrate	BNOM	562	4.8	54.89		10.9
Filter5May8	Citrate	BNOM	1000	4.8	54.89		10.9
Filter6May8	Citrate	BNOM	5	110.0	62.53		11.1
Filter6May8	Citrate	BNOM	10	64.3	62.53		11.1
Filter6May8	Citrate	BNOM	17.8	26.5	62.53		11.1
Filter6May8	Citrate	BNOM	25	30.0	62.53		11.1
Filter6May8	Citrate	BNOM	32	21.4	62.53		11.1
Filter6May8	Citrate	BNOM	42	20.3	62.53		11.1
Filter6May8	Citrate	BNOM	56.5	28.5	62.53		11.1
Filter6May8	Citrate	BNOM	100	19.1	62.53		11.1
Filter6May8	Citrate	BNOM	178	17.7	62.53		11.1
Filter6May8	Citrate	BNOM	317	22.8	62.53		11.1
Filter6Ma8	Citrate	BNOM	562	21.2	62.53		11.1

Legend

Filter: Identifier corresponding to the date Ag NPs were applied to the Anodisc filter.
SilverType: Identifier of the Ag NP stabilizing molecule
WaterType: A: Hardness = 200 mg/L $CaCO_3$ as $Mg(NO_3)_2 \cdot 6H_2O$, Alk = 200 mg/L $CaCO_3$ as $NaHCO_2$ **;** B: I = 10 mM as $NaNO_3$ Alk = 50 mg/L $CaCO_3$ as $NaHCO_2$ NOM = 5 mg/L Humic Acid (Suwannee River)
Volume_mL: Amount of water filtered. Sample collected at midpoint of 5 mL
Ag_ugL: Total silver concentration (particulate + soluable) in filtered water sample, measured using ICP-OES
SolAg_mgL: Total silver concentration of NP solution after soaking Anodisc filters for initial application of silver.
FilterAg_mg_final: Amount of silver desorbed from Anodisc filter (using concentrated HNO_3 and measured by ICP-OES) after filtration experiments were complete.
Filter_mg: Mass of Anodisc filter prior to application of Ag NPs

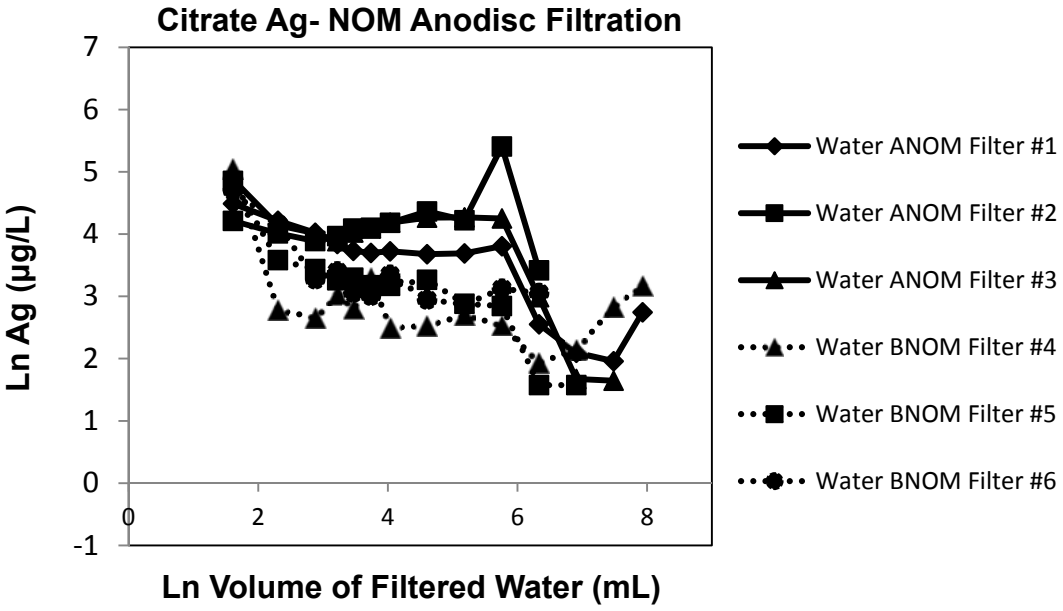
Citrate Ag- NOM Anodisc Filtration
Ln Ag (µg/L)
7
6
5
4
3
2
1
0
-1
0
2
4
6
8
Ln Volume of Filtered Water (mL)
Water ANOM Filter #1
Water ANOM Filter #2
Water ANOM Filter #3
Water BNOM Filter #4
Water BNOM Filter #5
Water BNOM Filter #6

APPENDIX E: CHAPTER 7 PARAMETER ESTIMATES AND SIGNIFICANCE TESTS

Parameter Estimate	Ag-Water			
	Cit-A	p-value	Cit - B	p-value
Intercept, γ00	6.8689	<0.0001	7.008	<0.0001
BPEI, γ01	-1.7217	0.619	0.1874	0.8275
Citrate, γ01	0	-	0	-
PVP,γ01	-3.2036	0.0014	-1.7546	0.0892
Water A,γ02	0	-	-0.1391	0.871
Water B, γ02	0.1391	0.871	0	-
BPEI Vol, γ11	-0.03555	0.8779	0.03555	0.8779
Cit Vol, γ11	0	-	0	-
PVP Vol,γ11	0.4316	0.1127	0.4316	0.1127
WaterA Vol, γ12	0	-	0.3199	0.1566
Water B Vol, γ12	-0.3119	0.1566	0	-
Vol,γ10	-1.0251	<0.0001	-1.337	<0.0001
Water A, BPEI, γ03	0	-	-1.9091	0.0046
Water A, Cit, γ03	0	-	0	-
Water A PVP,γ03	0	-	-1.4489	0.0324
Water B, BPEI, γ03	1.9091	0.0046	0	-
Water B, Cit, γ03	0	-	0	-
Water B, PVP, γ03	1.4489	0.0324	0	-

Parameter Estimate	Ag-Water			
	PVP-A	p-value	PVP-B	p-value
Intercept, γ00	3.6653	<0.0001	5.2534	<0.0001
BPEI, γ01	1.4819	0.1297	1.9421	0.0593
Citrate, γ01	3.2036	0.0014	1.7546	0.0892
PVP,γ01	0	-	0	-
Water A,γ02	0	-	-1.5881	0.0531
Water B, γ02	1.5881	0.0531	0	-
BPEI Vol, γ11	0.4671	0.0986	-0.4671	0.0986
Cit Vol, γ11	-0.4316	0.1127	-0.4316	0.1127
PVP Vol,γ11	0	-	0	-
WaterA Vol, γ12	0	-	0.3119	0.1566
Water B Vol, γ12	-0.3119	0.1566	0	-
Vol,γ10	-0.5935	0.0285	-0.9054	<0.0001
Water A, BPEI, γ03	0	-	0.4501	0.4924
Water A, Cit, γ03	0	-	1.4489	0.0324
Water A PVP,γ03	0	-	0	-
Water B, BPEI, γ03	0.4601	0.4924	0	-
Water B, Cit, γ03	-1.4489	0.0324	0	-
Water B, PVP, γ03	0	-	0	-

Parameter Estimate	Ag-Water			
	BPEI-A	p-value	BPEI-B	p-value
Intercept, γ00	5.1471	<0.0001	7.1955	<0.0001
BPEI, γ01	0	-	0	-
Citrate, γ01	1.7217	0.0619	-0.1874	0.8275
PVP,γ01	-1.4819	0.1297	-1.9421	0.0593
Water A,γ02	0	-	-2.0482	0.0172
Water B, γ02	2.0482	0.0172	0	-
BPEI Vol, γ11	0	-	0	-
Cit Vol, γ11	0.03555	0.8779	0.03555	0.8779
PVP Vol,γ11	0.4671	0.0986	0.4671	0.0986
WaterA Vol, γ12	0	-	0.3119	0.1566
Water B Vol, γ12	-0.3119	0.1566	0	-
Vol,γ10	-1.0607	<0.0001	-1.3726	<0.0001
Water A, BPEI, γ03	0	-	0	-
Water A, Cit, γ03	0	-	1.9091	0.0046
Water A PVP,γ03	0	-	0.4601	0.4924
Water B, BPEI, γ03	0	-	0	-
Water B, Cit, γ03	-1.9091	0.0046	0	-
Water B, PVP, γ03	-0.4601	0.4924	0	-
Error Terms	All combos	p-value		
uoj	2.4174	0.0123		
u1j	0.159	0.0281		
rij	0.7462	<0.001		

References

Adamczyk, Z., & Warszyński, P. (1996). Role of electrostatic interactions in particle adsorption. *Advances in Colloid and Interface Science*, *63*, 41–149. Retrieved from http://www.sciencedirect.com/science/article/pii/0001868695002812

Anandarajah, A., & Chen, J. (1995). Single Correction Function for Computing Retarded van der Waals Attraction. *Journal of Colloid and Interface Science*, *176*(2), 293–300. http://doi.org/10.1006/jcis.1995.9964

Anton Paar (2012). Instruction Manual SurPASS Electrokinetic Analyzer. Anton Paar, Austria. Available upon request from www.anton-paar.com

AshaRani, P.V., Low Kah Mun, G., Hande, M.P., Valiyaveetil, S. (2009). Cytotoxicity and Genotoxicity of Silver Naoparticles in Human Cells. *ACS Nano,* 3 (2), 279-290.

ATSDR (1990). Toxicological Profile for Silver. Available at: http://www.atsdr.cdc.gov/toxprofiles/tp.asp?id=539&tid=97 <Accessed November 2012>

Auffan, M., Rose, J., Wiesner, M. R., & Bottero, J.Y. (2009). Chemical stability of metallic nanoparticles: a parameter controlling their potential cellular toxicity in vitro. *Environmental Pollution*, *157*(4), 1127-33. doi:10.1016/j.envpol.2008.10.002

Battocchio, C., Porcaro, F., Mukherjee, S., Magnano, E., Nappini, S., Fratoddi, I., Polzonetti, G. (2014). Gold Nanoparticles Stabilized with Aromatic Thiols: Interaction at the Molecule–Metal Interface and Ligand Arrangement in the Molecular Shell Investigated by SR-XPS and NEXAFS. *The Journal of Physical Chemistry C*, *118*(15), 8159–8168. http://doi.org/10.1021/jp4126057

Bielefeldt, A. R., Kowalski, K., & Summers, R. S. (2009). Bacterial treatment effectiveness of point-of-use ceramic water filters. *Water Research*, *43*(14), 3559-65.

Benjamin, M. M.; Lawler D. F. (2013). *Water Quality Engineering*. John Wiley & Sons Inc.: Hoboken, 315-318.

Brown, J. (2007). *Effectiveness of ceramic filtration for drinking water treatment in Cambodia*. Retrieved from ProQuest Dissertations and Theses database. (AAT 3289142)

Byrd, T.L., Walz, J. Y. (2005). Interaction Force Profiles between Cryptosporidium parvum Oocysts and Silica Surfaces. *Environmental Science & Technology*, *39*(24), 9574–9582.

Byun, S., Davies, S. H., Alpatova, A. L., Corneal, L. M., Baumann, M. J., Tarabara, V. V, & Masten, S. J. (2011). Mn oxide coated catalytic membranes for a hybrid ozonation-membrane filtration: comparison of Ti, Fe and Mn oxide coated membranes for water quality. *Water Research*, *45*(1), 163–70. http://doi.org/10.1016/j.watres.2010.08.031

Box, E. P.; Jenkins, G. M.; Reinsel, Gregory C. (2014) Time Series Analysis : Forecasting and Control. Hoboken: Wiley. Ebook Library. Web. 31 Dec. 2014.

Cao, G. (2004). *Nanostructures & Nanomaterials Synthesis, Properties & Applications*. Imperial College Press: London, 15-48.

Carlson, C., Hussain, S.M., Schrand, A. M., Braydich-Stolle, L.K., Hess, K.L., Jones, R.L., Schlager, J.J. (2008). Unique Cellular Interaction of Silver Nanoparticles: Size-Dependent Generation of Reactive Oxygen Species. *J. Phys. Chem. B*, 112, 13608-13619

Chambers, B. A., Afrooz, A. R. M. N., Bae, S., Aich, N., Katz, L., Saleh, N. B., & Kirisits, M. J. (2014). Effects of Chloride and Ionic Strength on Physical Morphology, Dissolution, and Bacterial Toxicity of Silver Nanoparticles.

Chen, Y., Liu, X., Liu, L., Zhang, Y., Wang, Z., & Zhang, Q. (2013). Functional poly(vinylidene fluoride) membrane anchored with silver nanoparticle with antibacterial activity. *Synthetic Metals*, *174*, 1–5. http://doi.org/10.1016/j.synthmet.2013.04.021

Chemical Book (2015). Polyethlyleneimine, Branced. Website. Accessed June 4, 2015 <http://www.chemicalbook.com/ChemicalProductProperty_EN_CB9162514.htm>

Cho, H., Li, L., Bae, Y. H., Huh, K. M., & Kang, H. C. (2014). Bioreducible branched polyethyleneimine derivatives physically loaded with hydrophobic pheophorbide A: preparation, characterization, and light-induced cytotoxicity. *Macromolecular Bioscience*, *14*(10), 1483–94. http://doi.org/10.1002/mabi.201400145

Clasen, T. F., & Haller, L. (2008). *Water Quality Interventions to Prevent Diarrhoea : Cost and Cost-Effectiveness*. Geneva. Retrieved from http://www.who.int/water_sanitation_health/economic/prevent_diarrhoea.pdf?ua=1

Curry, A., Nusz, G., Chilkoti, A., & Wax, A. (2005). Substrate effect on refractive index dependence of plasmon resonance for individual silver nanoparticles observed using darkfield microspectroscopy. *Optics Express*, *13*(7), 2668. http://doi.org/10.1364/OPEX.13.002668

De Gennes, P. G. (1987). Polymers at an Interface; a Simplified View. *Advances in Colloid and Interface Science*, *27*, 189–209.

Diez-Roux, A. V. (2000). Multilevel analysis in public health research. *Annual Review of Public Health*, *21*, 171–92. http://doi.org/10.1146/annurev.publhealth.21.1.171

Eckhardt, S., Brunetto, P. S., Gagnon, J., Priebe, M., Giese, B., & Fromm, K. M. (2013). Nanobio Silver: Its Interactions with Peptides and Bacteria, and Its Uses in Medicine. *Chemical Reviews*. doi:10.1021/cr300288v

Edzwald, J.K, (2011). *Water Quality & Treatment A Handbook on Drinking Water Ed. 6.* Chapter 19. Formation and Control of Disinfection By-Products. McGraw Hill, Chicago, IL USA.

Entwisle, B., Mason, W. M., Hermalin A. (1986). The Multilevel Dependence of Contraceptive Use on Socioeconomic Development and Family Planning Program Strength. *Demography*, 23(2), 199-216

El Badawy, A. M., Luxton, T. P., Silva, R. G., Scheckel, K. G., Suidan, M. T., & Tolaymat, T. M. (2010). Impact of environmental conditions (pH, ionic strength, and electrolyte type) on the surface charge and aggregation of silver nanoparticles suspensions. *Environmental Science & Technology*, *44*(4), 1260–6. http://doi.org/10.1021/es902240k

El Badawy, A. M., Silva, R. G., Morris, B., Scheckel, K. G., Suidan, M. T., & Tolaymat, T. M. (2011). Surface charge-dependent toxicity of silver nanoparticles. *Environmental Science & Technology*, *45*(1), 283-7. doi:10.1021/es1034188

Elimelech, M., Jia, X.,Gregory J., Williams, R. (2013). Particle deposition & aggregation: measurement, modelling and simulation. Butterworth-Heinemann.

Filliben, J. J. (1975). The Probabiity Plot Correlation Coefficient Test for Normality. Technometrics, 17(1), 111-117.

Franks, G. V., & Gan, Y. (2007). Charging Behavior at the Alumina–Water Interface and Implications for Ceramic Processing. *Journal of the American Ceramic Society*, *90*(11), 3373–3388. http://doi.org/10.1111/j.1551-2916.2007.02013.x

Furneaux, R. C., Rigby W.R., Davidson, A.P. (1989). The formation of controlled-porosity membranes from anodically oxidized aluminum. *Nature* 337(12), 147-149.

Galjaard, G., Clement, J., Seng Ang, W., Lim, M.H., (2013). CeraMac®-19 Demonstration Plant Ceramic Microfiltration at Choa Chu Kang Waterworks. *Proceedings American Water Works Association AMTA/AWWA Membrane Technology Conference*. San Antonio, TX.

Gao, Y., Jiang, P., Liu, D. F., Yuan, H. J., Yan, X. Q., Zhou, Z. P., … Shen, D. Y. (2004). Evidence for the Monolayer Assembly of Poly(vinylpyrrolidone) on the Surfaces of Silver Nanowires. *The Journal of Physical Chemistry B*, *108*(34), 12877–12881. http://doi.org/10.1021/jp037116c

Gorham, J. M., MacCuspie, R. I., Klein, K. L., Fairbrother, D. H., & Holbrook, R. D. (2012). UV-induced photochemical transformations of citrate-capped silver nanoparticle suspensions. *Journal of Nanoparticle Research*, *14*(10), 1139. http://doi.org/10.1007/s11051-012-1139-3

Golas, P. L., Louie, S., Lowry, G. V, Matyjaszewski, K., & Tilton, R. D. (2010). Comparative study of polymeric stabilizers for magnetite nanoparticles using ATRP. *Langmuir : The ACS Journal of Surfaces and Colloids*, *26*(22), 16890–900. http://doi.org/10.1021/la103098q

Goldstein, N., & Greenlee, L. F. (2012). Influence of synthesis parameters on iron nanoparticle size and zeta potential. *Journal of Nanoparticle Research*, *14*(4), 760. http://doi.org/10.1007/s11051-012-0760-5

Grasso, D., Subramaniam, K., Butkus, M., Strevett, K., & Bergendahl, J. (2002). A review of non-DLVO interactions in environmental colloidal systems. *Reviews in Environmental Science and Bio/Technology*, *1*(1), 17–38. http://doi.org/10.1023/A:1015146710500

Gregory, J. (1973). Approximate expression for the interaction of diffuse electrical double layers at constant charge. *J. Chem. Soc., Faraday Trans*. 2., 69, 1723-1728.

Gregory, J. (1975). Interaction of unequal double layers at constant charge. *Journal of Colloid and Interface Science*., 51 (1) 44-51.

Gregory, J. (1981). Approximate Expressions for Retarded van der Waals Interaction. *Journal of Colloid and Interface Science*, *83*(1), 138–145.

Ha, C., Hamand, J., Kennedy, M.D., Amy, G.L., (2013). Uniform Pore-Structure Ceramic Membrane for Filtration of Impaired Quality Source Waters, American Water Works Association AMTA/AWWA Membrane Technology Conference, San Antonio, TX.

Hoek, E. M. V, & Agarwal, G. K. (2006). Extended DLVO interactions between spherical particles and rough surfaces. *Journal of Colloid and Interface Science*, *298*(1), 50–8. http://doi.org/10.1016/j.jcis.2005.12.031

Hogg, R., Henly, T.W. and Furstenau, D.W. (1966). Mutual Coagulation of Colloidal Dispersions. *Trans. Faraday Soc*., 62, 1638-1651

Holt, K. B., Bard, A. J. (2005). The Interaction of Silver (I) Ions with the Respiratory Chain of Escherichia coli: An Electrochemical and Scanning Electrochemical Microscopy Study of the Antimicrobial Mechanism of Micromolar Ag^{+}. *Biochemistry* 44(39), 13214-13223 doi:10.1021/bi0508542.

Hu, K., & Bard, A. J. (1997). Use of Atomic Force Microscopy for the Study of Surface Acid - Base Properties of Carboxylic Acid-Terminated Self-Assembled Monolayers, *Langmuir 13*(19), 5114–5119.

Huang, H. H., Ni, X. P., Loy, G. L., Chew, C. H., Tan, K. L., Loh, F. C., Xu, G. Q. (1996). Photochemical Formation of Silver Nanoparticles in Poly (N - vinylpyrrolidone), Langmuir (12), 909–912.

Hunter, A. C. (2006). Molecular hurdles in polyfectin design and mechanistic background to polycation induced cytotoxicity. *Advanced Drug Delivery Reviews*, *58*(14), 1523–31. http://doi.org/10.1016/j.addr.2006.09.008

Huynh, K. A., & Chen, K. L. (2011). Aggregation kinetics of citrate and polyvinylpyrrolidone coated silver nanoparticles in monovalent and divalent electrolyte solutions. *Environmental Science & Technology*, *45*(13), 5564–71. http://doi.org/10.1021/es200157h

Israelachvili, J. (1992). *Intermolecular & Surface Forces* Second Edition. Academic Press: San Diego.

Kallman, E. N., Oyanedel-craver, V. A., Asce, A. M., Smith, J. A., & Asce, M. (2011). Ceramic Filters Impregnated with Silver Nanoparticles for Point-of-Use Water Treatment in Rural Guatemala. *Glass*, (June), 407–415. http://doi.org/10.1061/(ASCE)EE.1943-7870

Kim I., (2014). *Transport and retention of silver nanoparticle in granular media filtration.* Dissertation, The University of Texas at Austin. <https://repositories.lib.utexas.edu/bitstream/handle/2152/26883/KIM-DISSERTATION-2014.pdf>

Kim J., Pitts, B. Steward, P.S., Camper, A. Yoon, J. (2008). Comparison of the Antimicrobial Effects of Chlorine, Silver Ion, and Tobramycin on Biofilm. *Antimicrobial Agents and Chemotherapy*, Volume 52. No. 4, 1446-1453

Kruger (2011). New Treatment Plan to Feature Ceramic Membranes. *Water World: Membranes*.
June 2009. Supplement. Accessed February 16, 2012.
http://www.krugerusa.com/lib/kruger/3FEBE49iar679sFW9y1Pp1gM.pdf

Kwok O., Underhill, A.T., Berry J.W., Luo, W., Elliott, T.R., and Yoon, M. (2008). Analyzing Longitudinal Data with Multilevel Models: An Example with Individuals Living with Lower Extremity Intra-articular Fracture. *Rehabilitation Psychology*. 53(3): 370-386.

Lantagne, D. (2001). *Investigation of the Potters for Peace colloidal silver impregnated ceramic filter. Report 1: Intrinsic effectiveness*. Alethia Environmental, Allston, MA, USA

Lantagne, D., Klarman, M., Mayer, A., Preston, K., Napotnik, J., & Jellison, K. (2010). Effect of production variables on microbiological removal in locally-produced ceramic filters for household water treatment. *International Journal of Environmental Health Research*, *20*(3), 171–87. http://doi.org/10.1080/09603120903440665

Li W.R., Xie X.B., Shi Q.S., Zeng H.Y., Ou-Yang Y.S., and Chen Y.B. (2010). Antibacterial activity and mechanism of silver nanoparticles on Escherichia coli. *Applied Microbiology and Biotechnology* 85:1115-1122.

Lin, S., Cheng, Y., Liu, J., & Wiesner, M. R. (2012). Polymeric coatings on silver nanoparticles hinder autoaggregation but enhance attachment to uncoated surfaces. *Langmuir : The ACS Journal of Surfaces and Colloids*, *28*(9), 4178–86. http://doi.org/10.1021/la202884f

Linnert T., Mulvaney, P., and Henglein, A. (1990). Long-lived nonmetallic silver clusters in aqueous solution: preparation and photolysis. *Journal of the American Chemical Society*. 112:4657-4664.

Liu, J., & Hurt, R. H. (2010). Ion release kinetics and particle persistence in aqueous nano-silver colloids. *Environmental science & Technology*, *44*(6), 2169-75. doi:10.1021/es9035557

Lv, Y., Liu, H., Wang, Z., Liu, S. Hao, L., Sang, Y., Liu, D. Wang, J. Boughton, R.I. (2009). Silver nanoparticle-decorated porous ceramic composite for water treatment. *Journal of Membrane Science*, Volume 331, Issues 1-2, Pages 50-56.

Ma, R., Levard, C., Marinakos, S. M., Cheng, Y., Liu, J., Michel, F. M., Brown, G. E. (2012). Size-controlled dissolution of organic-coated silver nanoparticles. *Environmental Science & Technology*, *46*(2), 752-9. doi:10.1021/es201686j

Metawater (2011). *Ceramic Membrane Image.* Accessed October 24, 2011. <http://www.metawater.co.jp/eng/product/drinking/membrane_clarify/application.html>.

Metawater (2015). *Ceramic Membrane Installations.* Accessed June 4, 2015. < <http://www.metawater.co.jp/eng/product/drinking/membrane_clarify/location.html >.

Mdluli, P. S., Sosibo, N. M., Revaprasadu, N., Karamanis, P., Leszczynski, J. (2009). Surface enhanced Raman spectroscopy (SERS) and density functional theory (DFT) study for understanding the regioselective adsorption of pyrrolidinone on the surface of silver and gold colloids. *Journal of Molecular Structure*, *935*(1-3), 32–38. http://doi.org/10.1016/j.molstruc.2009.06.039

Mdluli, P. S., Sosibo, N. M., Mashazi, P. N., Nyokong, T., Tshikhudo, R. T., Skepu, A., van der Lingen, E. (2011). Selective adsorption of PVP on the surface of silver nanoparticles: A molecular dynamics study. *Journal of Molecular Structure*, *1004*(1-3), 131–137. http://doi.org/10.1016/j.molstruc.2011.07.049

Millennium Project (2006). About MDGs. Website. Accessed December 9, 2014 <http://unmillenniumproject.org/goals/index.htm>

Moghimi, S. M., Symonds, P., Murray, J. C., Hunter, a C., Debska, G., Szewczyk, A. (2005). A two-stage poly(ethylenimine)-mediated cytotoxicity: implications for gene transfer/therapy. *Molecular Therapy : The Journal of the American Society of Gene Therapy*, *11*(6), 990–5. http://doi.org/10.1016/j.ymthe.2005.02.010

Nap, R. J., Park, Y., Wong, J. Y., Szleifer, I. (2013). Adsorption of acid and polymer coated nanoparticles: a statistical thermodynamics approach. *Langmuir : The ACS Journal of Surfaces and Colloids*, *29*(47), 14482–93. http://doi.org/10.1021/la403143a

Ng, L. Y., Mohammad, A. W., Leo, C. P., & Hilal, N. (2013). Polymeric membranes incorporated with metal/metal oxide nanoparticles: A comprehensive review. *Desalination*, *308*, 15–33. http://doi.org/10.1016/j.desal.2010.11.033

Oyanedel-Craver, V. A, & Smith, J. A. (2008). Sustainable colloidal-silver-impregnated ceramic filter for point-of-use water treatment. *Environmental science & technology*, *42*(3), 927-33.

Padilla, A.P., Rodríguez, J.A., Saitúa, H.A. (1997). Synthesis and water ultrafiltration properties of silver membrane supported on porous ceramics. *Desalination*, Volume 114, Issue 3, Pages 203-208.

Park, J. (2013). Interfacial properties of asymmetrically functionalized citrate-stabilized gold and silver nanoparticles related to molecular adsorption. The University of Utah Dissertation. UMI Number 3563410 ProQuest LLC Ann Arbor, MI.

Parsegian, V.A. and Weiss, G.H. (1981). Spectroscopic Parameters for Computation of van der Waals Forces. *J. Colloid Interface Sci* 81, 285-289

PATH (2012). *The Impact of Manufacturing Variable on Ceramic Pot Filtration Effectivenss.* Seatle. Accessed January 1, 2015 < http://www.ceramicwaterfilter.org/wp-content/uploads/manufacturing_variables_final_report.pdf>

Poortinga, A. T., Bos, R., Norde, W., Busscher, H. J. (2002). *Electric double layer interactions in bacterial adhesion to surfaces*. *Surface Science Reports* (Vol. 47, pp. 1–32). http://doi.org/10.1016/S0167-5729(02)00032-8

Potters for Peace (2015). Filter Factor Locations. Website. Accessed January 22, 2015 < http://pottersforpeace.com/filter-map/>

Quevedo, I. R., Tufenkji, N. (2009). Influence of Solution Chemistry on the Deposition and Detachment Kinetics of a CdTe Quantum Dot Examined Using a Quartz Crystal Microbalance. *Environmental Science & Technology*, *43*(9), 3176–3182. http://doi.org/10.1021/es803388u

Raudenbush, S.W. and Bryk A. W (2002). *Hierarchical Linear Models Applications and Data Analysis Methods*. Thousand Oaks, CA, Sage Publications Inc.

Rayner, J., Zhang, H., Schubert, J., Lennon, P., Lantagne, D., Oyanedel-Craver, V. (2013). Laboratory Investigation into the E ff ect of Silver Application on the Bacterial Removal Efficacy of Filter Material for Use on Locally Produced Ceramic Water Filters for Household Drinking Water Treatment.

Robinson, B.V., Sullivan, F.M., Borzelleca, J.F., Schwartz, S.L. (1990). *PVP: A Critical Review of the Kinetics and Toxicology of Polyvinylpyrrolidone (Povidone)*. Lewis Publishers, Inc., Chelsea, Michigan.

Shen, J., Ziaei-Azad, H., Semagina, N. (2014). Is it always necessary to remove a metal nanoparticle stabilizer before catalysis? *Journal of Molecular Catalysis A: Chemical*, *391*, 36–40. http://doi.org/10.1016/j.molcata.2014.03.027

Silva, T., Pokhrel, L. R., Dubey, B., Tolaymat, T. M., Maier, K. J., Liu, X. (2014). Particle size, surface charge and concentration dependent ecotoxicity of three organo-coated silver nanoparticles: comparison between general linear model-predicted and observed toxicity. *The Science of the Total Environment*, *468-469*, 968–76. http://doi.org/10.1016/j.scitotenv.2013.09.006

Stewart, M. W. (2010). Measuring the effect of water quality parameters on the release of silver nanoparticles from a ceramic surface using a quartz crystal microbalance by. The University of Colorado at Boulder Master's Thesis. Retrieved from ProQuest Dissertations and Theses database. ProQuest LLC Ann Arbor, MI (UMI Number: 1487918)

Swei, J., Talbot, J. B. (2003). Viscosity Correlation for Aqueous Polyvinylpyrrolidone (PVP) Solutions, *Journal of Applied Polymer Science. 90(4)* 1153-1155.

The Ceramics Manufacturing Working Group (2011). *Best Practice Recommendations for Local Manufacturing of Ceramic Pot Filters for Household WaterTreatment, Ed. 1.* Atlanta, GA, USA: CDC

Tobita, M., Yasuda, Y. (2008). Theoretical and Experimental Vibrational Characterizations of Amine-Coated Silver Nanoparticles. *The Journal of Physical Chemistry C*, *112*(36), 13851–13855. http://doi.org/10.1021/jp803195e

Tolaymat, T. M., El Badawy, A. M., Genaidy, A., Scheckel, K. G., Luxton, T. P., Suidan, M. (2010). An evidence-based environmental perspective of manufactured silver nanoparticle in syntheses and applications: a systematic review and critical appraisal of peer-reviewed scientific papers. *The Science of the Total Environment*, *408*(5), 999-1006. Elsevier B.V. doi:10.1016/j.scitotenv.2009.11.003

Tripathi, S. K., Singh, V. P., Gupta, K. C., & Kumar, P. (2013). Hydrophobic and membrane permeable polyethylenimine nanoparticles efficiently deliver nucleic acids in vitro and in vivo. *Journal of Materials Chemistry B*, *1*(19), 2515. http://doi.org/10.1039/c3tb00481c

Usui, S. (1973). Interaction of electrical double layers at constant surface charge. *J. Colloid Interface Sci.,* 44, 107-113.

Van Oss, C. J. (1990). DLVO and Non-DLVO Interactions in Hectorite. *Clays and Clay Minerals*, *38*(2), 151–159. http://doi.org/10.1346/CCMN.1990.0380206

Varner, K. E., El-Badawy, A., Feldhake, D.,Venkatapathy, R. State-Of-The-Science Review: Everything NanoSilver and More. U.S. Environmental Protection Agency, Washington, DC, EPA/600/R-10/084, (2010). Available at: http://oaspub.epa.gov/eims/eimscomm.getfile?p_download_id=498014 <Accessed November 2012>

van der Vegte, E. W., Hadziioannou, G. (1997). Acid - Base Properties and the Chemical Imaging of Surface-Bound Functional Groups Studied with Scanning Force Microscopy, *5647*(97), 9563–9569.

Verwey, E.J., Overbeek J.T. (1948). *Theory of the Stability of Lyophobic Colloids*; Elsevier: Amsterdam

Visser, J. (1972). On Hamaker Constants: A Comparison bewtween Hamaker constants and Lifshitz-van Der Waals Constants. *Advances in Colloid and Interface Science*, *3*, 331–363.

Wang, S., Yan, J., & Chen, L. (2005). Formation of gold nanoparticles and self-assembly into dimer and trimer aggregates. *Materials Letters*, *59*(11), 1383–1386. http://doi.org/10.1016/j.matlet.2004.12.045

Wegmann, M., Michen, B., Luxbacher, T., Fritsch, J., Graule, T. (2008). Modification of ceramic microfilters with colloidal zirconia to promote the adsorption of viruses from water. *Water Research*, *42*(6-7), 1726–34. http://doi.org/10.1016/j.watres.2007.10.030

Wulandari, P., Nagahiro, T., Fukada, N., Kimura, Y., Niwano, M., Tamada, K. (2015). Characterization of citrates on gold and silver nanoparticles. *Journal of Colloid and Interface Science*, *438*, 244–8. http://doi.org/10.1016/j.jcis.2014.09.078

Xiu, Z., Zhang, Q., Puppala, H. L., Colvin, V. L., Alvarez, P. J. J. (2012). Negligible particle-specific antibacterial activity of silver nanoparticles. *Nano letters*, *12*(8), 4271-5. doi:10.1021/nl301934w

Yakub, I., Soboyejo, W.O., (2012). Adhesion of E. coli to silver or copper coated porous clay ceramic surfaces. *Journal of Applied Physics,* 111, 124324. doi: 10.1063/1.4722326

Yen, H. J., Hsu, S. H., Tsai, C.-L. (2009). Cytotoxicity and immunological response of gold and silver nanoparticles of different sizes. *Small*, *5*(13), 1553-61. doi:10.1002/smll.200900126

Yu, F., Huang, Y., Cole, A. J., Yang, V. C. (2009). The artificial peroxidase activity of magnetic iron oxide nanoparticles and its application to glucose detection. *Biomaterials*, *30*(27), 4716–22. http://doi.org/10.1016/j.biomaterials.2009.05.005

Zhang, Y., Chen, Y., Westerhoff, P., Crittenden, J. (2009). Impact of natural organic matter and divalent cations on the stability of aqueous nanoparticles. *Water Research*, *43*(17), 4249–57. http://doi.org/10.1016/j.watres.2009.06.005

Zhang, Z., Zhao, B., Hu, L. (1996). PVP Protective Mechanism of Ultrafine Silver Powder Synthesized, *Journal of Solid State Chemistry,* (121), 105–110.

Ziebarth, J. D., Wang, Y. (2010). Understanding the protonation behavior of linear polyethylenimine in solutions through Monte Carlo simulations. *Biomacromolecules*, *11*(1), 29. doi:10.1021/bm900842d

Vita

Anne Marie Mikelonis was born and raised in Jackson, Michigan. After graduating from Lumen Christi High School, she entered Northwestern University in 2003. Anne graduated from Northwestern with a Bachelor of Science in Civil Engineering, a certificate in Music, and a passion for international development work. In 2008, she obtained a Master of Engineering in Environmental Engineering from the Massachusetts Institute of Technology (MIT). At MIT she studied chemically enhanced primary treatment of wastewater in Honduran Imhoff tanks. After the completion of her master's degree, Anne worked for two years as an Environmental Engineer for the consulting firm CDM Smith where she was involved in projects pertaining to sewer metering in the metro Detroit area. In 2010, she entered the doctoral program in Civil Engineering at the University of Texas at Austin under the supervision of Dr. Desmond Lawler.

Permanent email: amikelonis@gmail.com

This dissertation was typed by Anne Marie Mikelonis.